corewind

D1.4: Methods for multiple floaters and dynamic cables at farm level

Ozan Gözcü, Stavros Kontos, Henrik Bredmose
DTU

Tom Bailey, Friedemann Borisade
Rambøll

September 2021

Disclaimer:

This project has received funding from the European Union's Horizon 2020 Research and Innovation programme under grant agreement No 815083.

Project details:

Duration:
1 Sep 2019 - 28 Feb 2023
Grant agreement:
No: 815083

Document information

Deliverable number	D1.4
Deliverable name	Methods for multiple floaters and dynamic cables at farm level
Reviewed by	Climent Molins, UPC Valentin Arramounet
Date	29 September 2021
Work Package and Task	WP1, task 1.4: Development of mooring calculation models for accurate and efficient design
Lead Beneficiary for this Deliverable	DTU

Authors

Name	Organisation	E-mail
Ozan Gözcü	DTU	ozgo@dtu.dk
Stavros Kontos	DTU	stakon@dtu.dk
Henrik Bredmose	DTU	hbre@dtu.dk
Tom Bailey	RAMBOLL	Tom.bailey@ramboll.co.duk
Friedemann Borisade	RAMBOLL	Friedemann.borisade@ramboll.com

Version control

Version	Date	Author	Description of Changes
[Official versions only]	[yyyy-mm-dd]		
1.0	2021-09-29	Gözcü, Kontos, Bredmose, Bailey and Borisade	Final

Contents

1 Introduction and objective

Floating wind farms is the next step in the global exploitation of offshore wind energy. In the initial demonstration projects, all turbines have been moored individually. For sites of large depth however, cost reductions may be achieved by utilization of shared mooring lines and shared anchors. This leads to additional dynamics at the farm level, since the turbines are now structurally connected. The aero-servo-hydro-elastic design tools therefore needs adaptation to these new configurations such that the new dynamic effects can be captured.

This tool adaption is the focus of the present deliverable. The IEA 15 MW [20] reference wind turbine with the WindCrete spar floater is used as the through-going example, with configurations both in the Gran Canaria and Morro Bay sites. The HAWC2 model of DTU [18] is used to investigate the shared mooring line designs which are evaluated in terms of mooring line forces, equilibrium states, frequencies and corresponding mode shapes. The site properties, designs and their results are given in the detailed study sections along with the parameters for the shared mooring line designs.

1.1 Dynamic cables, shared mooring and shared anchors

Mooring lines and cables have many similarities with respect to dynamic modelling. Both are structural elements that mainly carry axial load and can have a softer bending stiffness. Both attract wave forcing and are coupled motion-wise to the main floater. Dynamic cables, though, are designed to provide a vanishing force contribution to the floater. All restoring force effects must come from the mooring and not from the cable, which is designed to move passively with the floater.

Due to this similarity and reduced dynamic impact from the cables, we here focus on three configurations, where mooring lines are connected between two or more turbines:

- One shared mooring line connected directly between two floating turbines (Section 4). This first test case is made for the Gran Canaria site at 200 m depth.
- One shared anchor with a vertical mooring line which is next connected to two floating turbines (Section 5). This configuration is made for the Morro Bay deep water site of 870 m depth, where pre-installed and shared anchors may be advantageous. Here also the effect of an added buoyancy element at the top end of the vertical mooring line is investigated.
- A four-turbine farm, where the turbines pair-wise share an anchor between them (Section 6). Also this configuration is made for Morro Bay.

The analysis method is applicable for dynamic cables too. For this reason, no specific treatment of dynamic cables is made, since the tools presented, can be directly applied to dynamic cables as well.

The industrial application of shared moorings and anchors are covered in two sections:

- A review section (Section 2) where state of the art within shared mooring, shared anchors and mooring technology is provided.
- A section on industrial load assessment for shared anchors at the sea bed (Section 7). The analysis is carried out with Orcaflex. The focus is on the anchor loads at

the farm level from wave forcing, wind-wave directionality under the simplified assumption of constant turbine thrust.

The objective of the deliverable is thus to show how the current load tools are capable of modelling wind farms with shared mooring line concepts and compute the dynamic characteristics of them. Further design optimizations and choice of 'most feasible designs' is left for a follow-on deliverable in WP2.

1.2 Key features

The IEA 15 MW turbine on a spar buoy floater is used in all configurations. This design with spar buoy is called WindCrete in COREWIND project. The turbine has 240 m rotor diameter and 1.012×10^6 kg total tower top mass. However, the floater, tower and mooring line designs are different for the two sites. The Gran Canaria site has 200 m depth and catenary mooring lines whereas the Morro Bay site has 870 m depth and taut mooring lines. The details of the site properties can be found in [23]. The floater and tower dimensions are also different and details of them can be found in [20]. The rest of the turbine specifications are identical for the two sites.

1.3 People and contributors

The HAWC2 developments and analysis of the three configurations have been carried out by Ozan Gözcü and Henrik Bredmose with support from Stavros Kontos (DTU). The background and state of the art section have been written by Tom Bailey and Fridemann Borisade (Ramboll). This also goes for the section on anchor load assesment.

2 Background and State of the Art

2.1 Mooring Characteristics

To provide a proper background for the present study, we here present the core requirements of moorings, the principle mooring performance characteristics, and an overview of existing industrial mooring experience with its relation to floating wind mooring systems.

The primary purpose of any offshore mooring is to maintain the floater's horizontal position relative to the seabed when the floater is subject to operational and environmental loading. The target for the floater position is generally referred to as the Theoretical Mooring Centre (TMC). The floater's horizontal movement away from the TMC is commonly referred to as offset or excursion. Historically and within Oil and Gas, the flexibility and configuration of riser systems combined with the site's water depth have governed the defined excursion limits used within mooring design. In floating wind applications, like flexible production risers, there is a flexible dynamic cable that requires the mooring to limit the floater excursion to prevent cable damage.

Mooring systems keep the floater close to its TMC by providing a restoring force (mooring stiffness) to oppose the net operational and environmental loads that are acting to move the floater away from its TMC. The mooring system stiffness properties should be calibrated to balance floater excursions against mooring loads as illustrated in the relationship shown in Figure 1, but also to balance the cost of material (line materials, but also anchor size and the structural weight of the connection points on the floater and any reinforcement of the mooring load path through the floater structure).

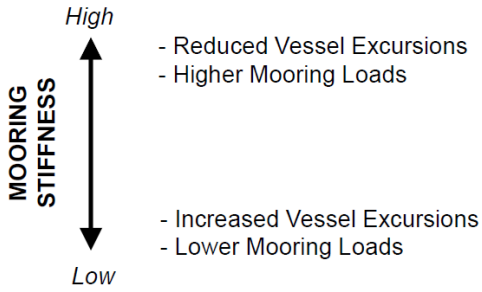

Figure 1: Qualitative influence of mooring stiffness [5].

Mooring systems must be designed to resist the following load sources:

1. Mean loads due to wind, wave and current ;
2. Slowly varying (low frequency) components of the wave loads and wind;
3. Wave period (high frequency) floater motion responses to waves.

The marine growth is more important for the dynamic cables, since its alteration on the mooring stiffness tends to be fairly minor.

Consider as an example two mooring systems with mooring stiffness curves shown in Figure 2. Indicated by their changing gradient, one exhibits reducing stiffness with increasing excursion on the left, whilst the other on the right has increasing stiffness with increasing excursion. It is important to note that all real mooring systems exhibit

increasing mooring stiffness with increased offset and that a reducing stiffness curve such as that in Figure 2 is purely theoretical. The exaggerated difference between the stiffness curves shown in Figure 2 does highlight the importance of the mooring stiffness gradient though.

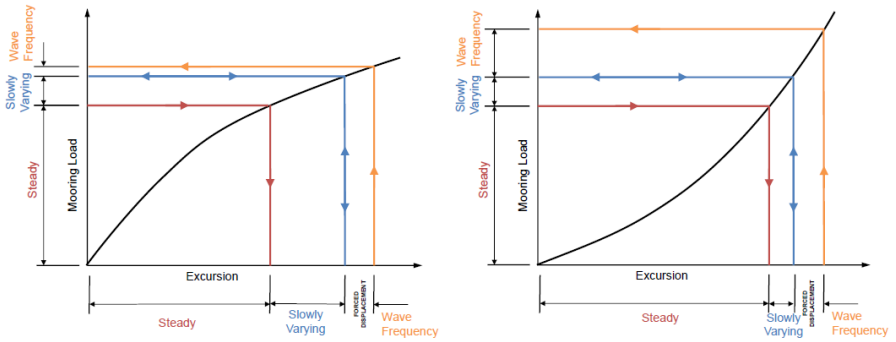

Figure 2: Exemplary mooring stiffness curves with different gradient (left: degressive curve, right: progressive curve) [5].

As noted earlier, the loads to be resisted by the mooring system consist of three main components. The first of these is the steady loads due to wind, wave and current. The steady (or static) loads are identical for both hypothetical mooring systems and result (arrows point from cause to effect) in less excursion in the softening system (left figure) due to its higher initial stiffness.

The slowly varying loads can have a more complex relationship with excursions, due to the low frequency load variations potentially exciting the natural frequencies of the coupled floater/mooring system. Comparing the two hypothetical systems in Figure 2 shows that the excursions due to steady loads on the softening system have put the floater at an offset where the mooring stiffness is reducing, resulting in larger excursions than observed for the stiffening system (right figure) under loads assumed to be identical.

Finally, the wave frequency motions of the floater result in forced displacements of the vessel (i.e. excursions that cause load). The effect of a forced displacement of equal magnitude on the mooring loads is significantly less for the softening system than the stiffening one due the difference in their stiffness's at large excursions.

Despite the degressive mooring stiffness curve not being feasible in a real mooring, it does highlight some of the advantages of a more linear mooring stiffness curve when compared to the progressive curve. A close to linear mooring stiffness curve minimises the steady load induced floater excursion as much as possible while reducing the slowly varying and wave frequency induced peak mooring loads. Many methods of altering the mooring stiffness curve exist outside of the specification of just mooring line materials, such as clump weights and buoyancy modules. However, many of these, in trying to reduce peak loads actually mainly soften the initial mooring stiffness, which is utilised by the steady load. When balancing mooring tensions and floater excursions, a close to linear mooring stiffness is a useful starting point.

2.2 Industrial Mooring Experience and Its Application to Floating Wind

Much of the industrial mooring expertise used within floating wind so far has originated in the Oil and Gas industry. This has many advantages, in that offshore moorings have been commonplace in that industry for many decades. This experience covers mooring challenges encountered both in shallow water, deep water and in severe environments. Considering the design life of a floating offshore wind turbine is approximately 25 years, no existing floating wind mooring has been installed for sufficient time to provide full, real-world, design life data to feed back into a tailored mooring design process.

Although mooring in the Oil and Gas industry has not undergone any significant changes or technology breakthroughs in quite some time, a steady but conservative optimisation of mooring design and mooring components has been in progress. Although further optimisation by the floating wind industry is required, it is important to note that despite a conservative approach to mooring design, the Oil and Gas industry has not been without numerous mooring line failures. Mooring line redundancy in the Oil and Gas industry is driven by the severity of the consequences of a floater losing position. It is perhaps worth highlighting that the loss of position of one floating offshore wind turbine within a wind farm puts the entire wind farm at risk and as the world becomes more reliant on the electricity produced by floating wind farms, the consequences of the loss or extended downtime of a wind farm become more tangible. Floating wind specific design standards provide more detail on the different design philosophies considering the issue of redundancy of the station keeping system.

As touched upon above, the mooring system of floating wind turbines has some notable differences to majority of offshore moorings in existence today. From the technical perspective, the major one is the wind turbine itself. The natural frequencies of the turbine and tower in operation add a key new parameter to mooring design. The avoidance or minimisation of mooring excitation and floater motion due to turbine operation is the primary consideration for many mooring designers.

From the project perspective, there is a far greater drive to reduce mooring costs within the floating wind industry. This has placed a cost focus on mooring optimisation, reducing mooring redundancy and the requirements for maintaining dynamic cable integrity. This may seem like unnecessarily fine margins, but it is important to remember that a floating wind farm could have hundreds of floaters all on their own moorings, when compared to the Oil and Gas industry where the numbers of floaters within a project is usually singular. The economies of scale for commercial floating wind farms are likely to change many of the cost considerations in place from Oil and Gas today.

2.3 Shared Moorings

The term shared moorings defines moorings of multiple floaters that share mooring lines. This usually includes mooring lines that pass between floaters, using fewer anchors.

As described in the section 2.2 on the background of moorings, worldwide mooring track record mainly revolves around single floaters in Oil and Gas applications. With the vast number of moorings required for floating offshore wind, some optimisation from the existing model is clearly required. In principle, shared moorings offer great potential to reduce the CAPEX of floating wind farm projects, but little research or

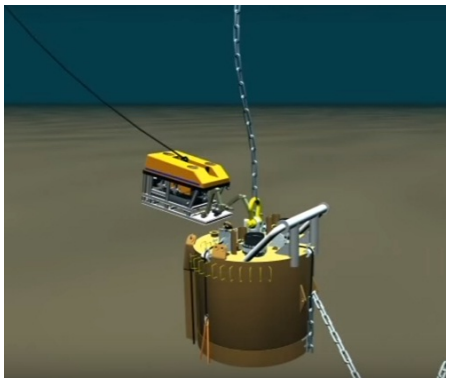

(a) A ROV pumps water out of the top suction port after sealing pile top valves. Pile top and ROV instrumentation contribute to a precise installation. [Source: `https://intermoor.com/press-releases/how-suction-piles-work/`].

(b) Wire rope mooring line birdcaging due to compression near socket termination. Birdcaging can happen when the mooring line goes slack under large heave or pitch motions of the floating structure [Source: BP [15]].

(c) Mooring chain on seabed showing no visible twist [Source: [17]].

(d) A suction pile is being lifted at a fabrication yard. The mooring chain connection padeye is visible. Padeye is generally designed for loads inline with the mainplate. Some side loads are tolerable, but not full mooring loads. [Source: `http://www.firstsubsea.com/products/smc/image-gallery.html`].

Figure 3: Various considerations on moorings and anchors

testing has been completed to validate the idea. This is made more difficult by the sheer number of possible shared mooring configurations and layouts.

The potential benefits of shared moorings include but are not limited:

- Reduction in the number of anchors affecting both material and fabrication costs as well as installation cost. This would also positively impact the project schedule as installation times considering the complete mooring system could potentially be reduced.
- Reduction in the amount of mooring line length required reducing material cost and production time.

However, to achieve these potential improvements, shared moorings may also present some challenges that will need to be considered. These include:

- Difficulty in installation;
- Difficulties in removal of single floater for O&M considering a tow-to port scenario with disconnection of mooring lines;
- Increased line component complexity increasing failure risk;
- Coupling effects of natural frequencies;
- Increased number of turbines affected by mooring line failure;
- Increased number of turbines affected by anchor failure.

Increasingly complex line configurations and line connections that can only be made subsea make the installation more difficult and time consuming. The use of divers or Remotely Operated Vehicles (ROV) to make connections (see Figure 3a), although possible, may significantly increase cost and time at wind farm scale, especially when considering their limited environmental operating envelope, for example regarding the maximum wave height until the operation can be performed, compared to an Anchor Handling Tug (AHT) or Construction Support Vessel (CSV). Trying to minimise connections made subsea when designing the mooring is likely to result in a mooring that is simpler to install, translating to cost and schedule reduction.

Other potential installation considerations include mooring lines that are shared between floaters but still utilise an anchor. Some may be more time consuming to pretension in the case of drag embedment anchors and to set the inverse catenary in the case of pile anchors. Mooring line pull in of shared mooring lines also has potential to cause increased complexity as it is unlikely floaters will be able to be installed simultaneously.

Similar complications are still present once installed and in operation as shared mooring line configurations make it more difficult to remove an individual floater from the wind farm for out of field replacement/maintenance using tow-in O&M scenarios. A temporary anchoring procedure could be devised to work around this but laying of any temporary anchor and mooring line would have to consider a potentially crowded subsea infrastructure of cables and other mooring lines.

It is natural of any system that the more complex it becomes, with an increased number of components, the higher the risk of failure, for example birdcaging as illustrated in Figure 3b. Almost all shared moorings involve an increase in the number of

inline connections, buoyancy modules or clump weights and it is this increased complexity that leads to an increase in the number of potential failure modes. Lessons learnt from Oil and Gas industry for permanent moorings include the use of shackles and other components that are Long Term Mooring (LTM) rated as well as trying to minimise clamp-on line attachments due to instances of them becoming detached.

As described before, one of the major differences in mooring design between Oil and Gas and floating wind, is the emphasis placed on the mooring natural frequencies. Using shared moorings and effectively coupling multiple floaters only increases the need to accurately identify natural frequencies and ensure that a larger coupled mooring system's natural frequency does not interfere with that of the floaters and their Wind Turbine Generators (WTG).

Through the use of a reduced number of mooring lines, the floating wind industry generally already has a reduced mooring line redundancy than the offshore Oil and Gas industry and this increases the risk to the wind farm as a whole due to a single mooring line failure. However, sharing mooring lines between floaters further increases the floaters co-dependence and a single mooring line failure could result in larger excursions and collisions for multiple turbines. It is important to note that both drag embedment and pile anchors are installed so that their connection point is orientated with the lay azimuth of the mooring line. In the case of a mooring line failure, the floater position changes and the lay azimuths of the remaining intact lines change, altering the load vector at the anchor connection points. In analytical software, this does not present an issue, but this load vector reversal is incompatible with drag anchors. With piles (see Figure 3d), the padeye orientation is set and so a different mooring load vector either applies acts to twist the pile or causes large out of plane forces on the shackle and padeye, resulting in the potential failure of the connection and loss of multiple mooring lines.

Further considerations on the benefits and challenges of shared moorings are provided in the Phase III Summary Report by the Carbon Trust Floating Wind Joint Industry Project [22].

In terms of other public literature, Matthew Hall from National Renewable Energy Laboratory (NREL) has published on shared moorings, for example in [16]. His paper describes the coupled, time-domain simulation of a full shared-mooring floating wind farm using a square-shaped configuration of four turbines in irregular waves and turbulent winds as illustrated in Figure 4. He concludes that the complex restoring properties of the shared mooring arrangement are reflected by the resulting surge displacements. Further, shared mooring lines see different excitation at each end and tend to be more sensitive towards resonance due to the absence of the seabed contact. In [21] Connolly et al. simulated several shared mooring floating wind turbine arrangements and concluded that the shared mooring lines were able to maintain platform spacings while reducing the number of anchors required. Furthermore, a cost analysis was presented that shows that significant cost savings over individually moored wind farms are possible for water depths that exceed 400 m.

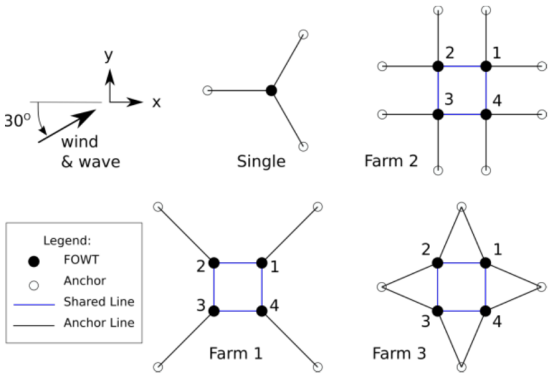

Figure 4: Schematic showing different configurations of shared mooring lines (blue lines), copied from [16].

2.4 Shared Anchors

The term shared anchors defines moorings of multiple floaters that use common anchors. Each floater will have its own mooring lines, but these lines will share anchor points with other floaters' lines, see examples in Figure 5.

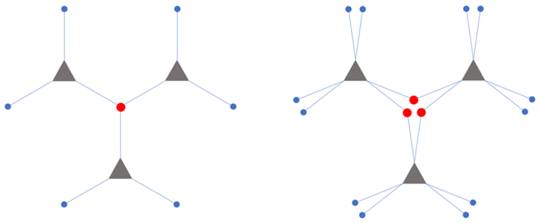

Figure 5: Illustration of exemplary configurations for shared anchors (red dots) [Source: Ramboll].

The use of shared anchors is perhaps a more conservative step towards shared mooring equipment building upon existing experience with classical dimensioning methodologies than full shared moorings in floating winds applications. Reducing the number of anchors required to be fabricated, transported and installed could result in a significant cost reduction for commercial scale floating wind farms if some challenges associated with shared anchors are mitigated. These include:

- Larger piles required;
- Increased monitoring during installation and slower installation of shared piles to avoid line twisting;
- Increased number of turbines affected by anchor failure;
- Ideal anchor positioning per floater may not be achievable with shared anchors;
- Pile refusal during installation results in potential for longer chain being required for at least one floater.

Using multiline anchors could result in larger anchors being required. It is important not only to consider the scalar loads on the anchor from multiple lines, but the vector load time histories from each line as in some configurations this could result in increased peak lateral loading in the resultant azimuth as well as increased pile load cycle magnitude. Opposing forces on the anchor, although unlikely due to similar environment loads acting on adjoining floating offshore wind turbines, could (in the case of taut and semi-taut mooring only) produce a resultant vertical load acting axially on the pile. Although larger anchors may be required, this may still prove to be more cost effective.

During any anchor installation, any portion of chain or rope should be twist free within certain tolerances (see Figure 3c). Many have some form of indication marked to make identification of twist easier. This can be a difficult and time consuming process offshore, but with multiple mooring lines attached to the same anchor, with different line lay azimuths, this has the potential to become far more complex and time consuming.

Through reducing the number of mooring lines, the floating wind industry already has a reduced anchor redundancy than the offshore Oil and Gas industry and this increases the risk to the wind farm as a whole due to a single anchor failure. However, sharing anchors between floaters further increases the floaters co-dependence and a single anchor failure could result in larger excursions or collisions for multiple turbines.

2.5 Geotechnical Considerations

Although the geotechnical properties of the seabed will be well surveyed before the installation campaign begins, it is important to have a pile refusal procedure in case the installation of a pile fails. This almost always requires the pile to be installed a certain distance away from the original piling attempt. With a pile connected to multiple mooring lines with different lay azimuths, the requirement for additional mooring line — i.e. reserve also known as “green” in mooring industry — to account for installation inaccuracy increases.

Geotechnical considerations of any anchor pile can be separated into axial load and lateral load. The axial uplift force has to be transferred to the ground through pile shaft friction. The self-weight of the pile and that of the enclosed soil column can be taken as additional uplift resistance. The shaft friction can be determined in accordance with the guidelines [13]. If Cone Penetration Tests (CPT) are available, a CPT-based design methodology is recommended. In the framework of the COREWIND project those are not required and typical shaft resistance has to be determined from tabulated values on basis of the given soil density. A degradation factor to account cyclic loading must be defined and considered in the design. Cyclic laboratory tests are typically used to define such degradation factors.

In lateral direction the pile-soil-interaction is typically modelled by so-called p-y curves which can be defined on basis of the standards referenced above. Those curves need to be modified to account for potential scour around the pile. Furthermore, the cyclic loading of the pile can lead to porewater pressure build-up in the soil which reduces its resistance. This must clearly be accounted for in design. A framework for defining the cyclic degradation in lateral direction is given in [13] which refers to concept presented e.g. in [2]. A special challenge in case of shared anchor points is the change of main loading directions that must be addressed in design by defining suitable simplified load cases and reduction factors.

Another specialty of the Morro Bay site is the risk of earthquakes. A heavy earthquake may also trigger porewater pressure build-up in loose or medium dense soil and can thereby significantly reduce its shear strength. In an extreme case, those layers can liquefy and provide no resistance at all.

2.6 Outlook

The cost advantages of using shared anchors may only reach their potential under certain conditions, hence, requiring site-specific evaluations. Turbine spacing and clustering should be dictated by the site-specific energy yield calculations and any savings on anchors could be diminished by an increase in mooring line lengths to reach a common mooring point while giving sufficient turbine spacing for the yield. Some sites where closer turbine spacing is possible may provide a more feasible system using shared anchor points.

Further considerations on the benefits and challenges of shared anchors are provided in the Phase III Summary Report by the Carbon Trust Floating Wind Joint Industry Project [22].

3 HAWC2 method for shared mooring lines

The turbine designs are modeled in HAWC2 [18] which is an aero-servo-hydro-elastic wind turbine analysis code. HAWC2 uses multibody dynamic formulation with linear Timoshenko beams for turbine structures and it can also use external super-elements to represent e.g. radiation-diffraction models of wind turbine floaters. It computes aerodynamic forces by the blade element momentum formulation. The hydrodynamic loads are computed either through the Morison equation in its full form, or by using the WAMIT [19] frequency response functions for the radiation and diffraction forces combined with the Morison drag. The controller is defined as an external dynamic link library (dll) and mooring line dynamics are also computed in its own dll developed by DTU Wind Energy and integrated to HAWC2. Figure 6 shows different levels of wind turbine load analysis depending on turbine configuration. The floating turbine analysis requires all sub-modules represented in the figure to model the physical problem accurately. The mooring line sub-module is highlighted since it is the main focus of this report.

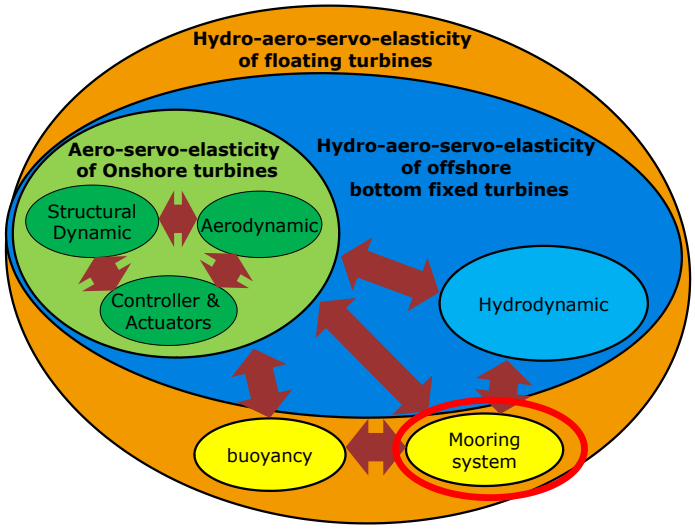

Figure 6: Wind turbine load computation sub-modules for different turbine configurations

The HAWC2 mooring line dll uses a dynamic mooring line formulation based on non-linear beam elements. The mooring line beam elements carry the loads only in axial direction and uses Green strain which is given in Equation (1). The current length and initial length of the element are shown as L and L_0 in the below equations. The current length L is computed at each iteration according to Equation (2) where x_n, y_n, z_n is the position of node number n in global HAWC2 coordinates.

$$\varepsilon_{Green} = \frac{L^2 - L_0^2}{2L_0^2} \tag{1}$$

where

$$L^2 = (x_{n-1} - x_n)^2 + (y_{n-1} - y_n)^2 + (z_{n-1} - z_n)^2 \tag{2}$$

The axial force that acts on an element can be found by using Equation (3) where E is the elastic modulus and A is the cross-section area. Cross-section properties are assumed constant and initial values are used.

$$f = EA\varepsilon_{Green} \tag{3}$$

There are 6 degrees of freedom (DoFs) in each mooring elements unlike turbine structures which have 12 DoFs for each beam element. The mooring line axial force has 3 force components in a three dimensional space. This result in 3 DoFs in each node and 6 DoFs in each element with 2 nodes. The element stiffness matrix is expressed in terms of axial force f and current length L as shown in Equation (4).

$$K_e = \frac{f}{L}\begin{bmatrix} 1 & 0 & 0 & -1 & 0 & 0 \\ 0 & 1 & 0 & 0 & -1 & 0 \\ 0 & 0 & 1 & 0 & 0 & -1 \\ -1 & 0 & 0 & 1 & 0 & 0 \\ 0 & -1 & 0 & 0 & 1 & 0 \\ 0 & 0 & -1 & 0 & 0 & 1 \end{bmatrix} \tag{4}$$

The internal force vector of an element can be found by multiplying K_e by the node coordinates. The result of this multiplication is shown in Equation (5).

$$K_e \begin{bmatrix} x_n \\ y_n \\ z_n \\ x_{n+1} \\ y_{n+1} \\ z_{n+1} \end{bmatrix} = \begin{bmatrix} -\delta f \\ \delta f \end{bmatrix} \quad \text{where, } \delta = \begin{bmatrix} \frac{x_{n+1}-x_n}{L} \\ \frac{y_{n+1}-y_n}{L} \\ \frac{z_{n+1}-z_n}{L} \end{bmatrix} \tag{5}$$

Mooring lines can be connected to each other or to the ground or to another structure such as a floater by using the constraint equations in the HAWC2 multibody formulation. These constraints lock the positions of the connection nodes of the structures or fix the position of the connection node to a point in space to represent e.g. a connectino to the ground. Rotations of nodes are allowed in the constraint equations (ball joint constraint) and only forces are transferred between the nodes. The mooring line elements are assumed to not carry moments, therefore there is no moment transfer at the constraints. This is consistent with the element definition of mooring lines.

Since mooring lines are defined by their initial lengths, first the equilibrium point of the system should be found. At the equilibrium state, mooring lines have some tension forces and turbines can move and rotate compared to their initial positions. When the equilibrium point is found, eigenvalue analysis can be run by using the mass and stiffness matrix of the whole system in HAWC2. The mass matrix has all added mass effects from Wamit or hydrodynamic formulation of HAWC2 and the effects of forces at constraint points are also included in stiffness matrix. Hence, the natural frequencies and corresponding mode shapes are computed at the equilibrium point by taking into account all mass and stiffness effects.

Mooring lines are integrated to the HAWC2 solver as super-elements. Superelements can connect to each other, other bodies and ground by constraints. Their internal dynamics including mass, stiffness, damping and forces are computed in their dynamic library which receives data from HAWC2 and send dynamic properties, forces and positions back to HAWC2. The integration of super-elements into HAWC2 equation of

motion (EoM) is done as shown in Figure 7. Details of superelement modelling in multibody dynamic formulation can be found in [1].

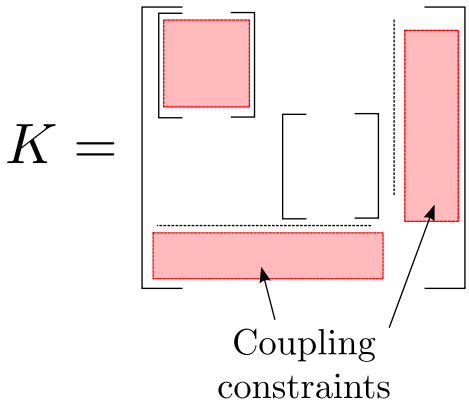

Figure 7: HAWC2 EoM includes body internal equations and its constraint equations

4 Configuration 1: Shared mooring line at the Grand Canaria site

We here consider as a first case, the configuration of a single shared mooring line between two turbines at the Gran Canaria site. The depth is 200 m. The mooring lines have 50 m long delta lines, and 565 m long main chain sections. There are 3 mooring lines in the single turbine design [8]. The lines are 120° apart from each other. Tower and floater properties are given in [20]. The floater diameter is 9.3 m at this site.

Figure 8 shows the single turbine design site design which has 3 catenary type mooring lines. It also shows the HAWC2 global coordinate system whose y axis is in the flow direction and z is in gravity direction. The center of the floater is at the (0.0,0.0) x and y coordinates and the z coordinate is 0.0 at the mean sea level.

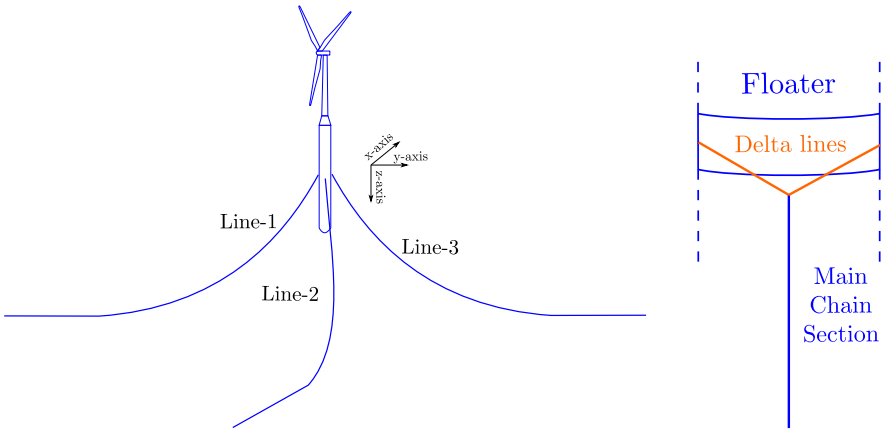

Figure 8: Single turbine design in Grand Canaria site and mooring line segments

The properties of the delta lines and main chain section are given in Table 1. The delta lines have the same cross-sectional properties as the main chain section. However, the main chain section is much longer than the Delta lines.

Table 1: Properties of mooring line sections for Grand Canaria site

	Delta line	Chain line
Length [m]	50.0	565.0
Nominal Diameter [mm]	160.0	160.0
Dry mass [kg/m]	561.25	561.25
Axial stiffness [kN]	2.304×10^6	2.304×10^6

Table 2 shows the anchor and fair-lead positions for the mooring lines. The coordinates are given in the HAWC2 global coordinate system which is shown in Figure 8 together with the single turbine case.

Table 2: Positions of anchor and fair-lead points of the mooring lines

	Anchor positions			Fair-lead pos. from tower bottom		
	x [m]	y [m]	z [m]	x [m]	y [m]	z [m]
Line-1	0.0	−600.0	200.0	8.05 / −8.05	−6.65	90.0
Line-2	−519.61	300.0	200.0	−8.05 / 0.00	−4.65 / 9.30	90.0
Line-3	519.61	300.0	200.0	8.05 / 0.00	−4.65 / 9.30	90.0

Design parameters for configuration 1 Figure 9 shows the shared mooring line design where the turbines are 1200 m (equals to five rotor diameter) away from each other. The shared mooring line has delta line sections at the floater sides, connected by a chain section whose length is a design parameter. The chain properties are the same as for the other chains.

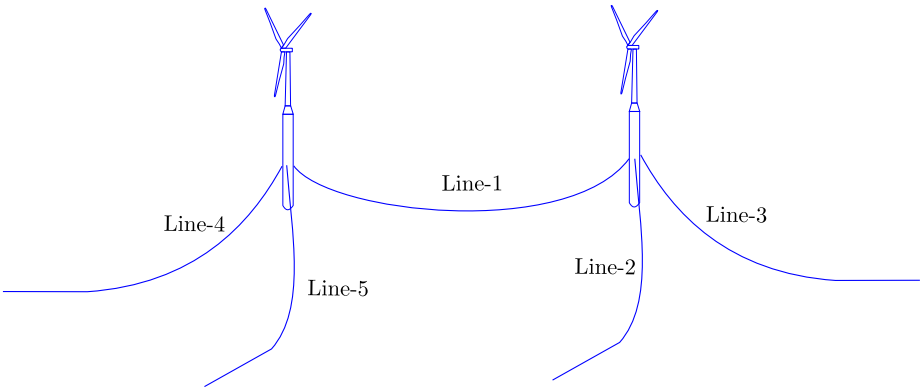

Figure 9: Shared mooring line design in Grand Canaria site. The length of Line-1 is a design parameter.

Two shared chain designs with different main chain lengths were investigated. The first design has a 1093.8 m long main chain section (called as Design-1) whereas the second design has a 1150.7 m long main chain section (called as Design-2). The results of these designs together with those of the single turbine design are given in the following sub-section.

4.1 Results

Table 3 shows the mooring line forces, turbine pitch angles and turbine surge motions at their equilibrium points. Figure 8 and 9 show the line numbers. The right turbine is the number one and left turbine is the number two. The pitch angles are given around the x axis of the global HAWC2 coordinate system which is also shown in Figure 8. Turbines with shared mooring line design are also away from their initial positions at their equilibrium points. They move in the surge direction which is parallel to the shared mooring line. The values are given in the global HAWC2 y axis. The turbines get 23.6 m closer to each other for Design-1 whereas they go 13.58 m away from each other for Design-2. The surge offset of the new designs can be prevented by adding buoyancy elements on main chains or replacing the chains with different mooring line material. The focus of this study is shared mooring line concepts and modelling them

in load analysis tools, so no effort was done to prevent the surge motion of the turbines in the study.

Table 3: Tension forces at the main chain sections and turbine pitch angles at equilibrium points

	Single WT	Design-1	Design-2
Line-1 [MN]	4.25	7.45	3.20
Line-2 [MN]	4.25	7.25	3.30
Line-3 [MN]	4.25	7.25	3.30
Line-4 [MN]	-	7.25	3.29
Line-5 [MN]	-	7.25	3.29
Pitch-1 [deg.]	−0.64	−0.66	−0.64
Pitch-2 [deg.]	-	−0.59	−0.66
Surge-1 [m]	0.00	6.79	−11.80
Surge-2 [m]	-	−6.79	11.80

Figure 10 shows the frequencies for the single turbine case, Design-1 (with 1093.8 m shared main chain section) and Design-2 (with 1150.7 m shared main chain section). The corresponding mode shapes of the frequencies are shown in Appendix A. Design-2 has lower first natural frequency compared to the single turbine design. On the other hand, Design-1 results in a higher first natural frequency than for the single turbine. The frequencies appear as groups around some frequencies such as 0.025 Hz. Design-1 does not have any natural frequency around 0.055 Hz which is the yaw natural frequency for the single turbine and Design-2. Design-1's first yaw frequency is at 0.082 79 Hz. The mode shapes around 0.025 Hz are dominated by roll or pitch motions. Mode shapes around 0.028 Hz are mainly in heave direction.

The two turbine designs generally have symmetric and asymmetric mode shapes in different directions. For example Design-1 has a symmetric pitch mode shape at 0.0247 Hz and an asymmetric pitch mode shape at 0.024 74 Hz. The higher frequencies after the first yaw frequencies are generally different yaw mode shapes.

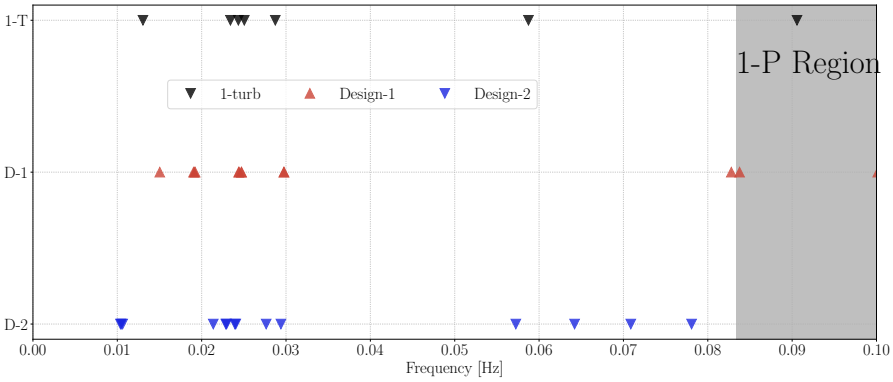

Figure 10: Frequencies for single and two turbine designs at Grand Canaria site

Table 4 shows the dominant directions of mode shapes and their frequency range from Figure 10. Some mode shapes have very strong coupling between two directions,

so both directions are written in some rows of the table. The frequencies are sometimes present as groups and their range is given in the table.

Table 4: Dominant directions of mode shapes and corresponding frequency range

	Single WT	Design-1	Design-2
Surge [Hz]	0.013	0.015	-
Sway - Surge [Hz]	-	0.019	0.010
Roll - Pitch [Hz]	0.023 - 0.025	0.024 - 0.025	0.021 - 0.024
Heave [Hz]	0.029	0.030	0.027 - 0.029
Yaw [Hz]	-	0.083 - 0.084	0.057 - 0.078

The first mode shapes for the different designs are shown in Figure 11. The single turbine and Design-1 configurations have motions in the surge directions whereas Design-2's surge motion is coupled with sway motion. The blue lines show the system in the equilibrium position and red lines show the system when it is moved according to the mode shapes. There are two views in each figure, left plot shows the system from side and right shows it from the front. All three axes have identical scale in the figures and dots on the lines are the connection point of bodies.

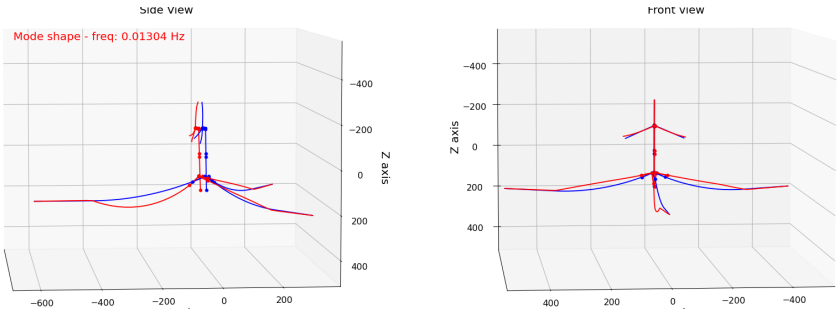

Figure 11: Single turbine case first mode shape

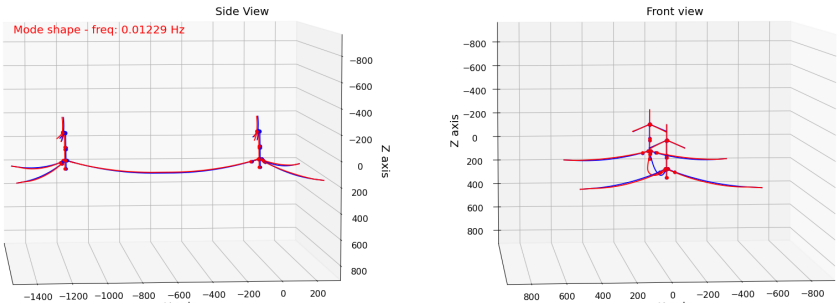

Figure 12: Design-1 first mode shape

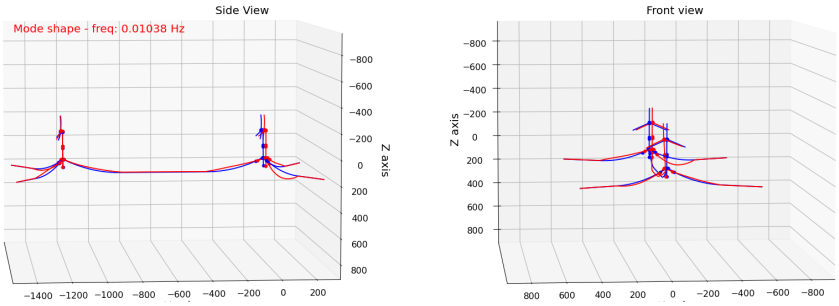

Figure 13: Design-2 first mode shape

The single turbine mode shape which stay in 1-P region is shown in Figure 14. Although the mode shape main motion occurs in the yaw direction, it is not the first yaw mode shape. Note that, the sea bed friction is not considered in natural frequency calculation. Also the mode shapes are normalized vectors and they are amplified in the plots for getting a better view of motions in the plots.

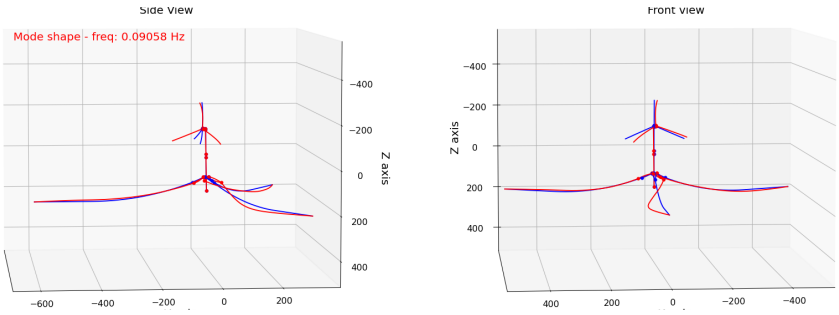

Figure 14: Single turbine mode shape at 0.0906 Hz

The mode shapes corresponds to the frequencies within the gray region are shown below for Design-1. They are in the yaw direction mainly but the first yaw mode shape is actually out of the gray zone. The gray zone marks the 1P region of the rotor forcing and therefore requires attention for design.

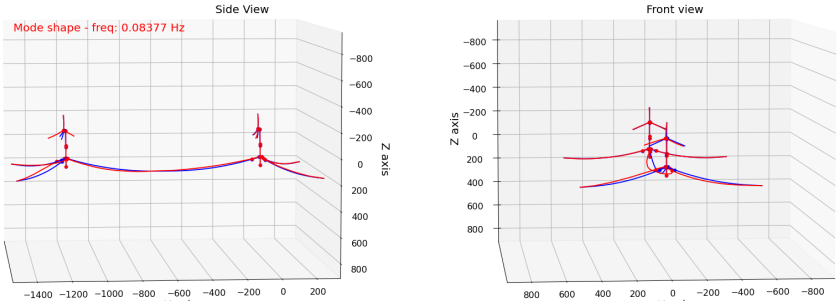

Figure 15: Design-1 mode shape at 0.0838 Hz

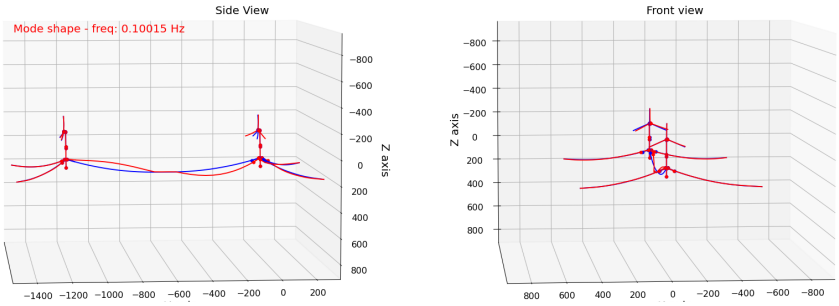

Figure 16: Design-1 mode shape at 0.1002 Hz

5 Configuration 2: Shared anchor at Morro Bay

We now go ahead with configuration 2, where a shared anchor between two turbines is modelled for the Morro Bay deep water site. Also an additional buoyancy element at the connection point is considered.

The single IEA 15 MW turbine design for the site has 4 mooring lines, with a slightly asymmetric configuration [9]. For the present investigation, this design was modified to a symmetric version, to be more generic. Each mooring line consists of a short chain section between sea bed and a main polyester section. The long polyester section is connected to the turbine by two delta lines which are also made of chain. Figure 17 shows the single turbine design and a detail view of a mooring line with its sections. The floater diameter is 9.7 m at the Morro Bay site.

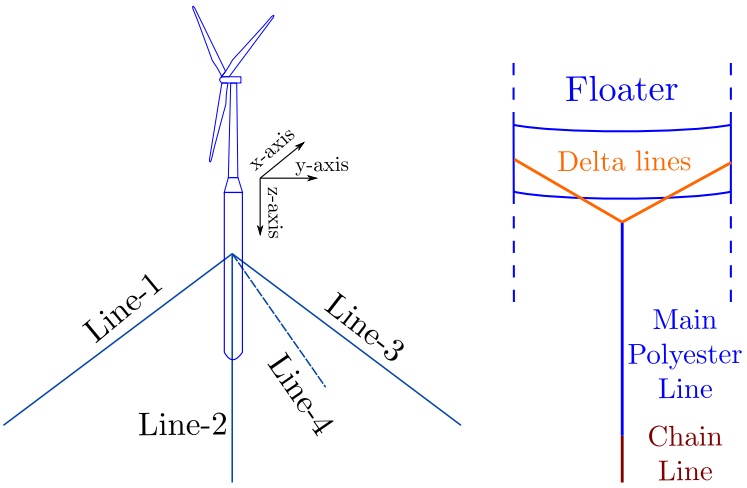

Figure 17: Single turbine design with 4 main mooring lines in Morro Bay site and the sections of a main mooring line

Table 5 shows the properties of the delta lines, main polyester line and chain section for the site. The longest part of the mooring lines is the polyester section. All sections are in taut condition similar to the lines shown in the above figure.

Table 5: Properties of mooring line sections

	Delta line	Main polyester	Chain line
Length [m]	50.0	1020.8	183.7
Diameter [mm]	90	205	85
Equivalent D [mm]	162	164	171
Dry mass [kg/m]	161.0	28.6	179.6
Axial stiffness [kN]	6.92×10^5	2.68×10^5	7.71×10^5

Table 6 shows the main mooring line anchor (connection to sea bed) and fair-lead positions. The fair-lead positions are measured from the tower bottom since they are not fixed in space but fixed on the floater. The tower bottom center position is 15 m above the mean sea level.

Table 6: Positions of the anchor and the fair-lead points of the mooring lines

	Anchor positions			Fair-lead pos. from tower bottom		
	x [m]	y [m]	z [m]	x [m]	y [m]	z [m]
Line-1	0.0	-1015.0	870.0	± 6.8589	-6.8589	105.0
Line-2	-1015.0	0.0	870.0	-6.8589	± 6.8589	105.0
Line-3	0.0	1015.0	870.0	± 6.8589	6.8589	105.0
Line-4	1015.0	0.0	870.0	6.8589	± 6.8589	105.0

The tower of the original HAWC2 model was modified for Morro Bay site. The tower properties can be found in [20]. The buoyancy force from the floater, turbine mass and floater mass values are given in Table 7.

Table 7: Total turbine, floater mass and buoyancy force of floater

Turbine mass [kg]	4.09×10^6
Floater mass [kg]	4.12×10^7
Buoyancy force [N]	4.58×10^8

The buoyancy force is larger than the total force due to the turbine mass and floater mass. The difference is about 1.35×10^7 N and is balanced by the mooring lines. Hence the mooring lines are in taut condition.

Design parameters for configuration 2 Two turbine designs with a shared mooring line and anchor is shown in Figure 18. The distance between the turbines is 1680 m which is equivalent to 7 rotor diameter of IEA 15 MW. The lines have the same properties as for the single turbine case except for Line-1, Line-7 and Line-9. Line-1 and Line-7 have delta lines on the floater side whose properties are same as the Delta line properties given in Table 5. After the Delta line sections the polyester section starts and Line-9 consist of only polyester section. The length of Line-9 is an important design parameter and its effect on the dynamics of entire system is part of the present investigation. The cross-section properties of the main polyester lines are identical to the properties given in Table 5. In some designs a buoyancy element is added to the intersection point of Line-1, Line-7 and Line-9 to see its effect on the entire system dynamics. Each set of design parameters and their results are given in Section 5.1.

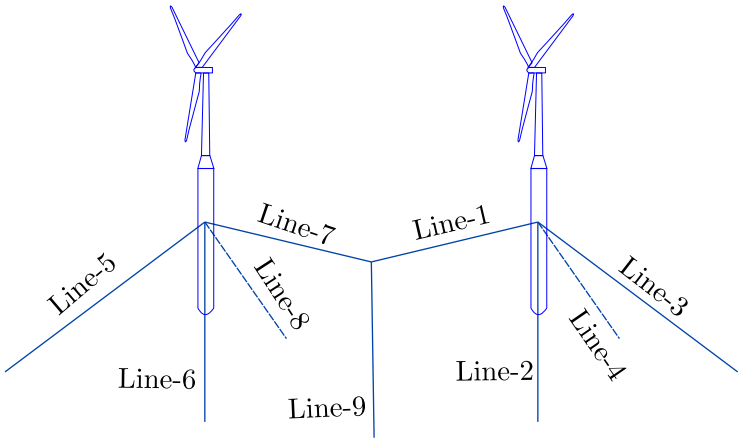

Figure 18: Shared mooring line design with 2 turbines in Morro Bay site

5.1 Results

We now analyse the dynamic properties of the configurations. Results are given for forces, orientation/position of turbines, and frequencies of the whole system and corresponding mode shapes. Different shared mooring line lengths and buoyancy elements are used and they are explained for each cases at corresponding sections. There are five designs whose polyester section lengths and buoyancy elements at the intersection point are given in Table 8.

Table 8: Different designs for Configuration-2

	Line-7 & 1 polyester length [m]	Line-9 polyester length [m]	Buoyancy force [MN]
Design-1	783.4	670.0	0.0
Design-2	783.4	670.0	2.0
Design-3	783.4	670.0	5.0
Design-4	783.4	670.0	10.0
Design-5	783.4	600.0	0.0

At the equilibrium position of the single turbine design, each mooring line has an 38.2° angle between the floater and each line. The floater has 0.46° pitch angle in the negative x-axis direction. Further, the center of gravity (CoG) position of the whole system which is very close to the mooring line attachments to the floater stays at its initial position. The elongations and forces on each line are very similar at the equilibrium point, therefore they are represented together. Table 9 shows the elongation of each line segment and the forces for the single turbine design.

Table 9: Elongations and forces of mooring line sections at equilibrium of single turbine design

	Delta line	Main polyester	Chain line
Initial Length [m]	50.0	1020.8	183.7
Elongation [m]	0.19	19.25	1.18
Elongation [%]	0.3	1.9	0.6
Force [MN]	2.69	5.18	5.03

As seen from the elongation results, the main polyester line has the largest elongation. The stiffness values in surge, sway and heave can be computed by giving a unit displacement to the top node of the main polyester line. We assume that the bottom node of the main polyester line doesn't move. Then, natural frequency estimates in surge, sway and heave directions can be computed quickly by using the stiffness values from the unit displacement analysis and mass of the entire system. Table 10 shows the natural periods computed from HAWC2 and by the simple method for the single turbine design.

Table 10: Periods of surge, sway and heave motions from HAWC2 and simple method

	HAWC2	Simple Method	Difference [%]
Surge [s]	105.5	103.6	1.8
Sway [s]	101.9	103.6	1.6
Heave [s]	30.9	30.4	1.6

In the simple method, first the internal force due to unit displacement in the selected direction is computed by Equation (3). Then the component of this force is computed by using the orientation of the mooring line and finally the force component in the selected direction is used as the stiffness value. The mass used in the natural frequencies includes turbine mass, floater mass and hydrodynamic mass. For the frequency estimation, the hydrodynamic mass coefficient is selected as 1.0 for the floater in surge and sway directions. For the heave stiffness, the change in buoyancy force due to unit displacement is also included and it is observed that it is the main contributor for the heave stiffness. The hydrodynamic mass coefficient is taken zero for heave motion in the simple calculations.

Figure 19-22 show surge, sway, heave and yaw mode shapes from HAWC2. The blue lines show the system in the equilibrium position and red lines show the system when it is moved by mode shapes. There are two views in each figure, left plot shows the system from side and right one shows it from the front. All three axes have same scale in the figures and dots on the lines are the connection point of bodies.

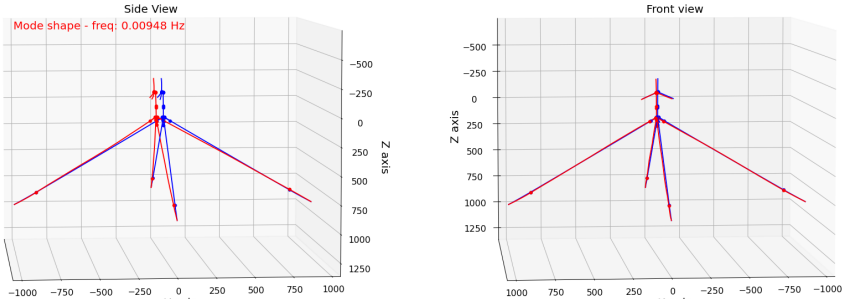

Figure 19: Single turbine surge mode shape in Morro Bay site

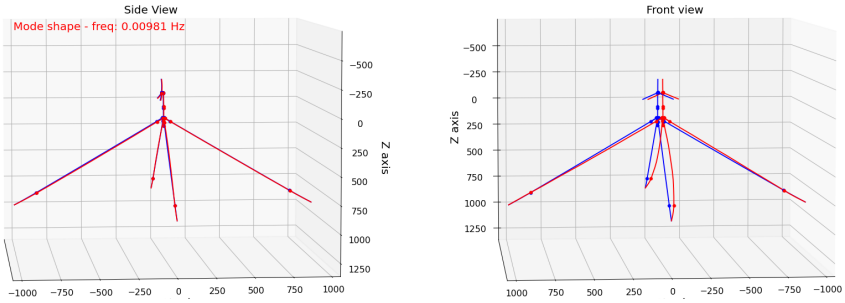

Figure 20: Single turbine sway mode shape in Morro Bay site

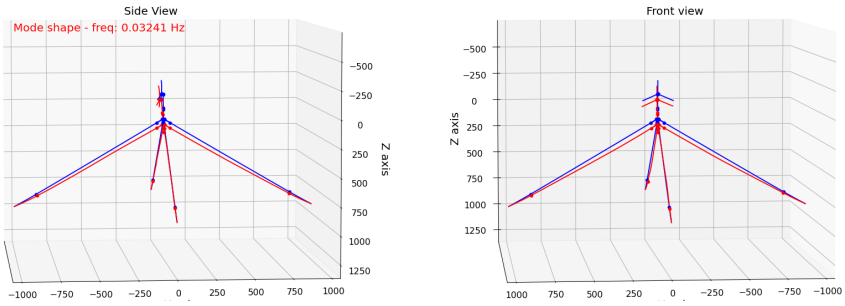

Figure 21: Single turbine heave mode shape in Morro Bay site

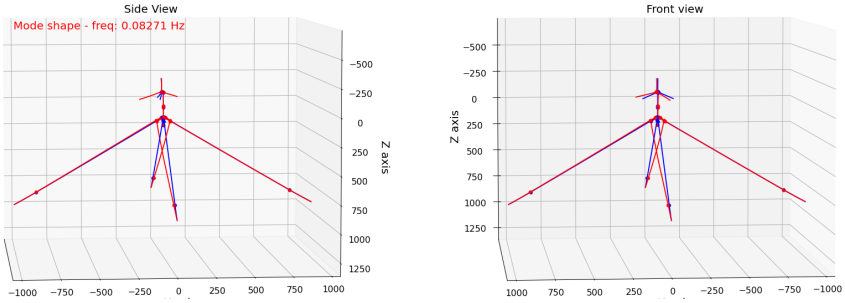

Figure 22: Single turbine yaw mode shape in Morro Bay site

As seen from the above figures the single turbine case is similar to a dynamic system with one mass where turbine and floater behaves like a rigid mass and the mooring system defines the stiffness in different directions. When two turbines are connected by a shared mooring line as shown in Figure 18, the system behaves as a dynamic system where two rigid masses are connected by springs. Therefore, extra mode shapes which are not present at the single turbine case can be observed in this design similar to shared mooring line designs in Configuration-1.

Figure 23 & 24 show the symmetric and asymmetric surge mode shapes for the configuration 2 designs given in Table 8. In the symmetric motion, the intersection point of Line-1 and Line-7 move together with the turbines and the system stiffness comes from mainly Line-3 (far right) and Line-5 (far left) similar to the single turbine case but the mass of the system is doubled in the shared mooring line design. Hence the frequency of symmetric surge motion is about $\sqrt{2}$ times smaller than the single turbine surge frequency. The mid-point does not move in the asymmetric surge mode shape where the turbines move towards each other. In this case Line-1 and Line-7 also contribute to the stiffness together with Line-3 and Line-5. As a result the frequency of the mode shape is larger than the symmetric mode shape. Symmetric and asymmetric mode shapes are also present in the sway, heave and yaw directions. However, their low frequencies are not affected as much as surge mode shape since the turbines are connected in surge direction in this design. A similar effect can be expected in sway frequencies when turbines are connected in sway direction.

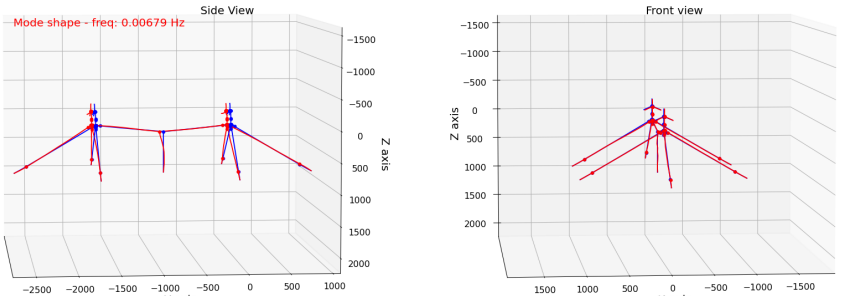

Figure 23: Symmetric surge mode shape for Design-1 which has zero buoyancy force at the intersection

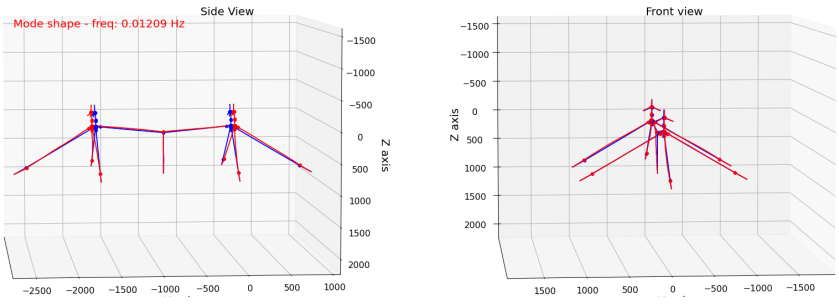

Figure 24: Unsymmetric surge mode shape for Design-1 which has zero buoyancy force at the intersection

Effect of a buoyancy element The motion of the mid-point in the symmetric mode shape can be prevented by applying tension force to Line-9 by a buoyancy element. In this case the symmetric motion of the mode shape is disturbed or completely removed in some cases due to the stiffness contribution of Line-9 in the surge direction. Buoyancy elements with different force effects are added to the intersection point of Line-1, Line-7 and Line-9. Table 11 shows the frequencies of surge, sway, heave and yaw motion for different buoyancy element forces. The frequencies are computed by HAWC2.

Table 11: Periods of surge, sway, heave and yaw motions for Design-1, Design-2, Design-3 and Design-4.

	Design-1	Design-2	Design-3	Design-4
Buoyancy force [MN]	0.0	2.0	5.0	10.0
Sym. Surge [s]	147.3	143.9	126.1	137.4
Unsym. Surge [s]	82.7	84.4	82.8	87.1
Sym. Sway [s]	102.4	102.7	107.5	103.2
Unsym. Sway [s]	100.6	101.6	102.4	103.2
Sym. Heave [s]	31.6	31.6	31.4	31.6
Unsym. Heave [s]	31.7	31.7	31.6	31.2
1^{st} Yaw [s]	11.1	11.9	12.1	12.6

The buoyancy element has stiffness and mass effect on the system. The mass effect comes form the added hydrodynamic mass and the stiffness effect can be estimated easily as given in Equation (6).

$$K_{buoy} = \frac{T}{L} \tag{6}$$

where T and L are the tension in the vertical mooring line and its length, respectively. K_{buoy} is in the surge direction stiffness contribution coming from the tension of the mooring line.

The results with different buoyancy forces show that adding a buoyancy force doesn't result in a significant change in the response of the full system. The reason is that if the buoyancy force is not large enough then its stiffness effect becomes limited since the length of mooring line is very long and decreases the K_{buoy} term in equation (6). So, a large buoyancy force needs to be applied to obtain a observable stiffness effect. However, large buoyancy force comes with large hydrodynamic added mass,

which also diminish the stiffness contribution since it increases the mass of the system. Therefore, system dynamics doesn't change significantly by adding buoyancy elements at the intersection point. Design-3 with 5 MN buoyancy force which corresponds to a sphere with a 4.9 m radius increases the first natural frequency 17 % compared to the original design with zero buoyancy force. The frequency increase comes with a coupling of the surge motion and sway motion in first two mode shapes. Figure 25 and 26 show the first two mode shapes for Design-3. The surge and sway motions are coupled unlike the mode shapes of Design-1 with zero buoyancy force shown in Figure 23.

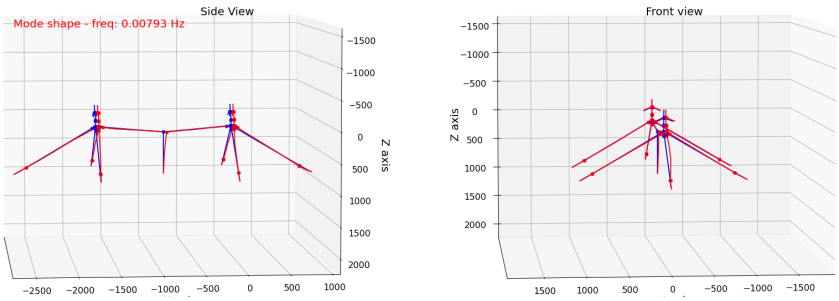

Figure 25: The first mode shape for Design-3 with 5 MN buoyancy force

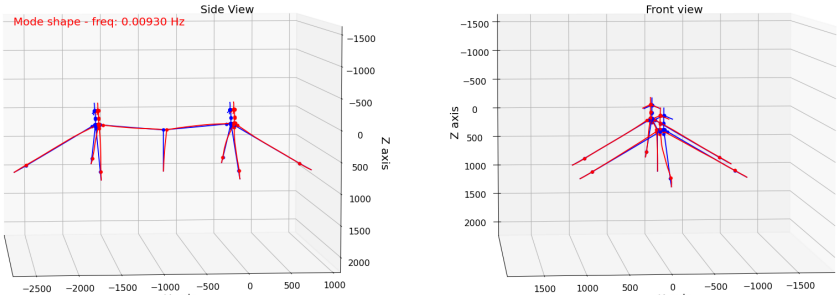

Figure 26: The second mode shape for Design-3 with 5 MN buoyancy force

The buoyancy study is a good example of how one can increase the natural frequency of the system. If we want to increase the natural frequency of the first mode shape without changing the stiffness of Line-5 and Line-3, we need to disturb the mode shape itself. So, the mid point should not follow the motions of the turbine at the symmetric surge mode shape. In that case it doesn't have pure symmetric surge motion. This is what happens in Design-3.

A similar effect can be obtained by changing the initial length of Line-9, so that its tension at equilibrium point can be controlled. The advantage of this approach is that there is no need to introduce any additional mass to the system for the tension force. Design-5 has Line-9 with a 657.12 m length which is almost 13 m shorter than the other designs. This results in almost 2 MN tension force at the equilibrium point without any buoyancy element and also results in higher tension force on Line -7 and Line-1 compared to the other designs. As a result of this, the first natural frequency is 33 % higher than Design-1 and only 8 % lower than the single turbine case.

Table 12 shows the mooring line tension forces at equilibrium point and Figure 27

shows the frequencies for single turbine, Design-1, Design-3 and Design-5. The 1-P region for the turbine also shown in the figure which corresponds to 5 to 7.56 rpm.

Table 12: Tension forces at the main polyester lines and turbine pitch angles at the equilibrium points for single turbine case, Design-1, Design-3 and Design-5

	Single WT	Design-1	Design-3	Design-5
F-Buoy [MN]	0	0	5.00	0
Line-1 [MN]	5.18	3.74	3.58	5.00
Line-2 [MN]	5.18	5.44	5.46	5.32
Line-3 [MN]	5.18	4.74	4.57	6.14
Line-4 [MN]	5.18	5.44	5.46	5.32
Line-5 [MN]	-	4.74	4.57	6.13
Line-6 [MN]	-	5.44	5.46	5.32
Line-7 [MN]	-	3.74	3.58	5.00
Line-8 [MN]	-	5.44	5.46	5.32
Line-9 [MN]	-	0.87	5.62	1.99
L-9 Length [m]	-	671.97	683.71	604.27
Pitch-1 [deg.]	−0.47	−0.35	−0.35	−0.35
Pitch-2 [deg.]	-	−0.59	−0.59	−0.58

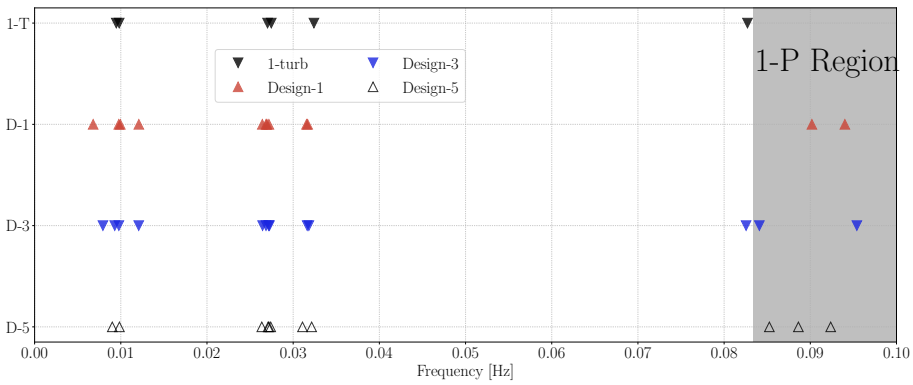

Figure 27: Frequencies for single turbine, Design-1, Design-3 and Design-5. The gray region represents the turbine 1-P region.

The frequencies appear as groups such as surge/sway group, roll/pitch group, heave group and yaw group similar to Configuration-1 results. The yaw group is the last one and, the first yaw frequencies of Design-1 and Design-5 stay in 1-P region.

Figure 28 shows Design-5 first mode shape where the surge and sway motions are coupled. The first mode shape of other designs are already given above in Figure 19, 23 and 25.

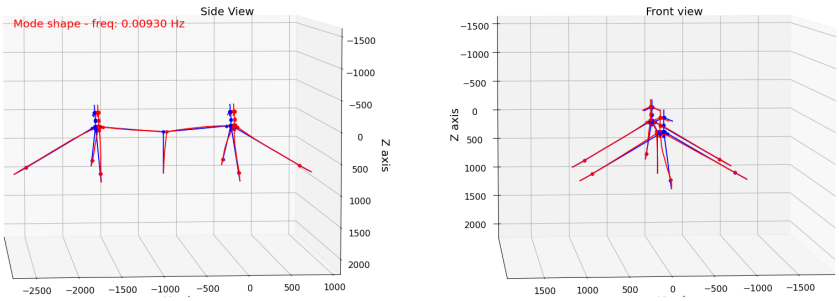

Figure 28: The first mode shape of Design-5

The first yaw mode shapes of the designs are shown in Figure 29 - 32. The first yaw frequencies of the single turbine design and Design-3 are out of the 1-P region, however Design-1 and Design-5 first yaw frequencies are in that region. The rest of the mode shapes for the frequencies shown in Figure 27 are given in Appendix B.1, B.2, B.3 and B.4.

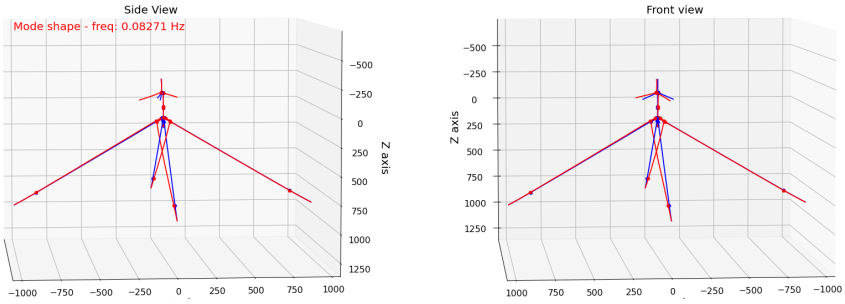

Figure 29: The first yaw mode shape of the single turbine design

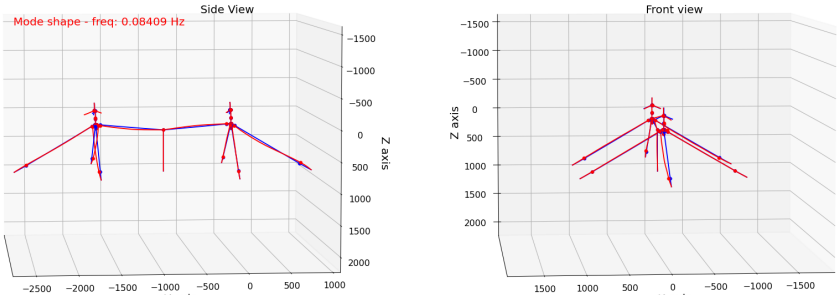

Figure 30: The first yaw mode shape of Design-1

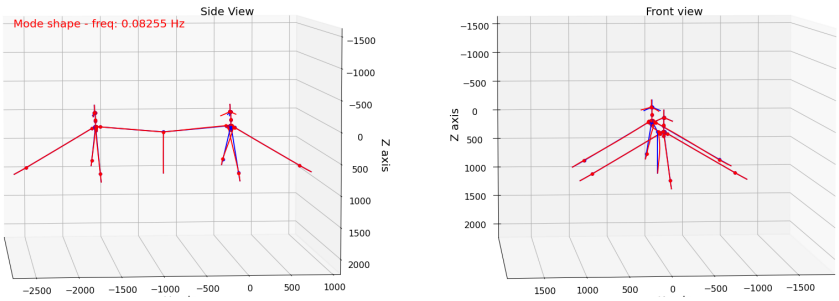

Figure 31: The first yaw mode shape of Design-3

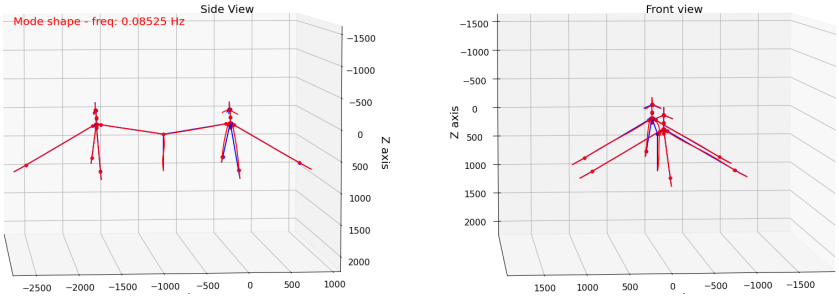

Figure 32: The first yaw mode shape of Design-5

6 Configuration 3: Four-turbine farm at Morro Bay

The final configuration is presented here. It consists of four turbines in a diamond configuration. Figure 33 shows the design where each turbine shares two of its mooring lines with another turbine. The shared lines have same cross sections as the designs in Configuration-2 (see Section 5). Long side mooring lines which goes directly to sea bed are applied with the properties as for the single turbine design. The diagonal of the square equals to 1680 m which result in 1187.94 m side length with the square edges as the turbine locations. The shared mooring lines attached to the turbines have 553.95 m initial length and vertical shared mooring lines have 600 m length.

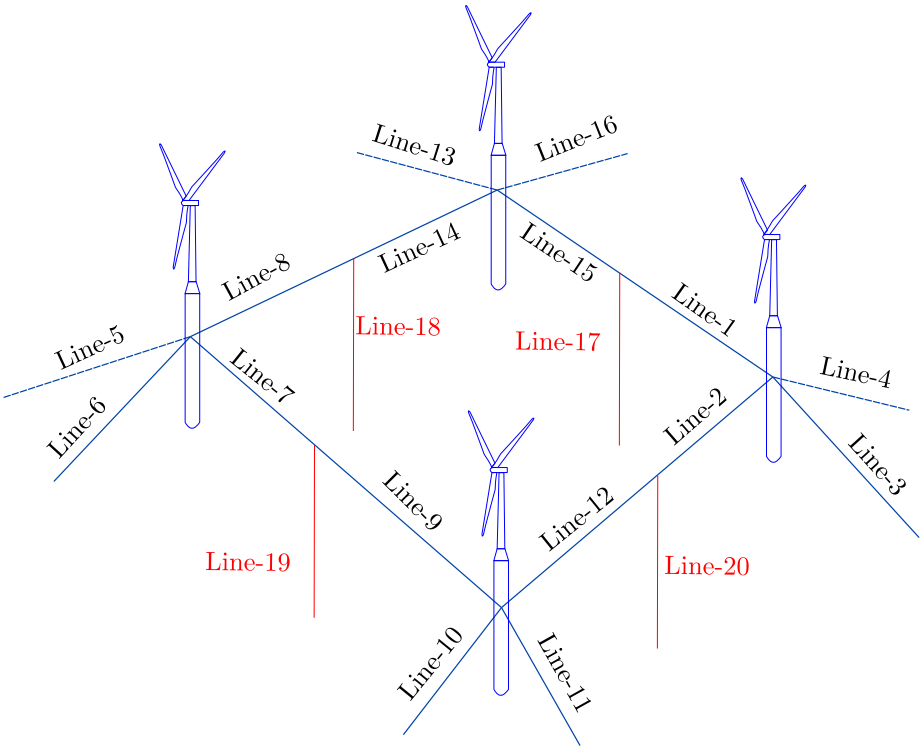

Figure 33: Shared mooring line design with four turbines in Morro Bay site

The system is now much more complex than the designs given in Configuration-1 and Configuration-2. Therefore there are many mode shapes for the design. Figure 34 shows the frequencies for the single turbine design and the four turbine design. The mode shapes corresponding to the frequencies are given in Appendix B.1 and C.

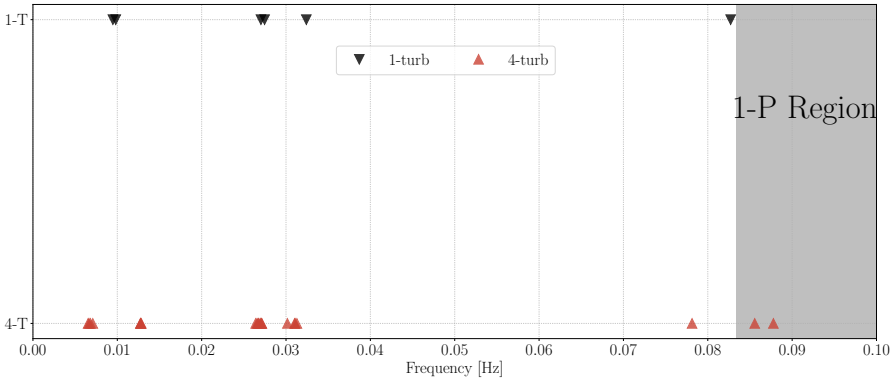

Figure 34: Frequencies for single and four turbine designs at Grand Canaria site

The first eight mode shapes between 0.0065 Hz to 0.0129 Hz have surge and sway motions in different combinations of symmetry. There are also eight mode shapes between 0.0264 Hz to 0.0271 Hz with roll and pitch motions. For heave motion, the system has four mode shapes which are between 0.0302 Hz to 0.0313 Hz.

Figure 35 & 36 shows the first surge-sway and roll mode shapes. As seen from the figure, surge and sway motions are coupled in the first mode shape. Roll and pitch mode shapes have a narrower frequency band (0.026 Hz - 0.027 Hz) than the surge-sway mode shapes and one turbine motion in a roll-pitch mode shape is common among them. Figure 36 provides a nice example with a first roll mode shape. The highest roll - pitch frequency is 0.027 Hz. Further roll-pitch mode shapes can be seen in Appendix C.

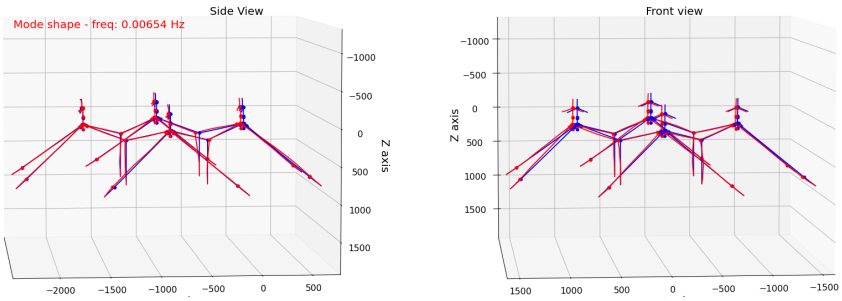

Figure 35: first surge-sway mode shape of the system at 0.006 54 Hz

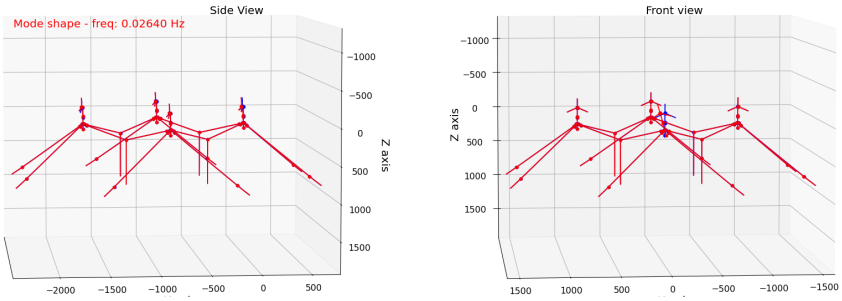

Figure 36: First roll mode shape of the system at 0.0264 Hz

Modes in the 1P region There are two frequencies which are in 1-P region in Figure 34. The mode shapes of these frequencies are shown in Figure 37 and 38 and are in the yaw directions mainly. Their frequency corresponds to 5.14 - 5.27 rpm which covers operation points up to 7.5 $\mathrm{m\,s^{-1}}$ wind speed. The yaw mode shapes also appear as combinations of turbines like for the surge-sway mode shapes.

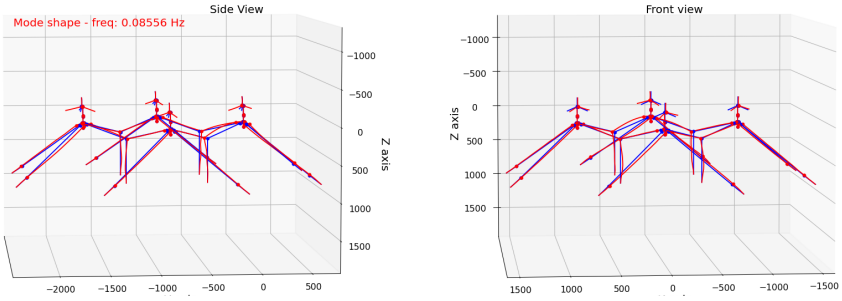

Figure 37: Mode shape of the system at 0.0856 Hz

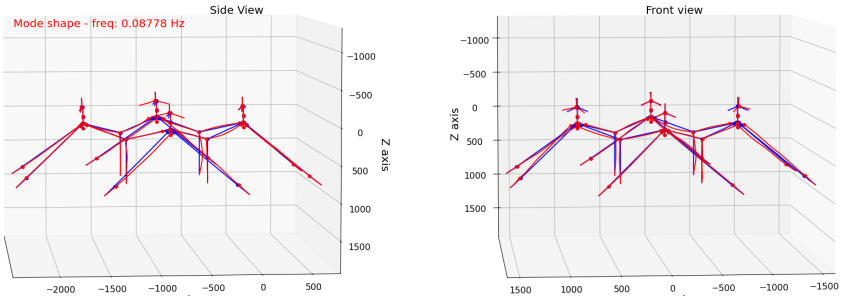

Figure 38: Mode shape of the system at 0.0878 Hz

Mooring line tensions The mooring line forces and turbine orientations are given in Table 13. The turbine numbers are given with respect to the mooring line numbers so that turbine-1 is attached to Line-4, turbine-2 is attached to Line-8, turbine-3 is attached to Line-12 and turbine-4 is attached to Line-16 given in Figure 33. The mooring line forces are given in groups for 4-turbine design since there is a symmetry. The pitch

results of turbine-3 and turbine-4 are also identical due to symmetry. The mooring line forces of the 4-turbine design are very similar to the single turbine case. The vertical mooring lines (Line-17,18,19,20) though have lower forces for the single turbine case. Turbine-3 and turbine-4 have very similar pitch angles to the single turbine case whereas the turbine-1 and turbine-2 pitch values are similar to the 2-turbine designs in Configuration-2.

Table 13: Tension forces at the main polyester lines and turbine pitch angles at the equilibrium points for single turbine case and 4-turbine design

	Single WT	4 WT
Line-1,7,9,15 [MN]	5.18	4.57
Line-2,8,12,14 [MN]	5.18	4.57
Line-3,6,10,13 [MN]	5.18	5.54
Line-4,5,11,16 [MN]	5.18	5.54
Line-17,18,19,20 [MN]	-	2.55
Pitch-1 [deg.]	-0.47	-0.34
Pitch-2 [deg.]	-	-0.62
Pitch-3,4 [deg.]	-	-0.48

7 Load assesment for shared anchors

7.1 Scope and Objectives

Preliminary mooring analysis has been undertaken to demonstrate a possible methodology for the design of mooring systems using piled shared anchors. The objectives of this part of the study were:

- Provide insight on turbine spacing and its impact on shared anchors;
- Demonstrate preliminary anchor load calculation through mooring analysis;
- Suggest suitable information interface between mooring analysis and geotechnical pile sizing;
- Discuss geotechnical aspects of shared anchor design versus anchors for a single mooring line;
- Highlight areas where method optimisation is possible or further work is required.

It is important to note that mooring optimisation is not the subject of this study and so although some degree of optimisation is covered, the focus is on the generation of shared anchor loads using the software OrcaFlex.

7.2 Design Parameters

COREWIND's deep water reference site Morro Bay and the Windcrete spar floater design were selected for the purposes of this study. Environmental data for the Morro Bay site was taken from Deliverable D1.2 [23].

7.2.1 Wind

Wind effects are represented in the OrcaFlex simulations using the 10 minute mean at the 10 m elevation wind velocity as a constant applied thrust force on the rotor and constant drag forces on the nacelle and tower. Wind is applied omnidirectionally. The operational and drag loads because of wind are not computed directly within OrcaFlex so are described separately using a different elevation within the Normal Sea State (NSS) and Extreme Sea State (ESS) mean wind speed profiles.

7.2.2 Wave

Waves in NSS and ESS states were applied omnidirectionally using the JONSWAP spectrum with peak enhancement factors set according to [10].

7.2.3 Current

No current velocity was provided in the design basis. Therefore conservative values for NSS and ESS were assumed based on [4].

7.2.4 Wind Turbine

The wind turbine used to calculate constant thrust and drag forces was the IEA 15 MW reference wind turbine (see for example in [6]). NSS and ESS thrust forces as well as NSS and ESS nacelle and tower drag were calculated using the NSS and ESS wind speeds at 140 m elevation and applied to the model as global loads. The tower height, weight and Nacelle/Rotor Assembly were also applied in the model using the data supplied in [6].

7.2.5 Anchor Design

As general guideline for designing anchoring systems for floating wind structures standards such as [11], [14] and [13] should be followed. Those guidelines provide a framework relevant for the geotechnical design of piled anchors for mooring systems. A safety concept and safety factors are provided in the standards. For the design of anchors for Deep Draught Floaters (DDFs) an increased safety factor of 1.7 on the pile axial resistance is advised in [11]. The design must generally fulfil Ultimate Limit State (ULS) and Accidental Limit State (ALS) analyses.

In the framework of the COREWIND project piled anchors are considered as feasible and cost-effective anchor type for the Morro Bay site. The piles are fabricated as steel pipe piles and can generally be installed by impact or vibratory driving or as suction piles. In the latter case the upper end of the pile is closed by a lid with valve openings where pumps can be connected to achieve the required negative pressure for installation.

The anchor points for the mooring lines are usually padeyes welded onto the outside of the pile below the mudline, see Figure 3d. Stiffening is often required to transfer the loads into the pipe pile structure. In case of shared anchors, each anchor line will be connected to its own padeye at the correct azimuth.

7.2.6 Mooring Arrangements

Three mooring configurations (also called patterns or unit cells) were considered. A 4 leg mooring, a 3 leg mooring and 6 leg mooring grouped 3 x 2. All three configurations were assumed to be symmetrical to facilitate the sharing of anchors. It is worth noting that asymmetric mooring designs either as a result of dominant metocean conditions or seabed slope are likely to make sharing anchors between wind turbines more difficult across a cluster. The models analysed here represent the least number of turbines to analyse the anchor pile shared by mooring lines in the centre. More turbines and their moorings could be modelled, but it would significantly increase computational time and have few benefits.

Factors of safety It is important to note that the three different mooring concepts studied here have differing levels of mooring line redundancy. A 3 leg mooring in a windfarm with tight enough turbine spacing to allow shared anchors is unlikely to avoid collision with a neighbouring turbine should one of its mooring lines fail. This could result in turbines that use a 3 leg mooring and shared anchors falling into consequence class 2 (no redundancy), requiring a higher factor of safety for the design of its mooring lines as prescribed in [11] and shown below.

Table 14: Mooring Line Factors of Safety [11]

Table 8-1 Load factor requirements for design of mooring lines

Limit state	*Load factor*	*Consequence class*	
		1	*2*
ULS	γ_{mean}	1.3	1.5
ULS	γ_{dyn}	1.75	2.2
ALS	γ_{mean}	1.00	1.00
ALS	γ_{dyn}	1.10	1.25

Fibre Rope Properties The stretch and axial stiffness characteristics of polyester rope have viscoelastic properties which are dependent on the magnitude of loads, load rates and cycles. The axial stiffness properties of the polyester rope have been based on publicly available vendor supplied data [7]. For the purposes of this study and others where approximate fibre rope size is to be determined, the use of non-linear load vs extension curves can be useful as they are scalable with the MBL of the fibre rope size. The worked Load vs Extension curve should be used. The curves are shown below in Figure 39.

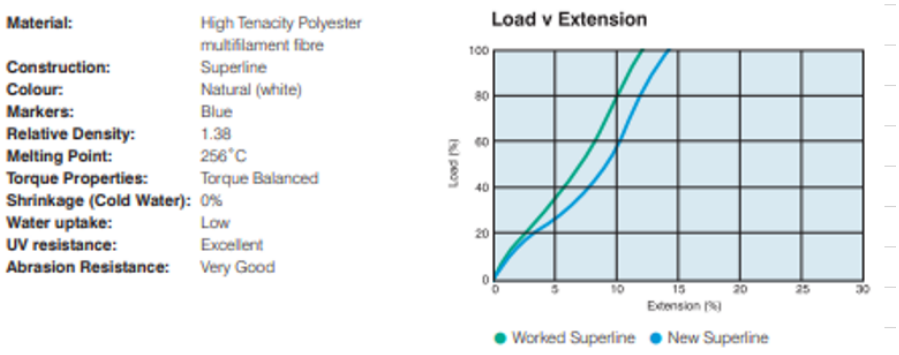

Figure 39: Polyester Superline Load vs Extension Curves [7]

It is important to note however that for detailed design that post installation drift stiffness and storm stiffness should be taken into account. The post installation rope stiffness properties are firstly input in the dynamic analysis to determine the floater's extreme excursions. The dynamic analyses are then re-run with storm stiffness properties applied to assess extreme line tensions. Both of these analyses conditions are to be assessed at the same pretension, by adjusting the length of storm stiffness polyester rope to suit.

4 Leg Mooring The 4 leg mooring configuration utilises a square grid pattern as shown below in Figure 40.

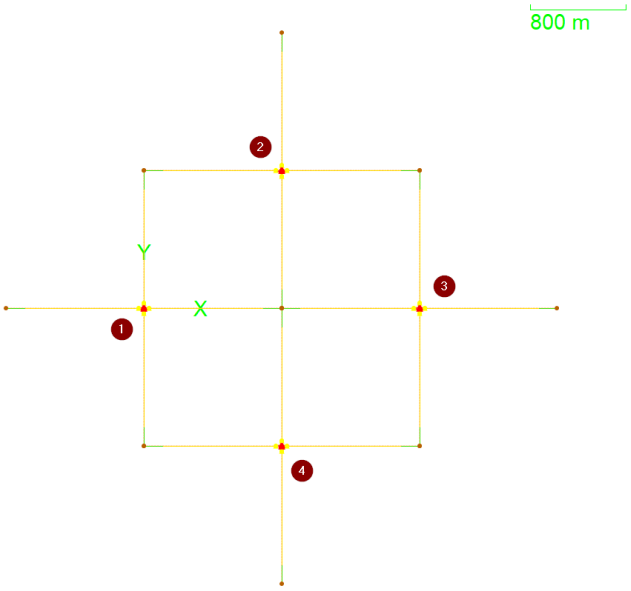

Figure 40: 4 Leg Mooring Configuration (Numbered Turbines in Red, Anchors in Brown)

Each mooring line consists a pair of 50 m long bridle lines connected to the spar to reduce occurrence of yaw (see Figure 41). The mooring system has been configured as a taut mooring comprising chain on the seabed and polyester rope through the water column. The advantage of such a system is that it utilises the elasticity of the fibre rope combined with some catenary action of the heavy mooring chain during extreme slack line events to provide the necessary restoring force. This also minimises rope abrasion issues during installation and during its design life. The mooring line pretension at the fairlead is equal in all lines at 5750 kN.

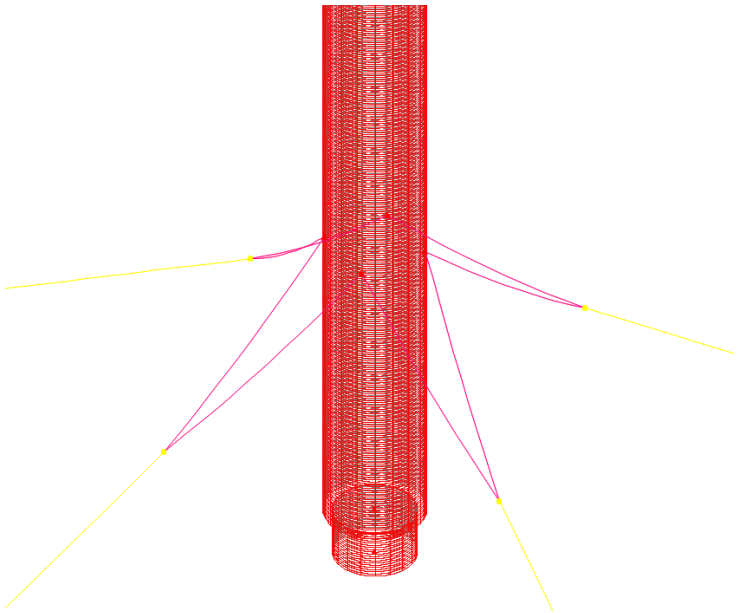

Figure 41: Bridle Chains Connecting to Spar

3 Leg Mooring The 3 leg mooring configuration forms a hexagonal grid pattern as shown below in Figure 42.

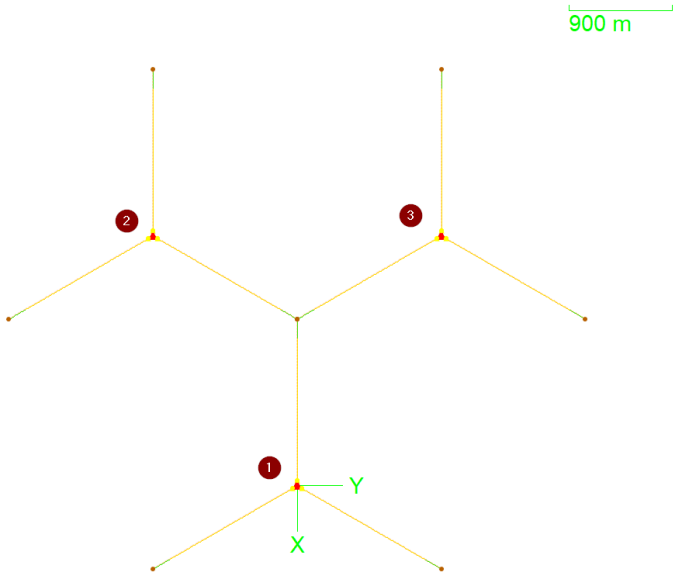

Figure 42: 3 Leg Mooring Configuration (Numbered Turbines in Red, Anchors in Brown)

The 3 x 1 mooring line components are similar to the 4 x 1 mooring design, but with increased cross section due to the reduced number of lines. The pretension at the

fairlead has been increased to 6500 kN.

3 x 2 Leg Mooring The 3 x 2 mooring does not have bridle lines connected to the spar as having two lines in each mooring line group has a similar effect on the yaw of the spar. Although the polyester and chain components are similar to the other two designs, it is important to note that they are significant smaller in cross section with lower pretensions at the fairlead of 4000 kN. The shared anchor configuration is shown below in Figure 43.

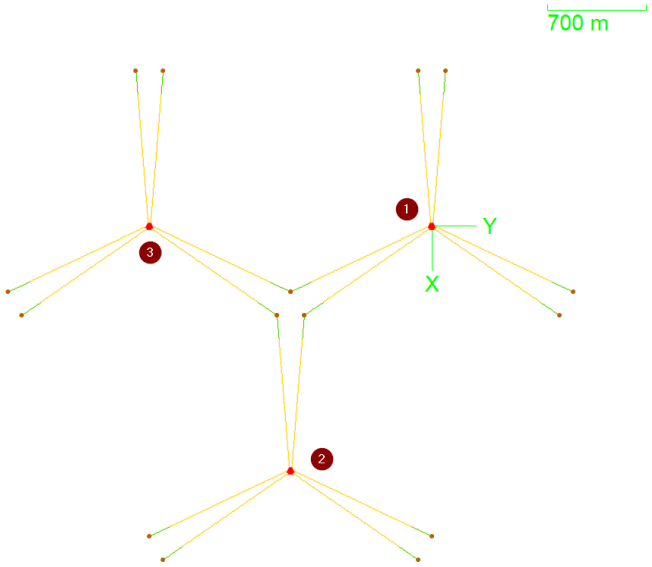

Figure 43: 3 x 2 Leg Mooring Configuration (Numbered Turbines in Red, Anchors in Brown)

7.3 Analysis Tools and Methodology

7.3.1 Software

OrcaFlex is a commonly used marine dynamics program developed by Orcina for static as well as both frequency domain and time domain dynamic analysis of a wide range of offshore systems, including all types of marine flexibles, global analysis, moorings, installation and towed systems. The program takes as input the mechanical, structural and other properties of the various component parts of the system, and calculates the static equilibrium configuration of the system, and its response to dynamic loading. Outputs include system geometry, forces and moments throughout the system.

In cases whereby detailed analysis of mooring systems is required such as the dynamic and non-linear behaviour of chain/fibre rope mooring lines, analyses are usually completed in the time domain. This is because frequency domain analysis is conducted by the application of a series of linear mappings to stochastic environmental or loading processes, but neither the wave elevation loading or the loading response is linear. In OrcaFlex's case (frequency domain), mooring stiffnesses are linearised after statics

have been run by using the tangent stiffness gradient at the point of evaluation, potentially underestimating peak mooring tensions due to a lack of increase in restoring force.

7.3.2 Methodology

Assumptions All mooring designs for the Morro Bay site were assumed to be of taut design. Due to the water depth, a catenary system was likely to be impractical due to the significant hang-off weight through the mid water column. Semi-taut configurations were also not considered for this site because the mooring footprint to achieve a catenary in the lower chain section and still utilise shared anchors would result in a turbine spacing far larger than required.

The analysis conducted so far only provides simulation time histories. No peak over threshold analysis or multiple seed simulations have been used, so values given will represent simulation maxima and could change given a more detailed level analysis and post-processing of results.

Mooring Design The anchor footprint was developed based on a minimum turbine spacing of 7 times the turbine rotor diameter. Once preliminary anchor positions were set, the preliminary mooring design process used a (Severe Sea State) SSS and iterated through mooring line sizes and pretension values until the 52 m NSS excursion acceptance criteria (see D1.2 [23]) was met. This resulted in a conservative mooring design that met the excursion criteria in both the NSS and ESS cases, but the design could be further optimised to reduce costs. This was completed on a single floater with mooring.

To speed up the iterative design process without automation, wave seeds were studied and using OrcaFlex's wave preview function, the wave elevation was examined. The largest wave elevation out of these seed time histories was selected and a 400 second simulation including the largest elevation with 100 second build up period was used to reduce computational time in achieving a basis single mooring system for each configuration.

The single WTG mooring design was repeated to the multi floater configurations described. NSS and ESS environmental conditions as well as their associated turbine thrust and drag applied loads were used. A simulation time of 3 hours was used.

Seastate Directionality As previously described, the metocean conditions have been applied omnidirectionally at this study's current level, despite the strong directionality of the Morro Bay site. Within the scope of the loadcase multiple metocean direction combinations that are suggested in [12], direction combinations have been applied based on those suggested in [3].

Table 15: Metocean Directionality Matrix

Orientation wrt Mooring	Metocean Combination	Example Directions (From)		
		Wave (°)	Wind (°)	Current (°)
Inline	Collinear	0	0	0
	Oblique	0	30	30
	Perpendicular	0	30	90
Bisecting	Collinear	45	45	45
	Oblique	45	75	75
	Perpendicular	45	75	135

Inline refers to the wave direction being aligned with one of the mooring lines, which usually results in the highest mooring line tensions and anchor loads. Bisecting describes the wave direction being half-way between mooring line azimuths, usually resulting in the largest floater excursions from TMC. Applying these metocean direction combinations, although not suitable for full detailed design, is useful during preliminary stages of a project because it significantly reduces the number of loadcases in an analysis that is already very computationally intensive.

Anchor Load Considerations The mooring lines of the DDFs are attached to the pile in a rather constant angle between XX and YY degrees. The loads can therefore be split up into a lateral and vertical load components with respect to the pile's main axis. According to the mooring design, vertical load components seen in taut and semi taut moorings result in permanent tensile pile loads with some cyclic load components. In case of a shared anchor, the tensile loads of the single anchors could sum up to an uplift load on the pile when at opposing azimuths.

The horizontal load components mainly introduce lateral one-way cyclic loads into the pile. In case of shared anchors, these load components have different directions in the X-Y plane that have the potential to reduce the lateral load component compared to a single line anchor which is beneficial for pile design. On the other hand, a changing main lateral loading direction may have more severe effects on the lateral pile bearing capacity. While the loads in the main direction are predominantly one-way cyclic loads, they may be of two-way nature in the secondary direction.

The load pattern may change significantly in case one of the mooring lines fails or during installation. This shall be considered as an ALS and temporary load case, respectively.

7.4 Results for 4 Leg Mooring

The directional combination of wind, waves and current were applied as per the directionality matrix. Maximum Line tensions and maximum floater excursions are shown in Table 16 with the conditions applied below.

Table 16: Comparison of Maximum Line Tensions and WTG Excursions to Loadcase Conditions - 4 Leg Mooring

	Wave			Wind		Current		Applied Loads				Results	
	Hs [m]	Tp [m]	Dir. [°]	Speed [m/s]	Dir. [°]	Speed [m/s]	Dir. [°]	Turbine Thrust [kN]	Nacelle Drag [kN]	Tower Drag [kN]	Dir. [°]	Max Line Tension [kN]	Max. WTG Excursion [m]
NSS	6.00	12.00	0.00	6.20	0.00	0.75	0.00	2450.00	11.00	44.00	0.00	7773.22	30.96
					30.00		30.00				30.00	7702.86	31.16
							90.00					7276.38	28.21
			45.00		45.00		45.00				45.00	7639.11	30.93
					75.00		75.00				75.00	7401.51	30.96
							135.00					6901.42	27.93
	6.00	16.00	0.00	6.20	0.00	0.75	0.00	2450.00	11.00	44.00	0.00	7754.48	31.85
					30.00		30.00				30.00	7691.75	31.61
							90.00					7298.45	28.80
			45.00		45.00		45.00				45.00	7619.50	31.78
					75.00		75.00				75.00	7392.24	31.36
							135.00					6941.97	28.49
ESS	9.90	16.00	0.00	26.84	0.00	1.50	0.00	1200.00	130.00	550.00	0.00	9419.00	45.13
					30.00		30.00				30.00	9159.09	43.87
							90.00					7493.48	35.47
			45.00		45.00		45.00				45.00	8816.28	44.79
					75.00		75.00				75.00	7902.75	43.73
							135.00					7210.49	35.07
	9.90	18.00	0.00	26.84	0.00	1.50	0.00	1200.00	130.00	550.00	0.00	9392.28	43.52
					30.00		30.00				30.00	9138.41	42.69
							90.00					7533.86	35.20
			45.00		45.00		45.00				45.00	8750.80	43.15
					75.00		75.00				75.00	7895.50	42.55
							135.00					7161.23	34.78

The largest mooring tensions can be seen in the inline cases, as highlighted by the cell shading. Contrary to expectation, the floater excursion is also highest in the inline cases, but only marginally. The ESS cases result in the higher mooring line tensions and floater excursions.

Table 17: Associated Maximum Global Anchor Loads (Yellow is Maximum) - 4 Leg Mooring

Mooring Line 3 - WTG1			Mooring Line 2 - WTG2			Mooring Line 1 - WTG3			Mooring Line 4 - WTG4		
End GX force [kN]	End GY force [kN]	End GZ force [kN]	End GX force [kN]	End GY force [kN]	End GZ force [kN]	End GX force [kN]	End GY force [kN]	End GZ force [kN]	End GX force [kN]	End GY force [kN]	End GZ force [kN]
5564.9	0.0	-1054.2	98.8	-4580.8	-2631.5	-4704.0	0.0	-2756.9	85.1	4769.5	-1648.1
5564.9	-200.5	-3202.6	72.8	-5720.8	-3308.6	-4884.3	-149.3	-2880.5	77.6	3809.2	-2188.8
3100.5	0.0	-1674.0	-119.5	-4659.7	-2683.0	-6296.8	0.0	-3704.4	-119.5	4659.7	-2683.0
2098.5	0.0	-1054.2	-284.1	-4699.0	-2708.7	-7536.0	0.0	-4426.2	-284.1	4699.0	-2708.7
5351.5	-199.9	-3065.5	98.8	-5945.2	-3455.4	-4977.6	-163.3	-2934.9	72.6	3566.1	-2029.0
2363.8	0.0	-1231.0	-277.5	-4580.8	-2631.6	-7627.9	0.0	-4493.4	-277.5	4580.8	-2631.6
2361.5	0.0	-1229.0	-277.6	-4581.1	-2631.5	-7627.8	0.0	-4493.6	-277.6	4581.1	-2631.5
5433.1	-196.8	-3121.2	63.9	-5536.5	-3176.6	-4704.0	-144.7	-2757.0	71.1	3681.5	-2107.2
3053.4	0.0	-1645.6	-120.9	-4648.4	-2676.0	-6266.3	0.0	-3677.8	-120.9	4648.4	-2675.0
5432.1	-196.7	-3120.5	64.0	-5537.2	-3176.8	-4704.3	-144.8	-2756.9	71.1	3681.0	-2106.9
5367.9	-202.4	-3081.7	66.5	-5729.5	-3307.6	-4889.8	-144.3	-2889.8	85.1	3633.1	-2074.2
2474.7	0.0	-1298.1	-288.5	-4769.5	-2753.7	-7327.3	0.0	-4291.2	-288.5	4769.5	-2753.7
3828.2	-238.4	-2166.9	-145.2	-6231.9	-3622.5	-6427.5	-240.7	-3776.4	-97.6	2976.3	-1648.1

For preliminary anchor sizing, supplying all of the simulation maxima and minima for each line, in each axis is simple and quick to extract using either OrcaFlex or from the load time histories. However, using all of the maximum loads simultaneously is likely to result in an overly conservative anchor design. The Tables 17 and 18 immediately above and below show the minima and maxima for each line and each axis, highlighted in yellow, but also display the loads on the other axes and lines that occur

at the same instance as the maxima or minima in yellow. Each row of loads would represent a loadcase for the pile design. The minima are shown here as well because the loads are given with reference to the OrcaFlex model's global axes, hence some of the largest loads are shown as negative. It is important to keep the direction of these loads so that the resultant load vectors on the mooring pile can be calculated accurately.

Table 18: Associated Minimum Global Anchor Loads (Yellow is Minimum) - 4 Leg Mooring

Mooring Line 3 - WTG1			Mooring Line 2 - WTG2			Mooring Line 1 - WTG3			Mooring Line 4 - WTG4		
End GX force [kN]	End GY force [kN]	End GZ force [kN]	End GX force [kN]	End GY force [kN]	End GZ force [kN]	End GX force [kN]	End GY force [kN]	End GZ force [kN]	End GX force [kN]	End GY force [kN]	End GZ force [kN]
2095.6	-250.1	-3202.6	-294.1	-6489.9	-3776.2	-7882.1	-275.8	-4652.2	-294.1	2976.3	-2753.8
2095.6	0.0	-1056.5	-284.1	-4697.8	-2707.7	-7512.9	0.0	-4410.8	-284.1	4697.8	-2707.7
4207.4	-250.1	-2419.8	-124.7	-6190.1	-3591.4	-6354.7	-243.3	-3734.1	-87.0	3442.7	-1959.3
5564.9	-200.5	-3202.6	72.8	-5720.8	-3308.6	-4884.3	-149.3	-2880.5	77.6	3809.2	-2188.8
2451.8	0.0	-1281.5	-294.1	-4705.2	-2711.4	-7423.5	0.0	-4351.4	-294.1	4705.2	-2711.4
3978.8	-239.3	-2265.3	-150.1	-6489.9	-3776.1	-6537.2	-265.1	-3848.0	-90.3	3198.8	-1789.3
3978.2	-239.3	-2265.0	-150.8	-6489.8	-3776.2	-6535.6	-265.2	-3846.5	-90.5	3198.6	-1789.1
2482.9	0.0	-1316.1	-284.1	-4705.5	-2713.0	-7882.1	0.0	-4652.0	-284.1	4705.5	-2713.0
3953.3	-236.2	-2248.8	-133.4	-6438.6	-3742.7	-6464.6	-275.8	-3803.2	-90.0	3200.9	-1788.8
2479.5	0.0	-1314.1	-284.1	-4705.5	-2713.0	-7881.8	0.0	-4652.2	-284.1	4705.5	-2713.0
0.0	-1281.5	-294.1	-4705.2	-2711.4	-7423.5	0.0	-4351.4	-294.1	-294.1	4705.2	-2711.4
3828.2	-238.4	-2166.9	-145.2	-6231.9	-3622.5	-6427.5	-240.7	-3776.4	-97.6	2976.3	-1648.1
2478.1	0.0	-1300.7	-288.4	-4769.2	-2753.8	-7327.5	0.0	-4291.0	-288.4	4769.2	-2753.8

The directionality of these global anchor loads is also shown within the Figure 44 below. X, Y and Z axis contributions from all four mooring lines are visible with some being negative due to their incidence angle to the anchor.

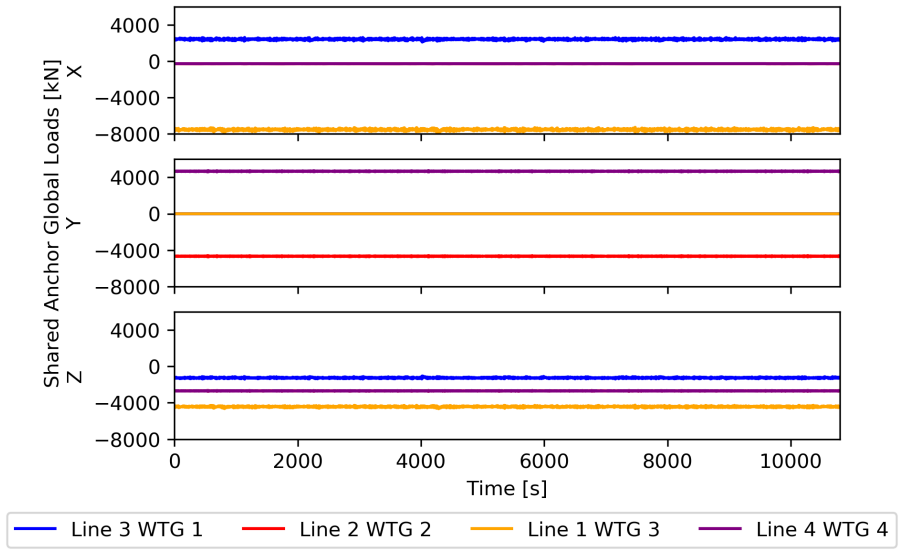

Figure 44: Global Anchor Loads Time History - 4 Leg Mooring

At the above scale where all sets of loads can be viewed simultaneously, the variation in each anchor load can be difficult to appreciate. The Figure 45 below displays the axial mooring tension time histories for the tension critical loadcase. These axial

loads are all positive due to being in tension rather than compression. This highlights some of the load variations with time history, but it is apparent that there are no significant outliers. Line 2's time history in red is similar to Line 4's in purple as they are both orientated normal to the net environmental load. Line 1 is to windward, giving the highest loads while Line 3 in blue is to leeward and exhibits the lowest loads.

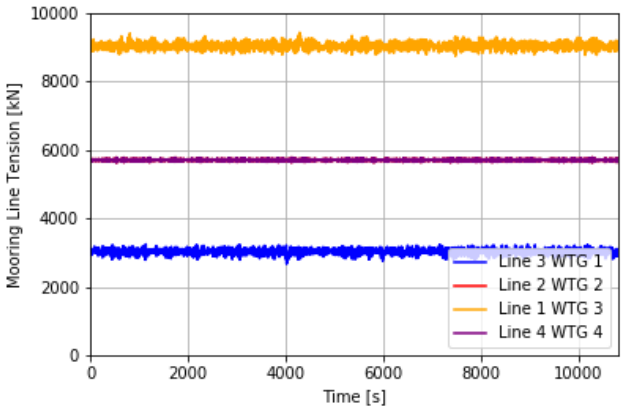

Figure 45: Maximum Mooring Line Tension Time History - 4 Leg Mooring

The Figure 46 below displays the time history of the floater excursion for the excursion critical loadcase. It is clear to see that the largest excursion from TMC is an isolated peak but it does align with the trough seen in the Line 3 mooring line tension. The floater excursions are within the acceptance criteria.

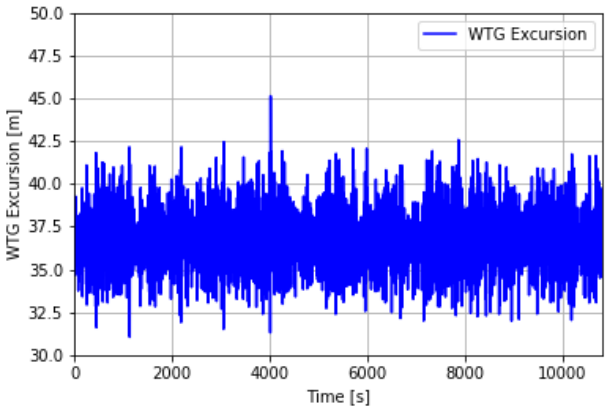

Figure 46: Maximum Turbine Excursion Time History - 4 Leg Mooring

7.5 Results for 3 Leg Mooring

The directional combination of wind, waves and current were applied as per the directionality matrix. Maximum line tensions and maximum floater excursions are shown

with the conditions applied below in Table 19. The ESS cases are clearly shown to be the most critical.

Table 19: Comparison of Maximum Line Tensions and WTG Excursions to Loadcase Conditions - 3 Leg Mooring

	Wave			Wind		Current		Applied Loads				Results	
	Hs [m]	Tp [m]	Dir. [°]	Speed [m/s]	Dir. [°]	Speed [m/s]	Dir. [°]	Turbine Thrust [kN]	Nacelle Drag [kN]	Tower Drag [kN]	Dir. [°]	Max Line Tension [kN]	Max. WTG Excursion [m]
NSS	6.00	12.00	0.00	6.20	0.00	0.75	0.00	2450.00	11.00	44.00	0.00	9110.52	34.85
					30.00		30.00				30.00	9029.49	35.41
							90.00					8508.09	32.41
			60.00		60.00		60.00				60.00	8824.25	35.50
					90.00		90.00				90.00	8500.40	35.53
							150.00					7946.81	31.98
	6.00	16.00	0.00	6.20	0.00	0.75	0.00	2450.00	11.00	44.00	0.00	9089.56	35.78
					30.00		30.00				30.00	9017.68	35.95
							90.00					8529.95	32.94
			60.00		60.00		60.00				60.00	8778.21	36.40
					90.00		90.00				90.00	8466.67	36.01
							150.00					7967.18	32.54
ESS	9.90	16.00	0.00	26.84	0.00	1.50	0.00	1200.00	130.00	550.00	0.00	11028.84	50.52
					30.00		30.00				30.00	10723.08	49.78
							90.00					8791.67	40.52
			60.00		60.00		60.00				60.00	9951.75	51.43
					90.00		90.00				90.00	8753.44	49.85
							150.00					7951.71	39.79
	9.90	18.00	0.00	26.84	0.00	1.50	0.00	1200.00	130.00	550.00	0.00	11022.20	48.83
					30.00		30.00				30.00	10710.44	48.26
							90.00					8808.37	40.18
			60.00		60.00		60.00				60.00	9816.19	49.76
					90.00		90.00				90.00	8645.99	48.32
							150.00					7768.82	39.50

The largest mooring tensions can be seen in the inline cases, as highlighted by the cell shading. As expected, the floater excursion is also highest in the bisecting cases.

Table 20: Associated Maximum Global Anchor Loads (Yellow is Maximum) - 3 Leg Mooring

Mooring Line 3 - WTG1			Mooring Line 2 - WTG2			Mooring Line 1 - WTG3		
End GX force [kN]	End GY force [kN]	End GZ force [kN]	End GX force [kN]	End GY force [kN]	End GZ force [kN]	End GX force [kN]	End GY force [kN]	End GZ force [kN]
2713.5	4161.5	-790.0	3548.0	-3503.4	-1612.0	-5455.4	0.0	-2437.6
2713.5	4127.5	-2103.1	3279.9	-5626.8	-2842.1	-5594.4	-120.2	-2509.2
2278.6	4161.5	-2014.7	2245.0	-4093.6	-1978.0	-7840.7	0.0	-3575.7
1169.4	2025.5	-790.0	2781.6	-5434.4	-2670.5	-8493.5	-279.3	-3876.3
2501.5	3803.0	-1916.4	3548.0	-6088.1	-3116.0	-5712.1	-112.7	-2572.5
1926.7	3816.1	-1799.4	1748.1	-3503.4	-1612.2	-9699.8	0.0	-4466.4
1927.7	3818.1	-1800.7	1748.2	-3503.8	-1612.0	-9688.6	0.0	-4460.9
2624.6	3990.0	-2016.5	3321.0	-5692.0	-2893.2	-5455.4	-127.5	-2438.7
2265.0	4134.8	-1998.9	2244.9	-4099.9	-1979.0	-7758.1	0.0	-3521.0
2558.9	3892.9	-1961.8	3331.1	-5720.8	-2908.0	-5464.0	-115.5	-2437.6

The Tables 20 and 21 immediately above and below show the minima and maxima for each line and each axis, highlighted in yellow, but also display the loads on the other axes and lines that occur at the same instance as the maxima or minima in yellow. Each row of loads would represent a loadcase for the pile design. The minima are

shown here as well because the loads are given with reference to the OrcaFlex model's global axes, hence some of the largest loads are shown as negative.

Table 21: Associated Minimum Global Anchor Loads (Yellow is Minimum) - 3 Leg Mooring

Mooring Line 3 - WTG1			Mooring Line 2 - WTG2			Mooring Line 1 - WTG3		
End GX force [kN]	End GY force [kN]	End GZ force [kN]	End GX force [kN]	End GY force [kN]	End GZ force [kN]	End GX force [kN]	End GY force [kN]	End GZ force [kN]
1165.7	2019.1	-2103.7	1748.1	-6303.8	-3170.7	-9752.7	-341.8	-4493.9
1165.7	2019.1	-793.5	2820.1	-5509.7	-2715.7	-8504.3	-279.3	-3883.0
1165.7	2019.1	-793.5	2820.1	-5509.7	-2715.7	-8504.3	-279.3	-3883.0
2713.1	4127.2	-2103.7	3285.9	-5638.4	-2848.6	-5588.0	-119.7	-2506.1
1926.7	3816.1	-1799.4	1748.1	-3503.4	-1612.2	-9699.8	0.0	-4466.4
1518.6	2437.7	-1086.0	3362.6	-6303.8	-3170.7	-7377.1	-310.3	-3350.1
1518.6	2437.7	-1086.0	3362.6	-6303.8	-3170.7	-7377.1	-310.3	-3350.1
1888.4	3740.4	-1756.1	1761.2	-3524.9	-1628.6	-9752.7	0.0	-4493.7
1651.2	2660.9	-1207.3	3157.3	-5880.1	-2938.0	-7545.0	-341.8	-3432.1
1888.7	3741.0	-1756.5	1759.8	-3522.3	-1626.9	-9752.4	0.0	-4493.9

The directionality of these global anchor loads is also shown within the Figure 47 below. X, Y and Z axis contributions from all four mooring lines are visible with some being negative due to their incidence angle to the anchor.

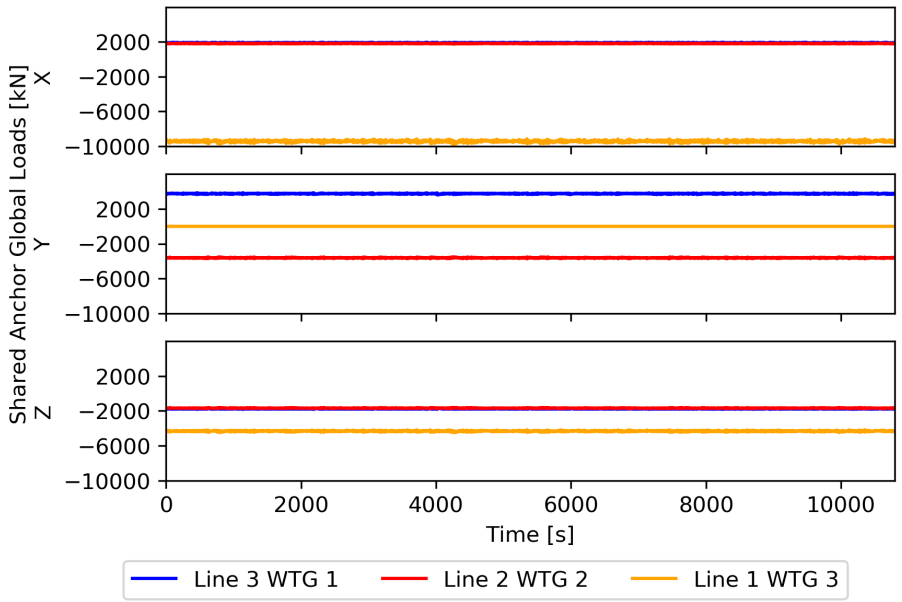

Figure 47: Global Anchor Loads Time History - 3 Leg Mooring

The Figure 48 below displays the axial mooring tension time histories for the tension critical loadcase. These axial loads are all positive due to being in tension rather than compression. This highlights some of the load variation with time history, but it

is apparent that there are no significant outliers. Line 2's time history in red is similar to Line 3's in blue as they are both orientated at similar angles to the net environmental load. Line 1 is to windward, giving the highest loads.

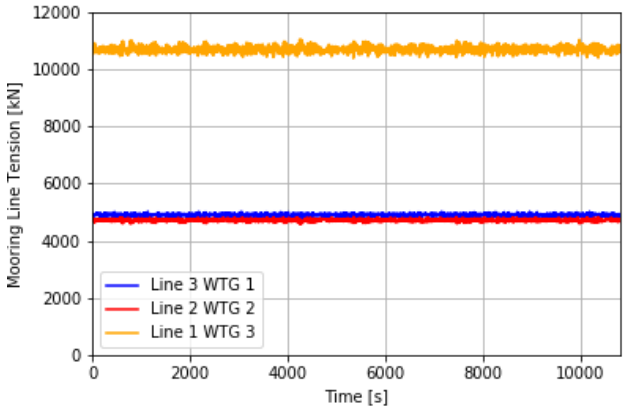

Figure 48: Maximum Mooring Line Tension Time History - 3 Leg Mooring

The Figure 49 below displays the time history of the floater excursion for the excursion critical loadcase. It is clear to see that the largest excursion from TMC is an isolated peak at approximately 4000 seconds. The floater excursions are within the acceptance criteria.

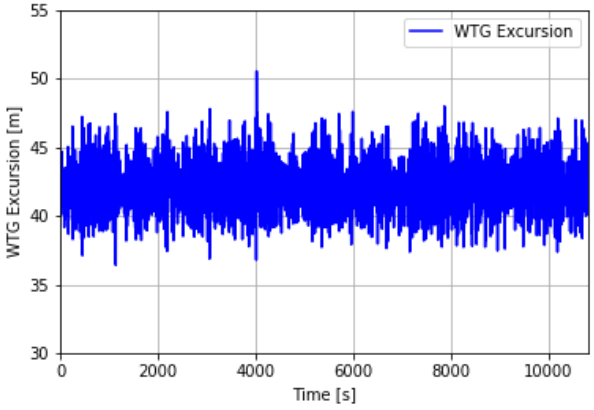

Figure 49: Maximum Turbine Excursion Time History - 3 Leg Mooring

7.6 Results for 3 by 2 Leg Mooring

The largest mooring tensions can be seen in the inline cases, as highlighted by the cell shading in Table 22. Similar to the 3 x 1 mooring, the floater excursion is also highest in the bisecting cases.

Table 22: Comparison of Maximum Line Tensions and WTG Excursions to Loadcase Conditions - 3 x 2 Leg Mooring

	Wave			Wind		Current		Applied Loads				Results	
	Hs [m]	Tp [m]	Dir. [°]	Speed [m/s]	Dir. [°]	Speed [m/s]	Dir. [°]	Turbine Thrust [kN]	Nacelle Drag [kN]	Tower Drag [kN]	Dir. [°]	Max Line Tension [kN]	Max. WTG Excursion [m]
NSS	6.00	12.00	0.00	6.20	0.00	0.75	0.00	2450.00	11.00	44.00	0.00	5341.03	29.59
					30.00		30.00				30.00	5079.93	29.56
					60.00		90.00				60.00	4779.97	26.71
			60.00		90.00		60.00				90.00	4903.38	29.89
							90.00					4807.64	29.51
							150.00					4755.17	26.62
	6.00	16.00	0.00	6.20	0.00	0.75	0.00	2450.00	11.00	44.00	0.00	5333.26	30.58
					30.00		30.00				30.00	5061.09	30.50
					60.00		90.00				60.00	4800.18	27.77
			60.00		90.00		60.00				90.00	4900.89	30.78
							90.00					4793.74	30.42
							150.00					4750.47	27.74
ESS	9.90	16.00	0.00	26.84	0.00	1.50	0.00	1200.00	130.00	550.00	0.00	6231.98	43.07
					30.00		30.00				30.00	6109.34	42.48
					60.00		90.00				60.00	5516.87	35.11
			60.00		90.00		60.00				90.00	5597.41	44.11
							90.00					5605.11	42.46
							150.00					5446.36	34.26
	9.90	18.00	0.00	26.84	0.00	1.50	0.00	1200.00	130.00	550.00	0.00	6268.93	41.54
					30.00		30.00				30.00	6153.82	41.31
					60.00		90.00				60.00	5550.94	34.61
			60.00		90.00		60.00				90.00	5567.92	42.50
							90.00					5623.84	41.26
							150.00					5469.25	33.74

Simultaneous loads are not provided for the 3 x 2 configuration at this stage, however the Figure 50 below displays the axial mooring tension time histories for the tension critical loadcase. These axial loads are all positive due to being in tension rather than compression. This highlights some of the load variations with time history. All of the 6 lines exhibit larger tension fluctuation at approximately 600 seconds.

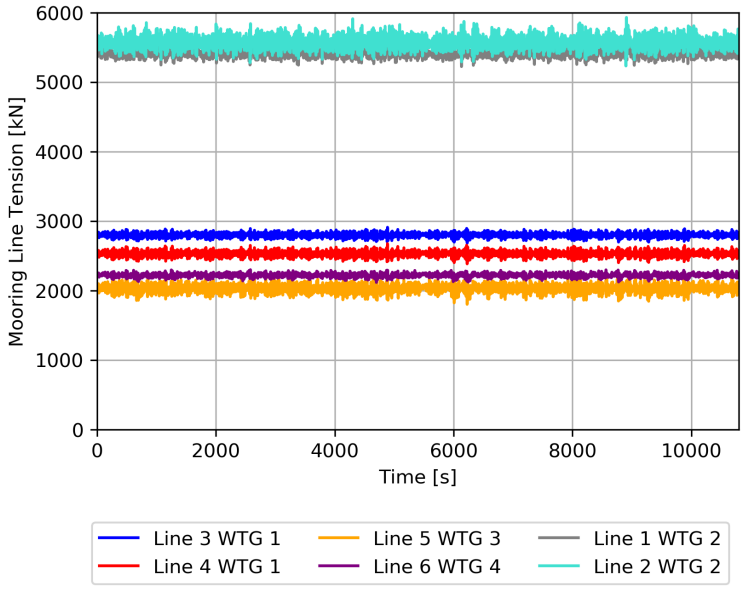

Figure 50: Maximum Mooring Line Tension Time History - 3 x 2 Leg Mooring

The Figure 51 below displays the time history of the floater excursion for the excursion critical loadcase. The largest excursion does align with the tension fluctuation at around 6000 seconds. The floater excursions are within the acceptance criteria.

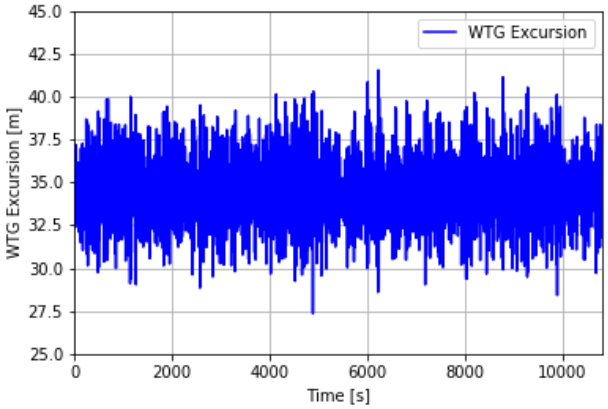

Figure 51: Maximum Turbine Excursion Time History - 3 x 2 Leg Mooring

7.7 Conclusion from shared anchor load assesement

7.7.1 Turbine Spacing

A minimum spacing of 7D has been assumed in this study focusing on the Morro Bay site. This study has used symmetrical, taut mooring design configurations to achieve a turbine spacing this compact in a water depth of 870 m. As such, it is thought that

semi-taut mooring configurations would not be able to accommodate shared anchor points at this turbine spacing and water depth.

Turbine spacing coupled with a lack of mooring redundancy in 3 line configurations could result in mooring line failure causing collision with adjacent turbines. This would likely make the mooring design consequence class 2, requiring larger factors of safety and thus larger sized mooring lines, potentially removing much of the cost advantage of shared anchors.

7.7.2 Anchor Load Generation

Mooring analysis has been used to generate preliminary anchor loads taking into account the multiple lines potentially attached to the anchor pile. Multiple floater analysis is required to achieve this so as to account for phase differences in mooring response as wave trains pass through the mooring site. Time domain analysis is required for anchor load generation, accounting for the system's non-linearities once design is past frequency domain initial concept stage. Time domain analysis is computationally intensive and this only increases when analysing multiple floating bodies and their mooring systems. With the aim of reducing the work and time required during initial design stages, a simplified method of generating anchor loads using a reduced number of loadcases and without resorting to over-conservative simultaneous maximums has been demonstrated in this study. Associated loads have been produced from the mooring line time histories in terms of the global axes to ensure load directionalities are fully accounted for.

7.7.3 Areas for Optimisation

Despite the reduction in loadcases and simplification of the process in the time domain, a brute force approach to running the OrcaFlex simulations was used, utilising cloud computing with the ability to run many simulations simultaneously. Looking at the results of the analyses completed within this study, many of the critical cases for each configuration become obvious. However, in the case of the 4 leg mooring one the the cases expected to be critical to the floater excursion wasn't, so assumptions shouldn't be made on critical cases before some sort of screening analyses have been completed. To reduce the time it takes to complete such a screen analysis, the use of equivalent regular wave transformation and regular wave analyses in OrcaFlex would be an approach to investigate further.

This study has focused on the generation of loads useful to shared anchor design, but being able to continue the geotechnical considerations past the qualitative and test a pile sizing and design methodology for shared anchor loads is a key further step, allowing the clearer comparison of anchor sizing for shared anchors and single line anchors. Coupled with this would be an investigation into the effects of mooring lines' inverse catenaries from padeye to mudline on a shared anchor pile.

8 Conclusion and Future Work

Two modelling approaches for shared mooring and shared anchors has been developed and demonstrated in the present deliverable. First, within HAWC2, a method for shared mooring lines that can connect to shared anchors has been established with application to three generic mooring examples. The method is directly applicable to dynamic cables as well. Next, an Engineering method in Orcaflex has been demonstrated on three solutions for shared anchors at the sea bed.

8.1 Dynamic analysis of shared mooring and anchor lines in HAWC2

The work shows that shared mooring line designs for floating wind turbine farms can be modelled in HAWC2. The equilibrium points, frequencies and corresponding mode shapes at the equilibrium points are computed by HAWC2 for shared mooring line designs. The design parameters are lengths of shared mooring lines and buoyancy force at the line intersections for Configuration-2. It is observed that the frequencies can be adjusted by tuning the mooring line lengths and buoyancy elements.

Configuration-1 has catenary type mooring lines which consist of heavy chains. This design requires very long shared chain to connect two turbines since the mid part of the chain section tends to touch the sea bed even for a short and tight mooring line design. For short mooring line design (Design-1 in Configuration-1), the mooring line forces are very large compared to the original single turbine design. Naturally, this design has a much higher first frequency compared to Design-2 which has a longer shared mooring line.

Configuration-2 has taut mooring lines in a very deep water (870 m depth). Additional to the HAWC2 calculated natural frequencies, a simple method was developed to estimate the frequencies of designs with taut mooring lines as an independent check. Its results are very accurate when compared to HAWC2 results for single turbine design.

Configuration-2 has more design parameters than the designs in Configuration-1 such as length of mooring lines and buoyancy forces. Designs with 2 turbines have $\sqrt{2}$ times lower first frequency than the single turbine design when the intersection point moves with the turbines in symmetric surge motion. This frequency can be increased by adjusting the mooring line lengths and buoyancy forces. On the other hand, these changes introduces coupling between surge and sway motion.

Configuration-3 is the most complex design in the report and can be considered as a first step of a turbine web design with shared mooring lines in a floating wind farm. The complexity is present in mode shapes but it can still be modeled in one HAWC2 simulation. Similar results to Configuration-2 was observed such as $\sqrt{2}$ times lower first frequency compared to single turbine design, however there are much more mode shape combinations for a certain direction such as surge-sway with symmetric and unsymmetric motion of turbines.

In all configurations, there are some frequencies at 1-P turbine revolution region. A decay test would be very useful to see the damping values for those mode shapes before load cases are run. Those frequencies are generally in yaw direction, however many of them are not the first yaw mode shape.

In the future, this work can be extended by load analysis by including the hydrodynamic and aerodynamic loads from waves and turbulent wind. Since the space dimensions are very large for a single turbulence box used in HAWC2, a proper method for parallel HAWC2 simulations for each turbine in a design needs to be developed first. There are two levels for parallel simulation of shared mooring line designs: the

first level is the flow coupling with a proper wake model and the second one is the structural coupling between mooring lines where forces and displacements needs to be exchanged between different turbine simulations. There would be another coupling level in terms of control algorithm where individual turbine controller can be coupled with a full system controller to overcome the instabilities of whole system and increase the power production.

8.2 Load assessment for shared anchors

As an example of dynamic load analysis, the study on shared anchor loads was carried out for a configuration of 4-leg mooring, 2-leg mooring and 3 x 2-leg mooring. Calculations were made for normal sea states and extreme sea states taking load directionality for current, wind and waves into account. The rotor loads were represented by constant forces, precomputed conditional to the actual sea states. The analysis was carried out in the time domain, to allow for nonlinear response in the mooring system, which will directly impact on the extreme anchor loads. Calculations of the type demonstrated provides background for determination of safety factors and risk analysis, where redundancy in the mooring system has a strong influence.

References

[1] Cardona A. "Superelements modelling in flexible multibody dynamics". In: *Mutibody System Dynamics* 4 (1999), pp. 245–266.

[2] K.H. Andersen. "Cyclic soil parameters for offshore foundation design". In: *Proc. Of the 3rd International Conference on Frontiers in Offshore Geotechnics (ISFOG)*. 2015.

[3] API. *Design and Analysis of Stationkeeping Systems for Floating Structures*. Tech. rep. API, 2005.

[4] Aurora. *Ocean surface current estimates updated every five days*. `https://earth.nullschool.net/about.html`. Sept. 2021.

[5] Tom Bailey. "An Investigation into the Design of a Disconnectable Turret Mooring for Very Shallow Waters". MA thesis. UK: University of Strathclyde, August 2015.

[6] Henrik Bredmose et al. *Definition of the 15 MW Reference Wind Turbine*. Tech. rep. D1.1. Corewind, 2020.

[7] Bridon. *Bridon Polyester Superline*. 2020.

[8] Florian Castillo. *WindCrete Optimized Mooring System: Chain configuration*. Tech. rep. D1.3. Corewind, 2020.

[9] Florian Castillo. *WindCrete Optimized Mooring System: Chain-Polyester configuration for Site C*. Tech. rep. D1.3. Corewind, 2020.

[10] Det Norske Veritas. *Environmental Conditions and Environmental Loads*. Tech. rep. Det Norske Veritas, 2019.

[11] Det Norske veritas. *Floating wind turbine structures*. Tech. rep. Det Norske Veritas, 2018.

[12] Det Norske veritas. *Loads and site conditions for wind turbines*. Tech. rep. Det Norske Veritas, 2016.

[13] Det Norske veritas. *Offshore soil mechanics and geotechnical engineering*. Tech. rep. Det Norske Veritas, 2019.

[14] Det Norske veritas. *Support structures for wind turbines*. Tech. rep. Det Norske Veritas, 2018.

[15] Guy Drori (from British Petroleum). *Underlying Causes of Mooring Lines Failures Across the Industry*. `https://mcedd.com/wp-content/uploads/2014/04/00_Guy-Drori-BP.pdf`. Mar. 2015.

[16] Matt Hall and Patrick Conolly. "Coupled Dynamics Modelling of a Floating Wind Farm with Shared Moorings". In: *Proc. of the ASME 2018 37th International Conference on Ocean, Offshore and Arctic Engineering*. OMAE2018. Madrid, Spain: ASME, 2018.

[17] Joint Industry Project Steering Committee. *Remote Operated Vehicle (ROV) inspection of long term mooring systems for floating offshore installations, Mooring Integrity Joint Industry Project Phase 2*. Tech. rep. Health and Safety Executive, 2017.

[18] Torben J. Larsen and Anders M. Hansen. *How 2 HAWC2, the user's manual*. Tech. rep. DTU Wind, 2020.

[19] CH Lee. *Wamit Theory Manual*. Tech. rep. 95-2. Massachusettes Institute of Technology Department of Ocean Engineering, 1995.

[20] Mohammad Youssef Mahfouz et al. *Public design and FAST models of the two 15MW floater-turbine concepts*. Tech. rep. D1.3. Corewind, 2020.

[21] Connolly P. and Hall M. "Comparison of pilot-scale floating offshore wind farms with shared moorings". In: *Ocean Engineering* 171 (2019), pp. 172–180. DOI: 10.1016/j.oceaneng.2018.08.040.

[22] Sam Strivens et al. *Floating Wind Joint Industry Project: Phase III Summary Report*. Tech. rep. The Carbon Trust, 2021.

[23] Fernando Vigara et al. *Design Basis*. Tech. rep. D1.2. Corewind, 2019.

A Configuration-1: Grand Canaria site

A.1 Single turbine

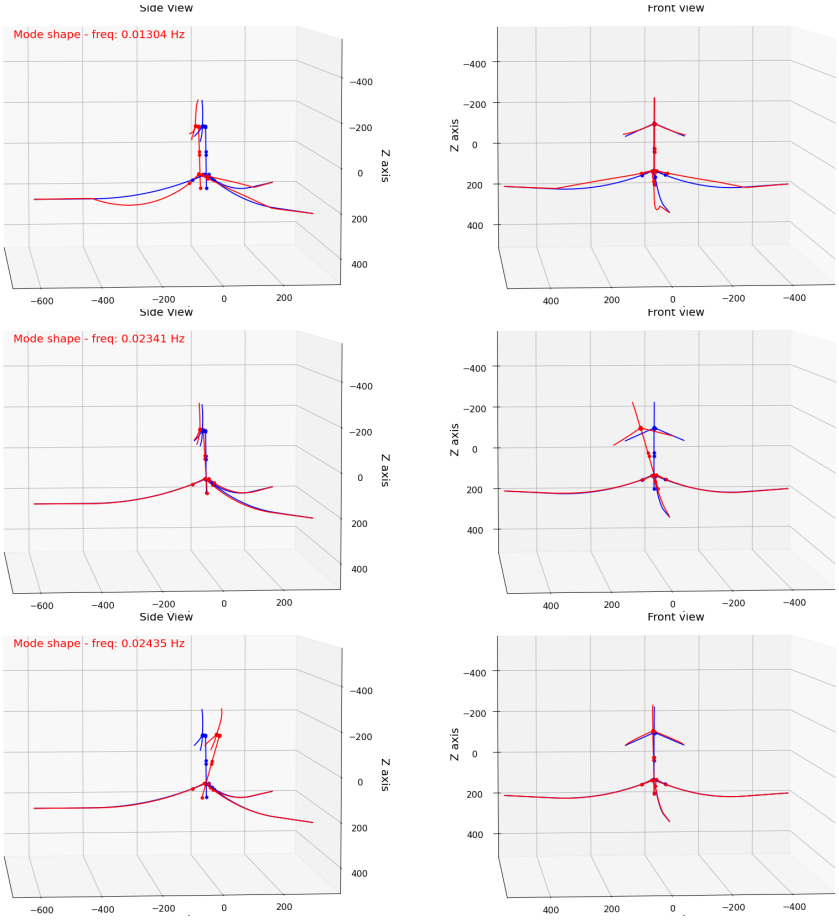

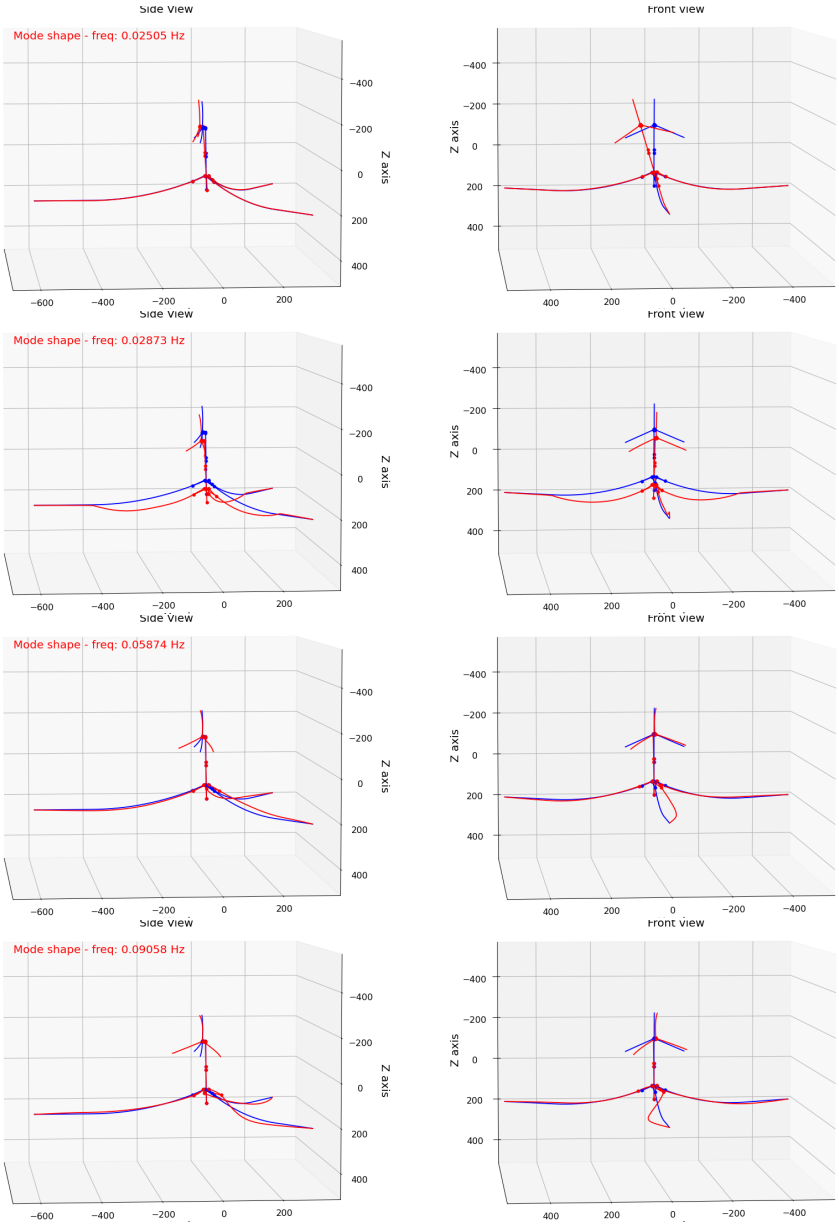
Side View
Mode shape - freq: 0.02505 Hz
Z axis
Front View
Z axis
Side View
Mode shape - freq: 0.02873 Hz
Z axis
Front View
Z axis
Side View
Mode shape - freq: 0.05874 Hz
Z axis
Front View
Z axis
Side View
Mode shape - freq: 0.09058 Hz
Z axis
Front View
Z axis

A.2 Design-1

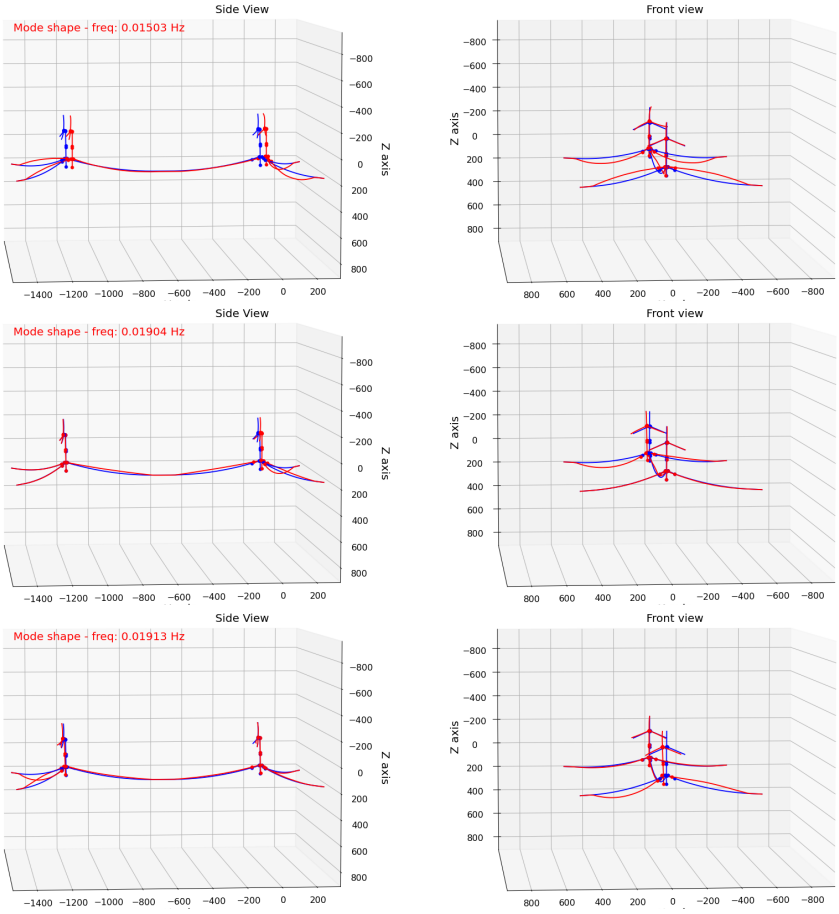
Side View
Mode shape - freq: 0.01503 Hz
Front view
Z axis
Side View
Mode shape - freq: 0.01904 Hz
Front view
Z axis
Side View
Mode shape - freq: 0.01913 Hz
Front view
Z axis

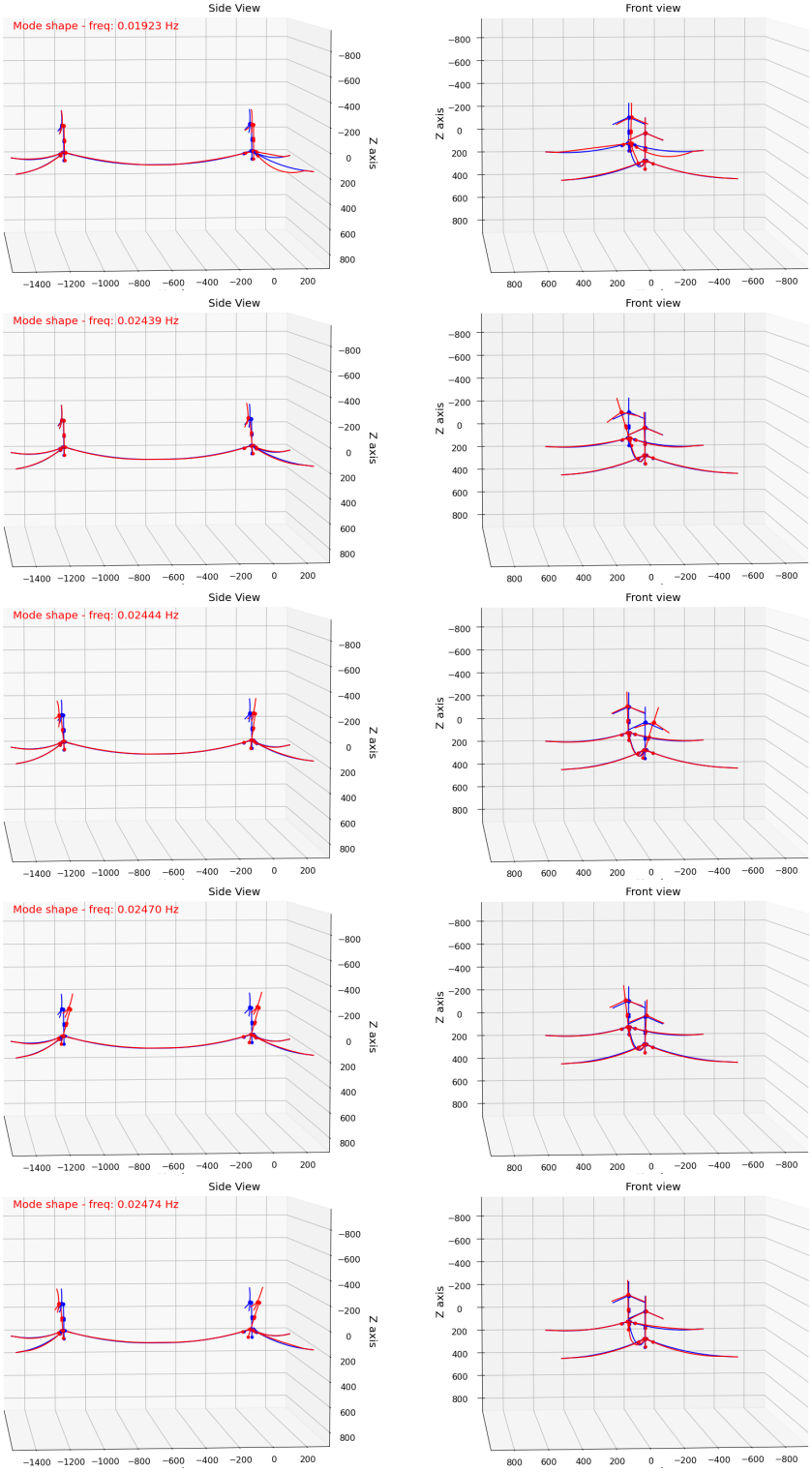
Side View
Mode shape - freq: 0.01923 Hz
Front view
Side View
Mode shape - freq: 0.02439 Hz
Front view
Side View
Mode shape - freq: 0.02444 Hz
Front view
Side View
Mode shape - freq: 0.02470 Hz
Front view
Side View
Mode shape - freq: 0.02474 Hz
Front view
Z axis

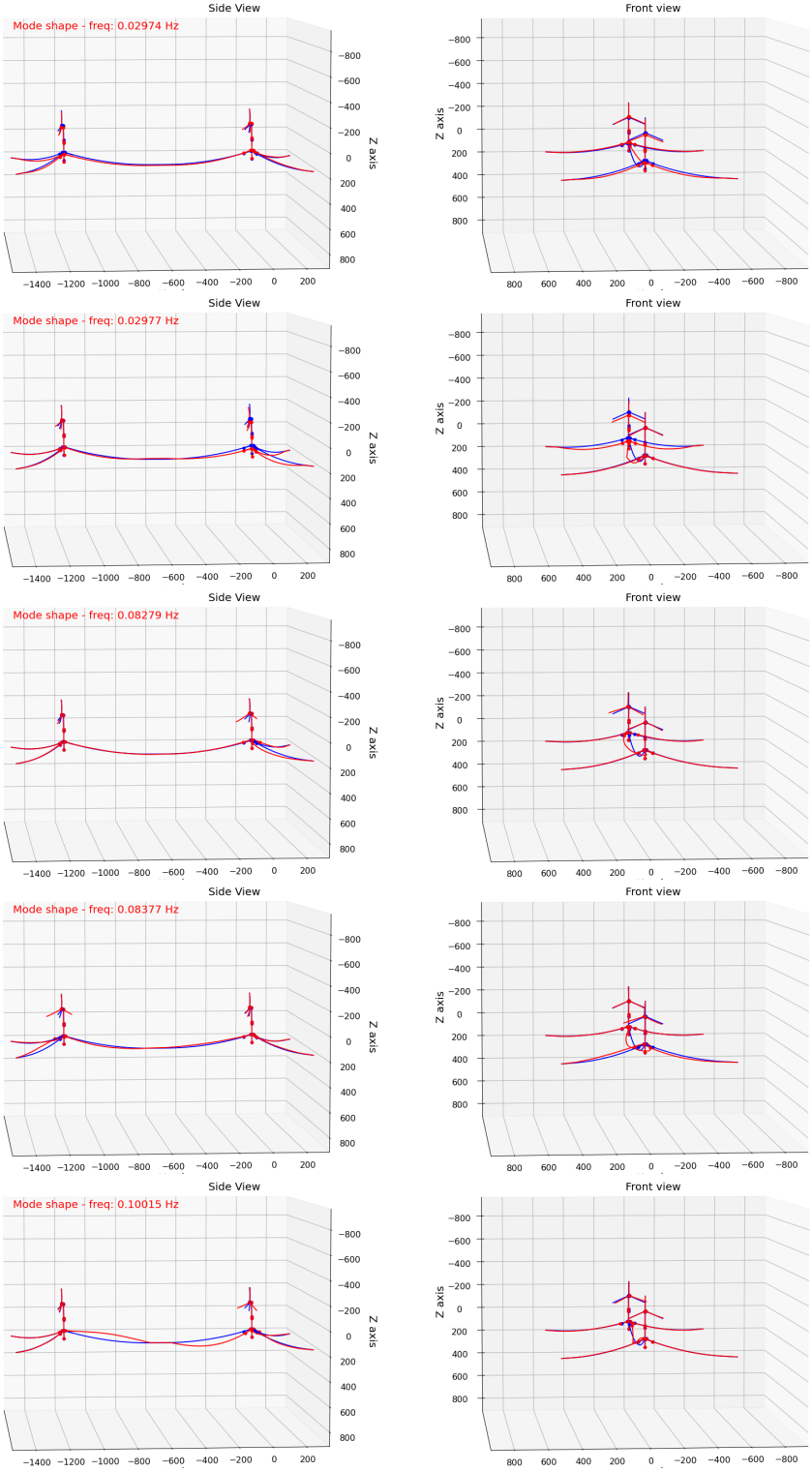
Side View
Mode shape - freq: 0.02974 Hz
Front view
Side View
Mode shape - freq: 0.02977 Hz
Front view
Side View
Mode shape - freq: 0.08279 Hz
Front view
Side View
Mode shape - freq: 0.08377 Hz
Front view
Side View
Mode shape - freq: 0.10015 Hz
Front view
Z axis

A.3 Design-2

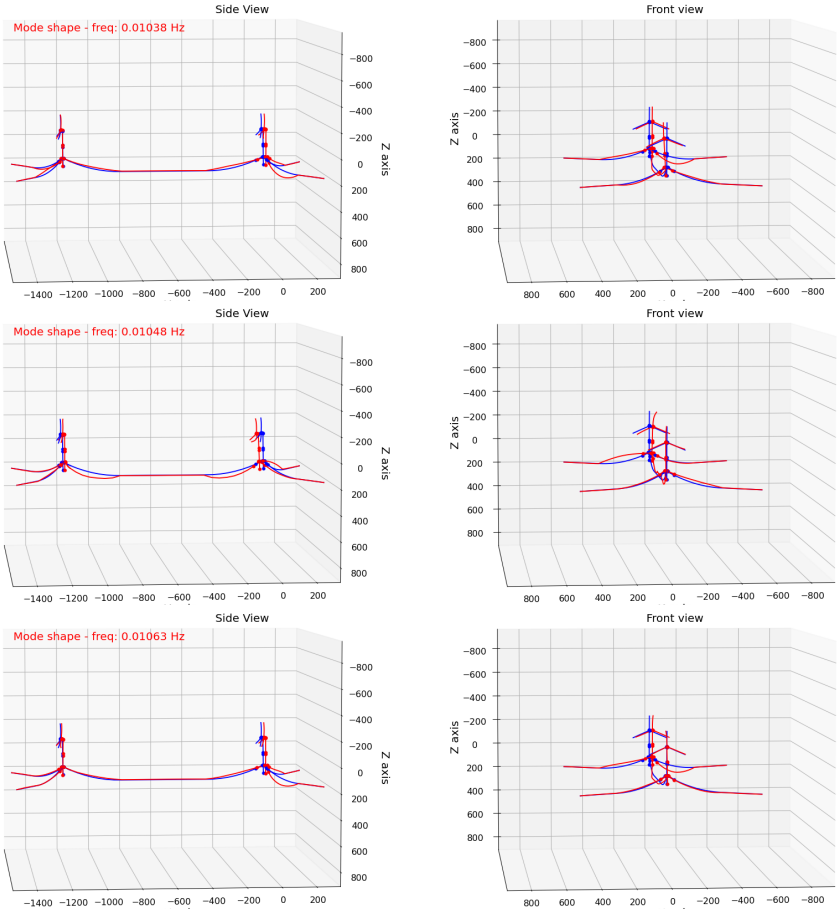
Side View
Mode shape - freq: 0.01038 Hz
Front view
Side View
Mode shape - freq: 0.01048 Hz
Front view
Side View
Mode shape - freq: 0.01063 Hz
Front view
Z axis

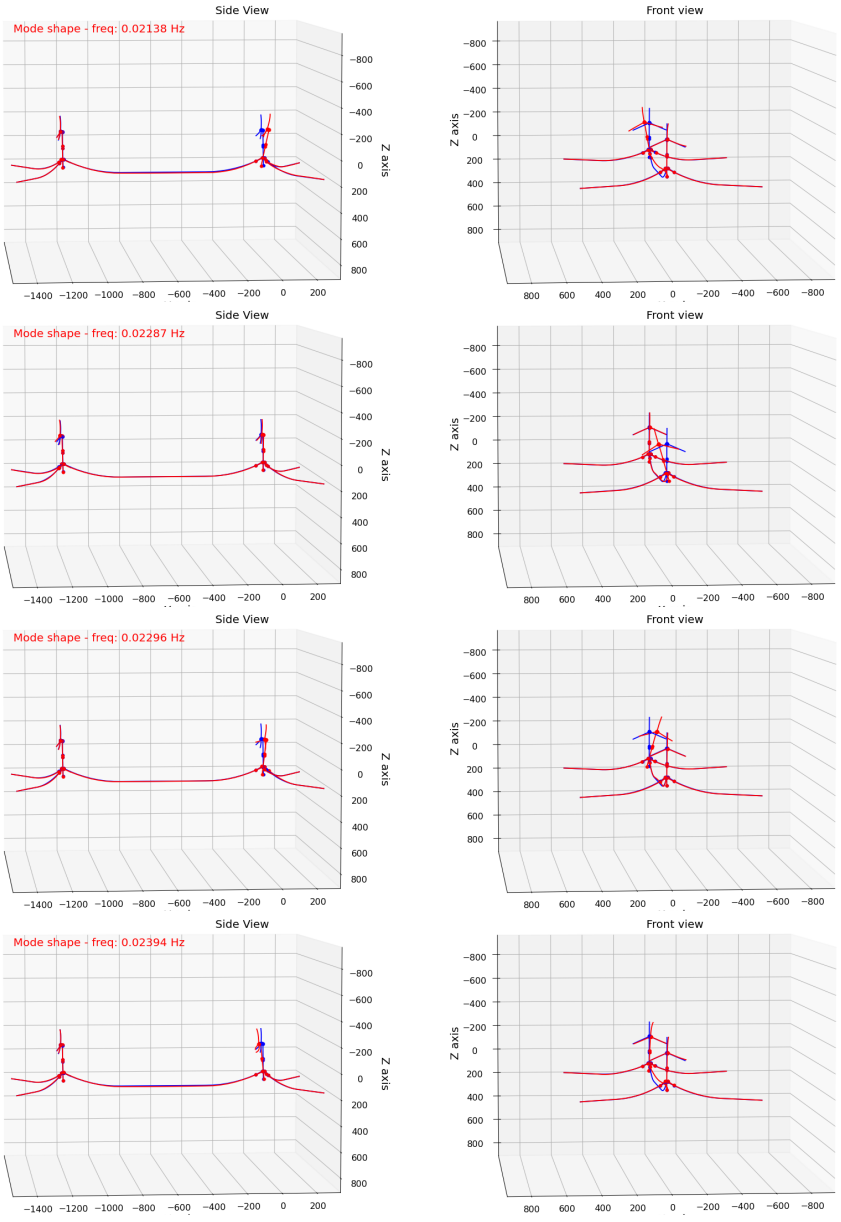
Side View
Mode shape - freq: 0.02138 Hz
Front view
Side View
Mode shape - freq: 0.02287 Hz
Front view
Side View
Mode shape - freq: 0.02296 Hz
Front view
Side View
Mode shape - freq: 0.02394 Hz
Front view
Z axis

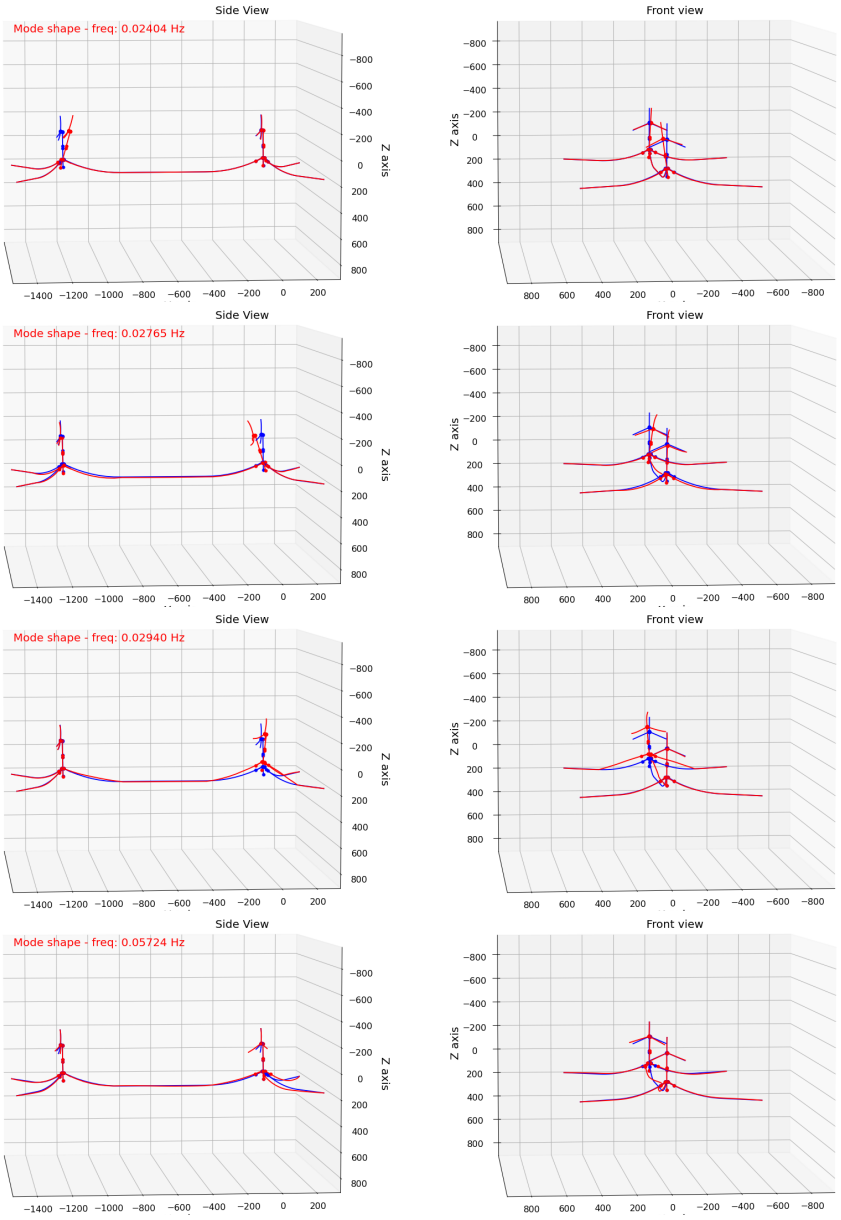
Side View
Mode shape - freq: 0.02404 Hz
Front view
Side View
Mode shape - freq: 0.02765 Hz
Front view
Side View
Mode shape - freq: 0.02940 Hz
Front view
Side View
Mode shape - freq: 0.05724 Hz
Front view
Z axis

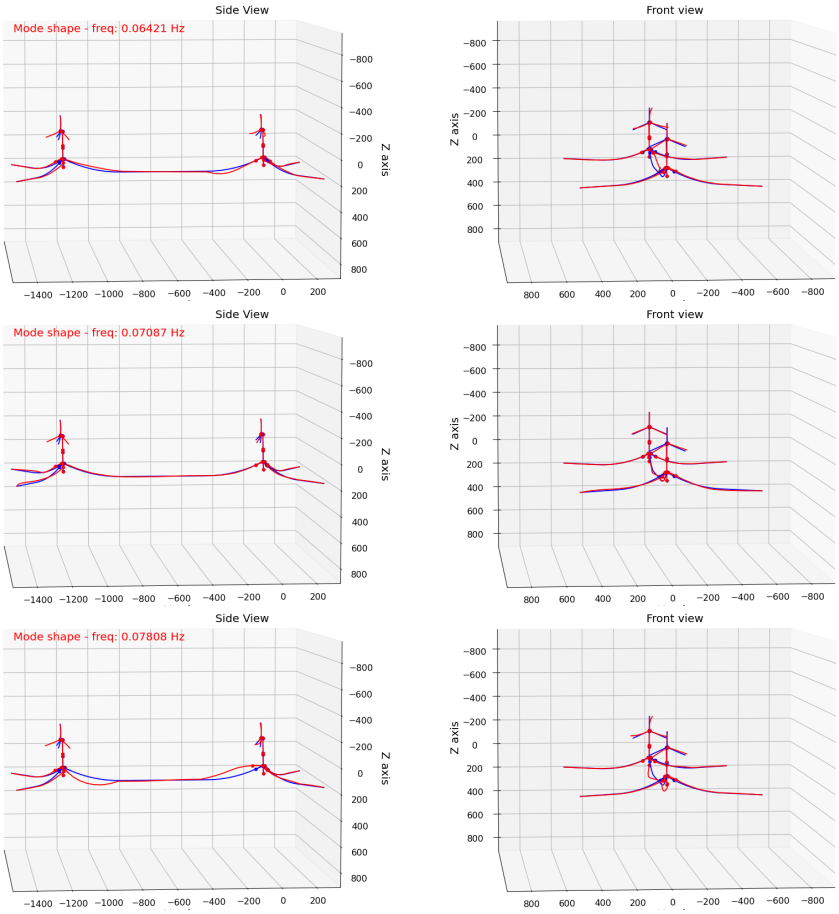
Side View
Mode shape - freq: 0.06421 Hz
Z axis
Front view
Z axis
Side View
Mode shape - freq: 0.07087 Hz
Z axis
Front view
Z axis
Side View
Mode shape - freq: 0.07808 Hz
Z axis
Front view
Z axis

B Configuration-2: Morro site

B.1 Single turbine

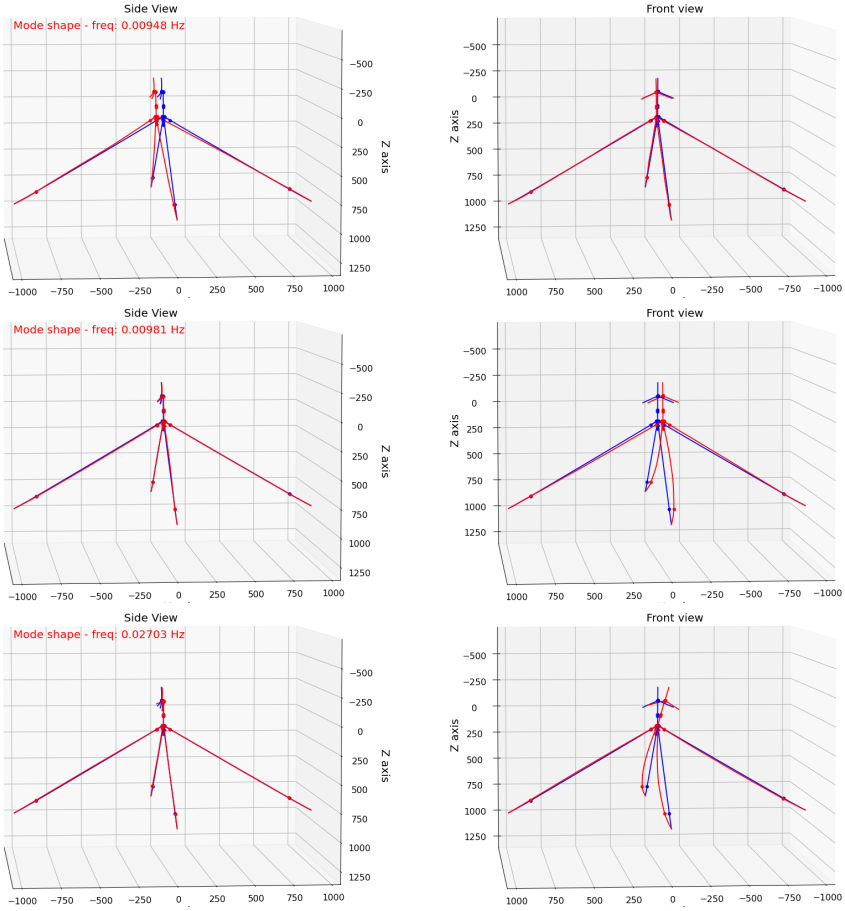

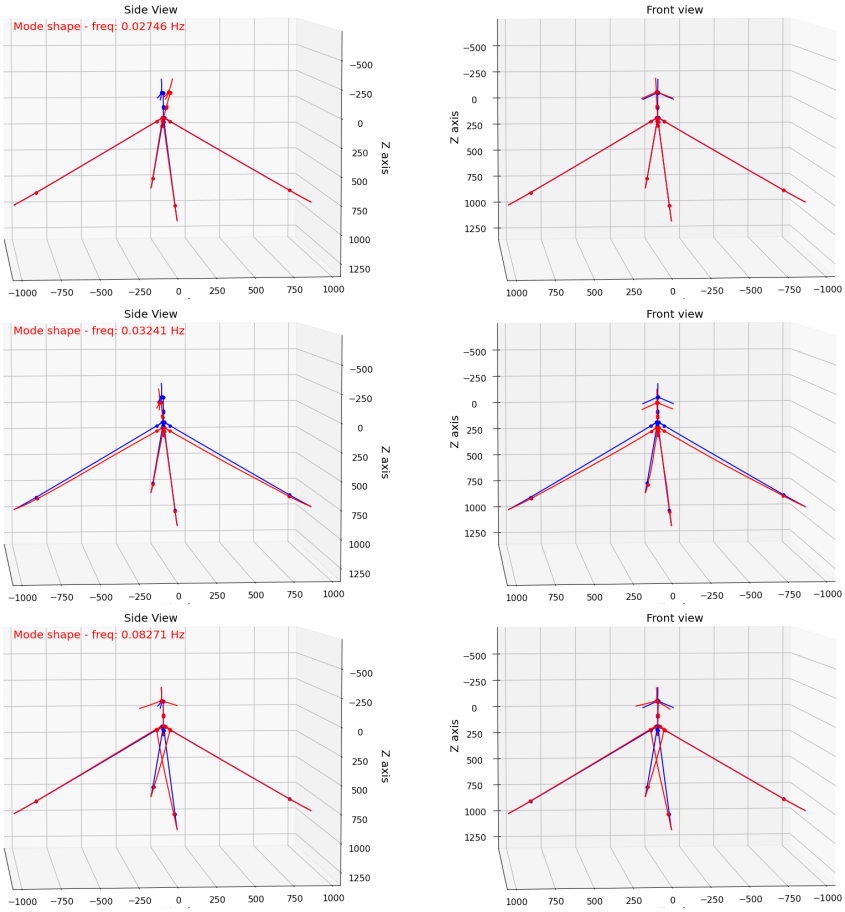
Side View
Mode shape - freq: 0.02746 Hz
Front view
Side View
Mode shape - freq: 0.03241 Hz
Front view
Side View
Mode shape - freq: 0.08271 Hz
Front view
Z axis

B.2 Design-1

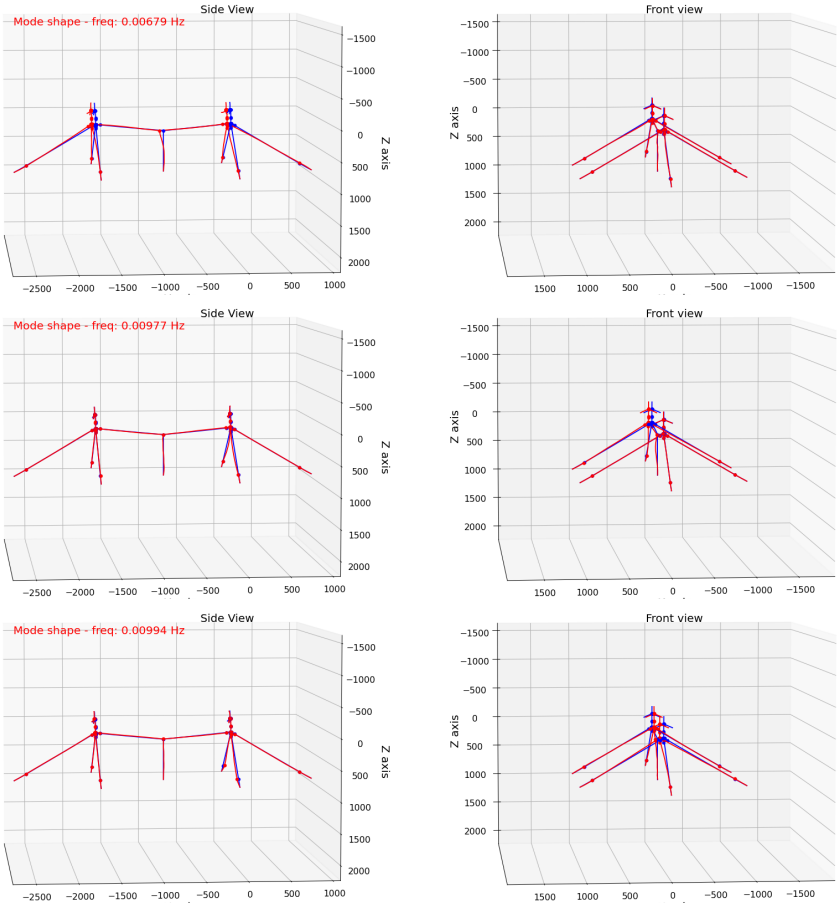
Side View
Mode shape - freq: 0.00679 Hz
Front view
Z axis
Side View
Mode shape - freq: 0.00977 Hz
Front view
Z axis
Side View
Mode shape - freq: 0.00994 Hz
Front view
Z axis

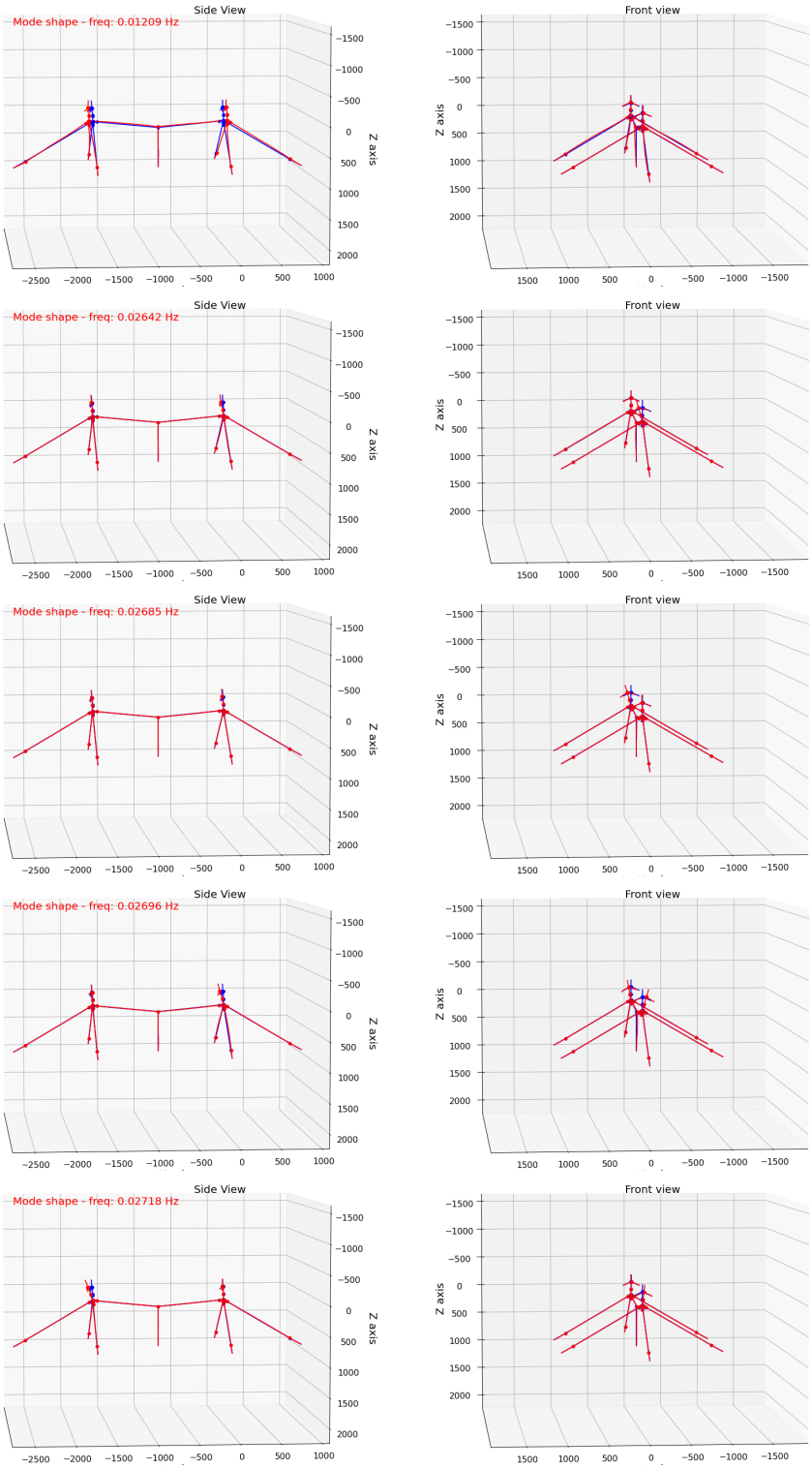
Side View
Mode shape - freq: 0.01209 Hz
Front view
Side View
Mode shape - freq: 0.02642 Hz
Front view
Side View
Mode shape - freq: 0.02685 Hz
Front view
Side View
Mode shape - freq: 0.02696 Hz
Front view
Side View
Mode shape - freq: 0.02718 Hz
Front view
Z axis

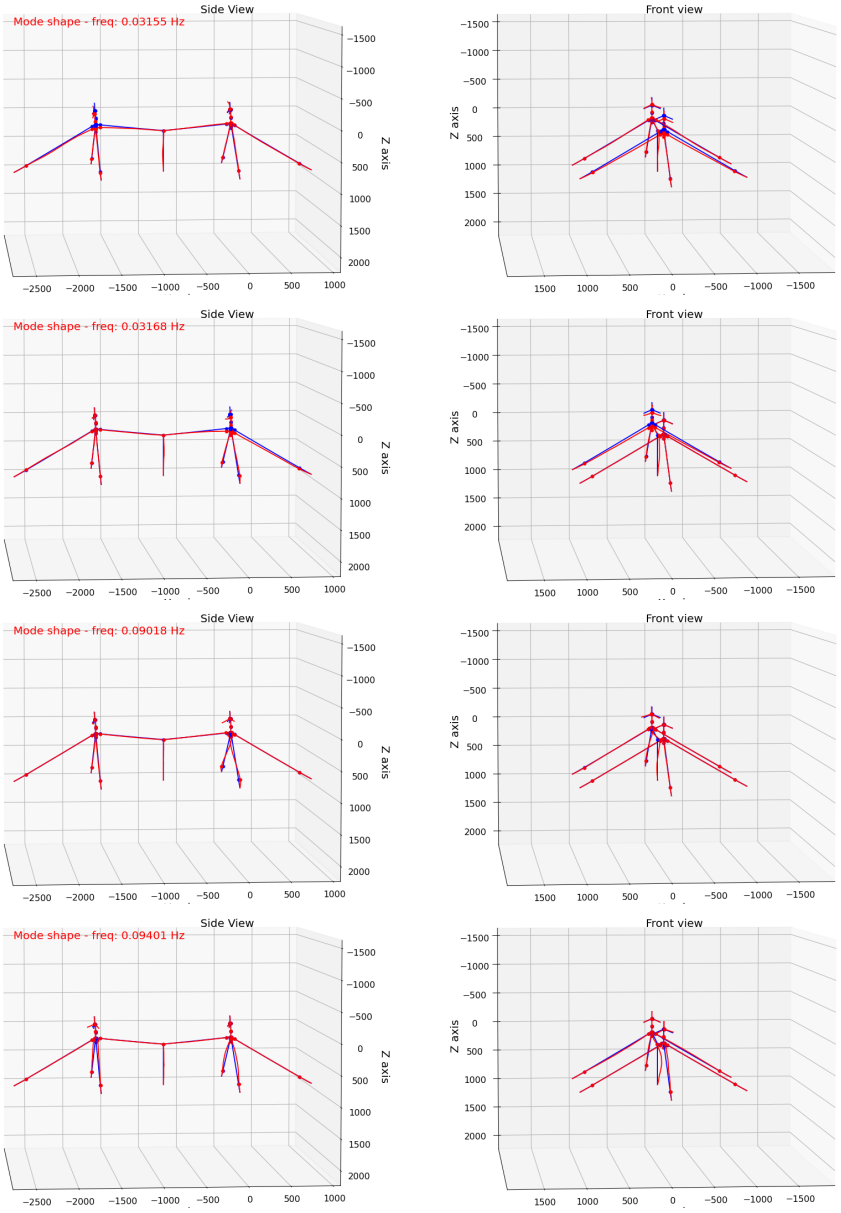
Side View
Mode shape - freq: 0.03155 Hz
Front view
Side View
Mode shape - freq: 0.03168 Hz
Front view
Side View
Mode shape - freq: 0.09018 Hz
Front view
Side View
Mode shape - freq: 0.09401 Hz
Front view
Z axis

B.3 Design-3

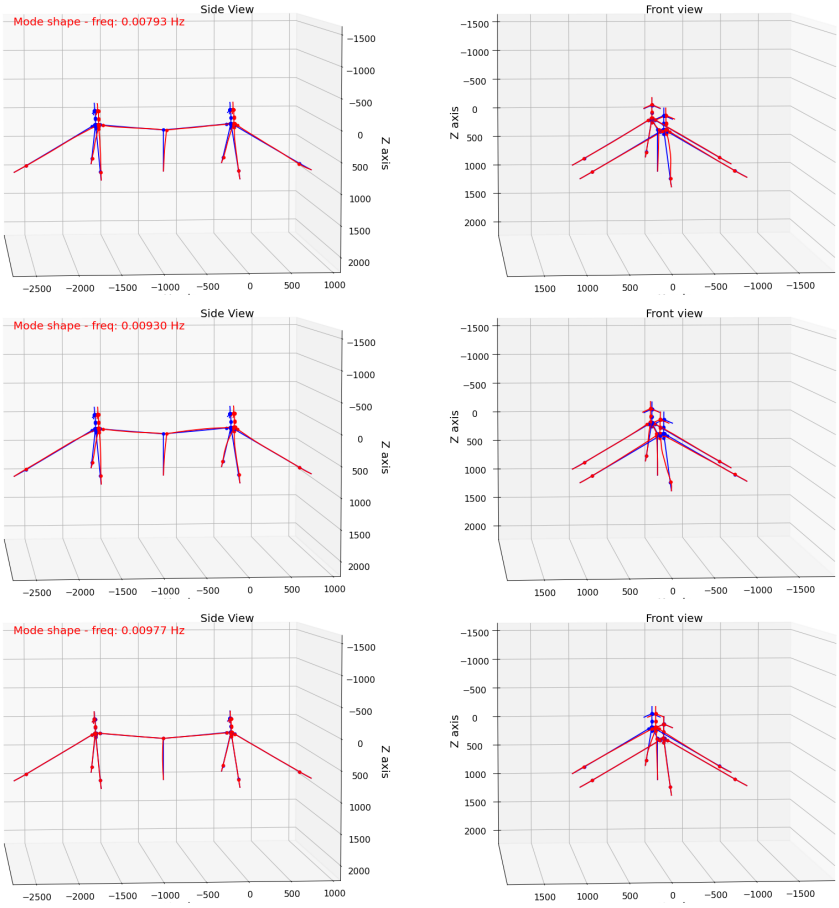
Side View
Mode shape - freq: 0.00793 Hz
Front view
Side View
Mode shape - freq: 0.00930 Hz
Front view
Side View
Mode shape - freq: 0.00977 Hz
Front view
Z axis

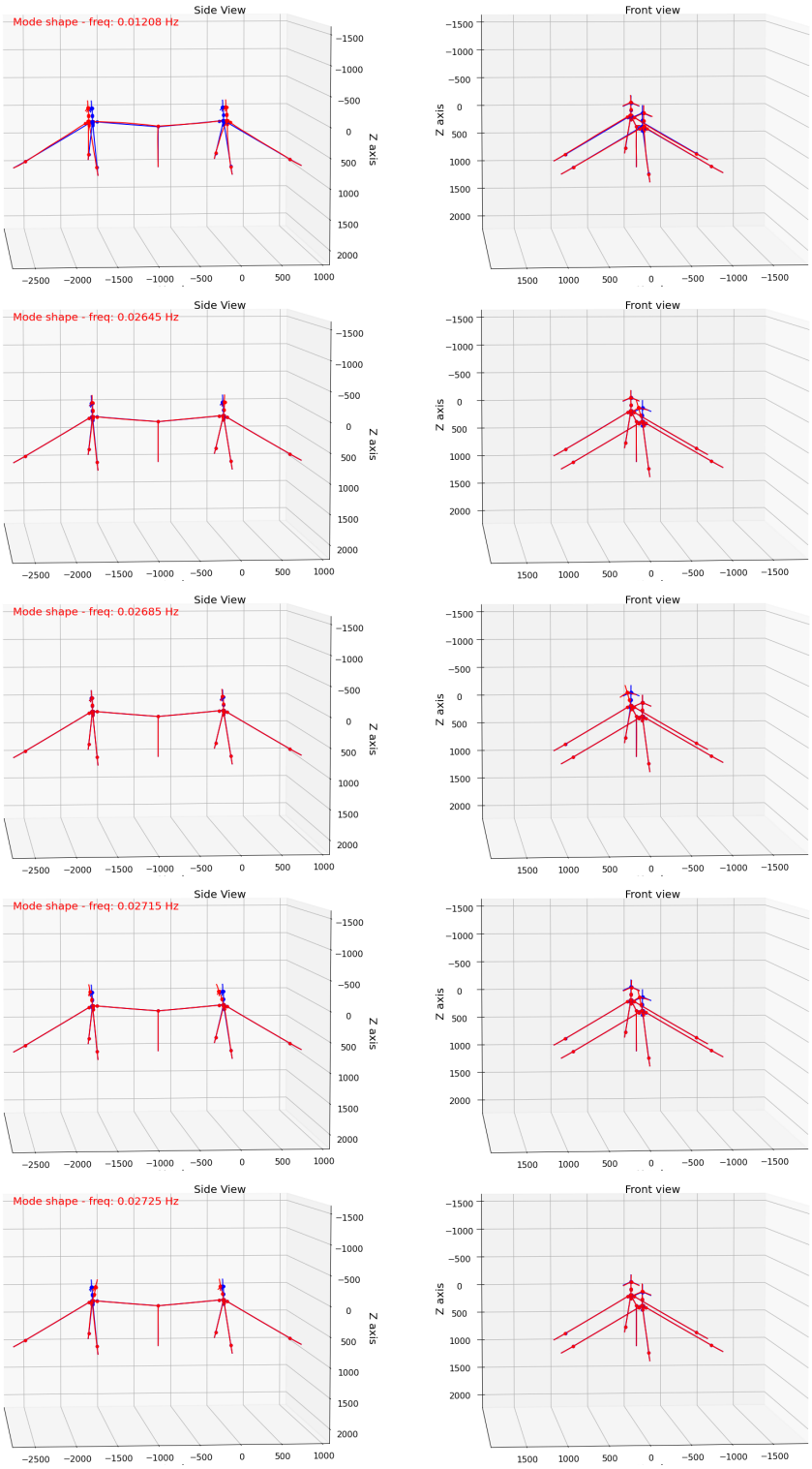
Side View
Mode shape - freq: 0.01208 Hz
Front view
Side View
Mode shape - freq: 0.02645 Hz
Front view
Side View
Mode shape - freq: 0.02685 Hz
Front view
Side View
Mode shape - freq: 0.02715 Hz
Front view
Side View
Mode shape - freq: 0.02725 Hz
Front view
Z axis

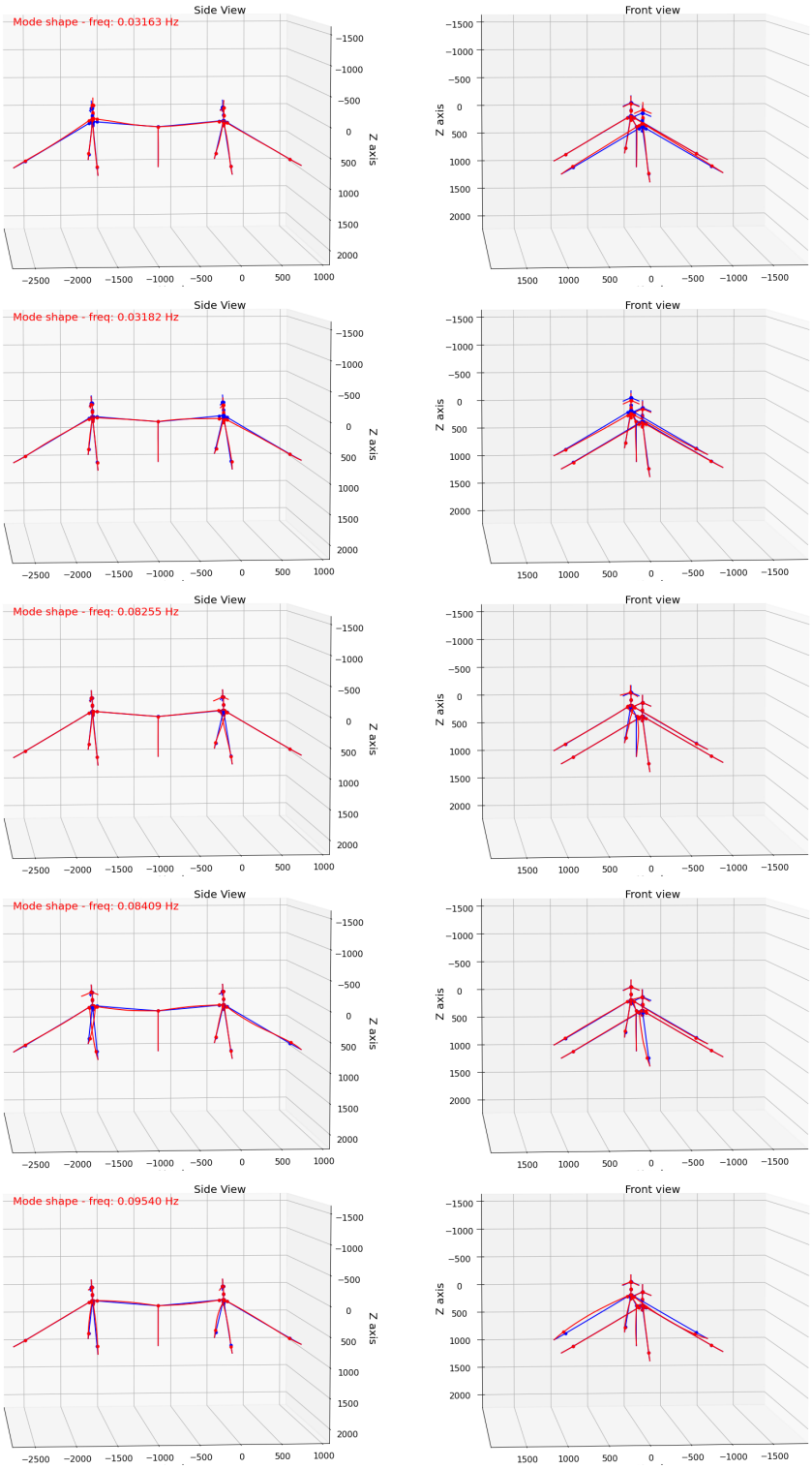
Side View
Mode shape - freq: 0.03163 Hz
Front view
Side View
Mode shape - freq: 0.03182 Hz
Front view
Side View
Mode shape - freq: 0.08255 Hz
Front view
Side View
Mode shape - freq: 0.08409 Hz
Front view
Side View
Mode shape - freq: 0.09540 Hz
Front view
Z axis

B.4 Design-5

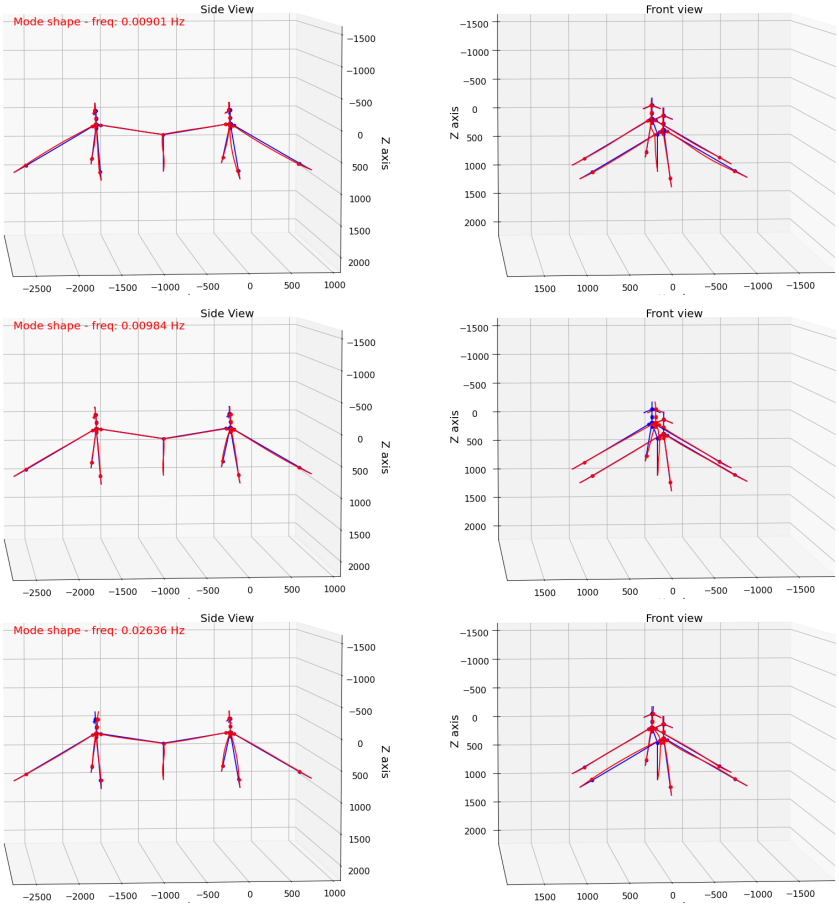
Side View
Mode shape - freq: 0.00901 Hz
Front view
Side View
Mode shape - freq: 0.00984 Hz
Front view
Side View
Mode shape - freq: 0.02636 Hz
Front view
Z axis

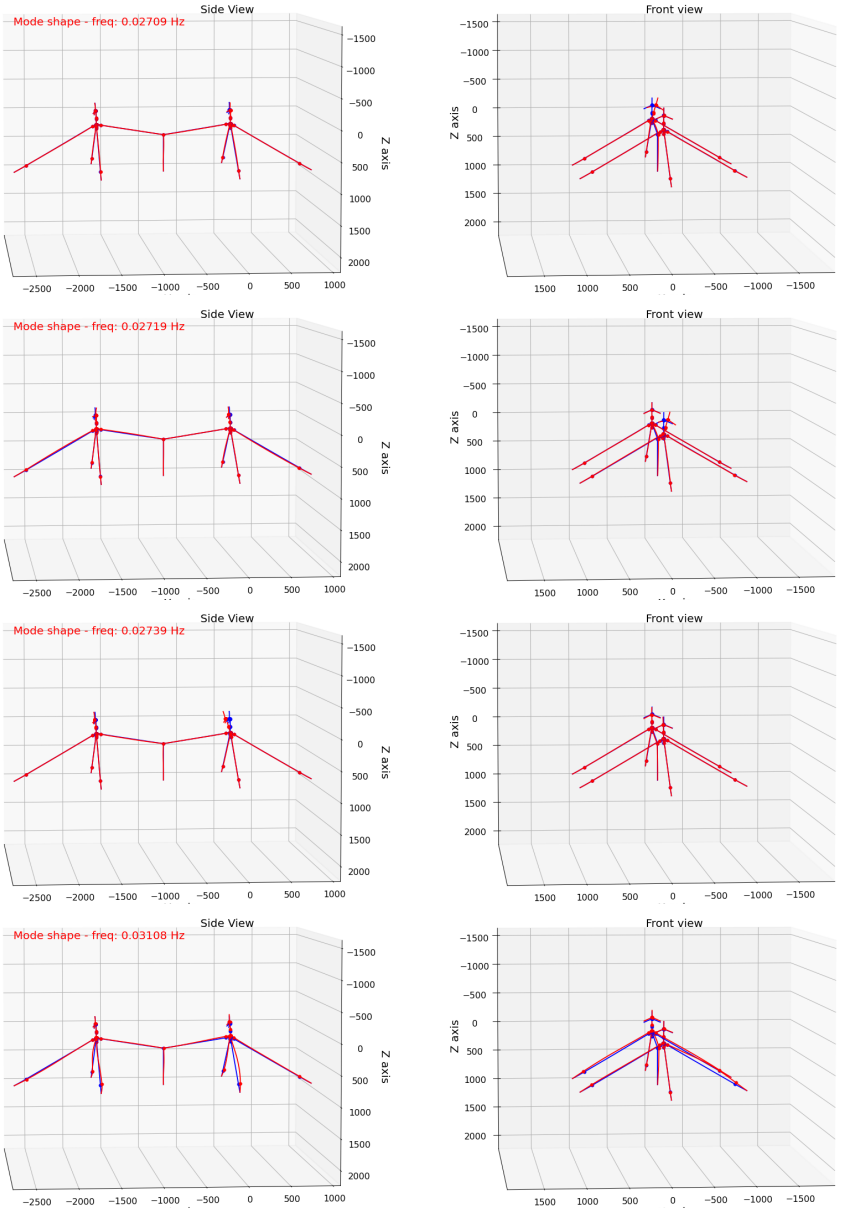
Side View
Mode shape - freq: 0.02709 Hz
Front view
Side View
Mode shape - freq: 0.02719 Hz
Front view
Side View
Mode shape - freq: 0.02739 Hz
Front view
Side View
Mode shape - freq: 0.03108 Hz
Front view
Z axis

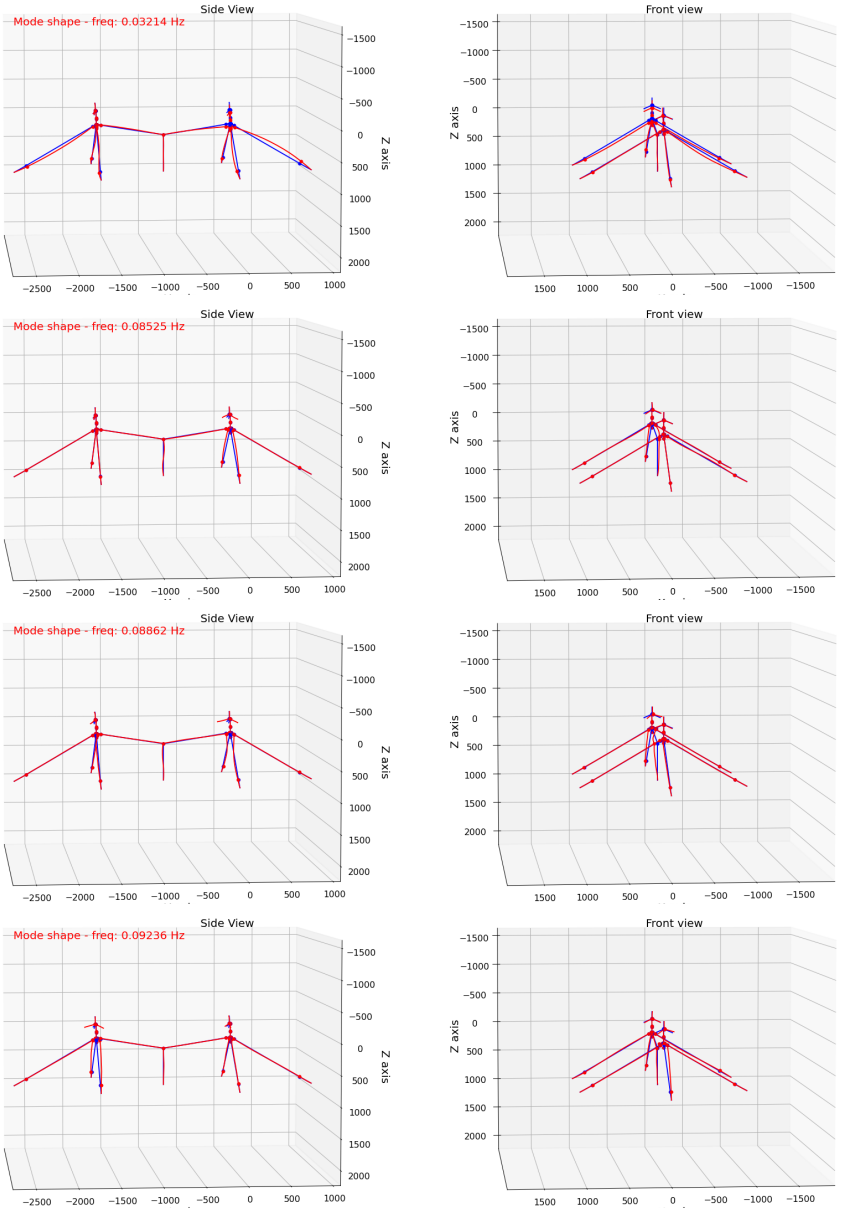
Side View
Mode shape - freq: 0.03214 Hz
Front view
Side View
Mode shape - freq: 0.08525 Hz
Front view
Side View
Mode shape - freq: 0.08862 Hz
Front view
Side View
Mode shape - freq: 0.09236 Hz
Front view
Z axis

C Configuration-3: Four turbines in Morro Bay

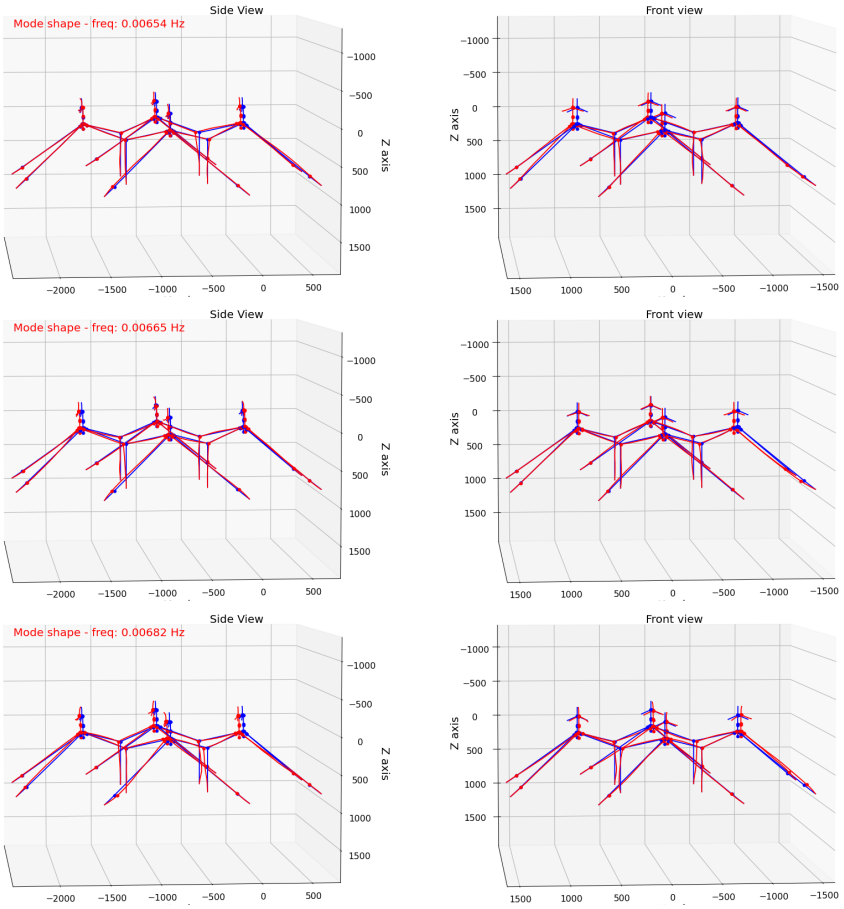

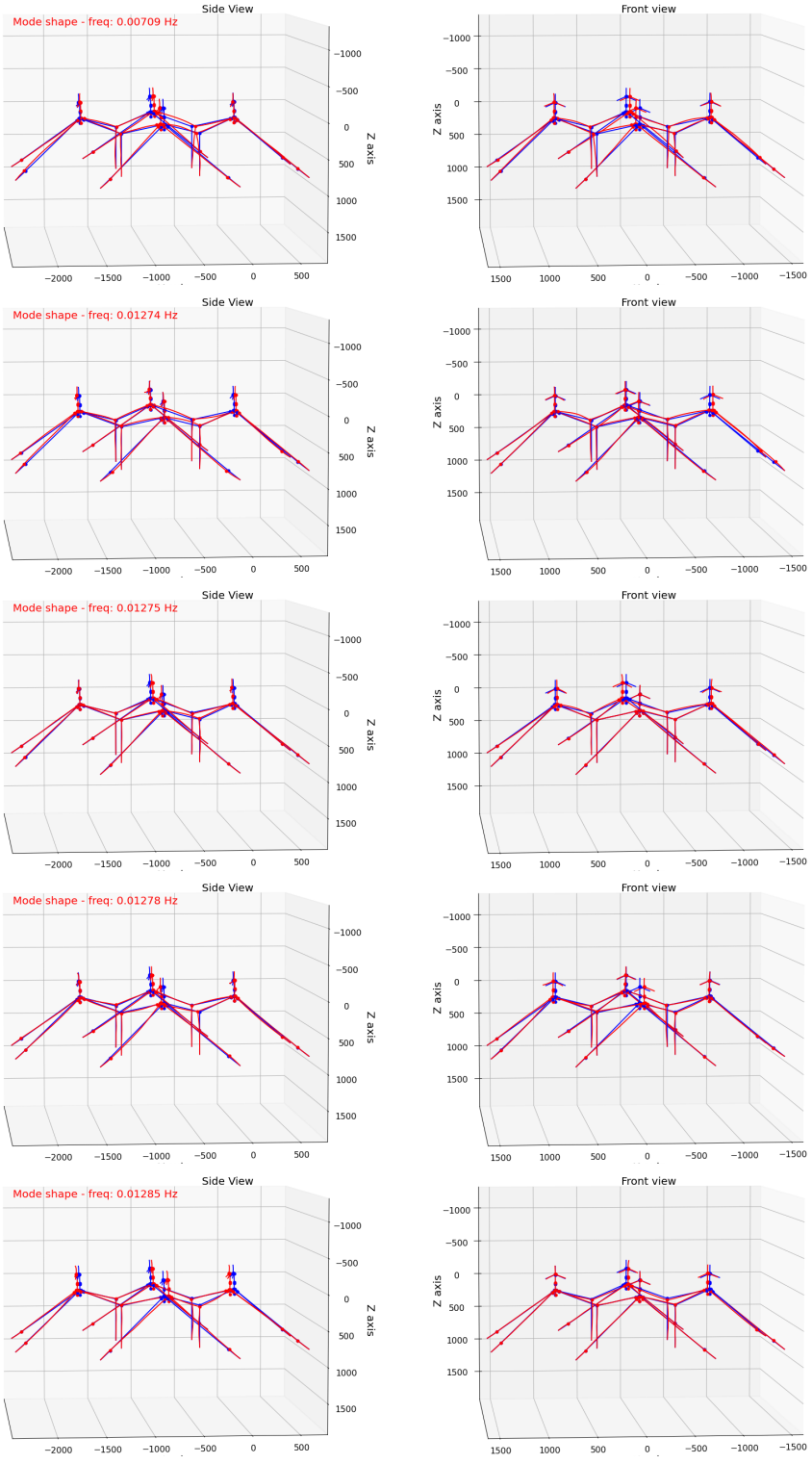
Side View
Mode shape - freq: 0.00709 Hz
Front view
Side View
Mode shape - freq: 0.01274 Hz
Front view
Side View
Mode shape - freq: 0.01275 Hz
Front view
Side View
Mode shape - freq: 0.01278 Hz
Front view
Side View
Mode shape - freq: 0.01285 Hz
Front view
Z axis

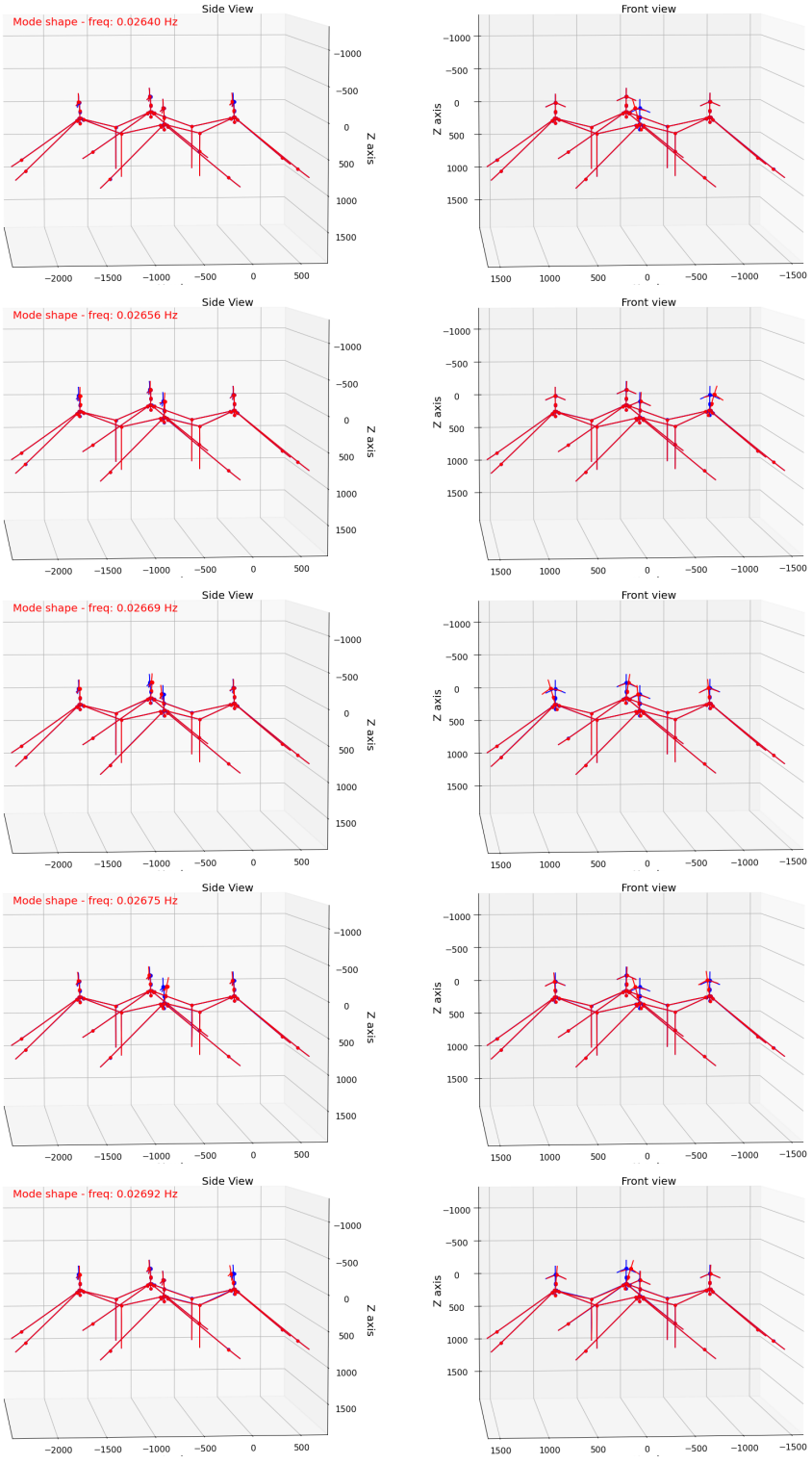
Side View
Mode shape - freq: 0.02640 Hz
Front view
Z axis
Side View
Mode shape - freq: 0.02656 Hz
Front view
Z axis
Side View
Mode shape - freq: 0.02669 Hz
Front view
Z axis
Side View
Mode shape - freq: 0.02675 Hz
Front view
Z axis
Side View
Mode shape - freq: 0.02692 Hz
Front view
Z axis

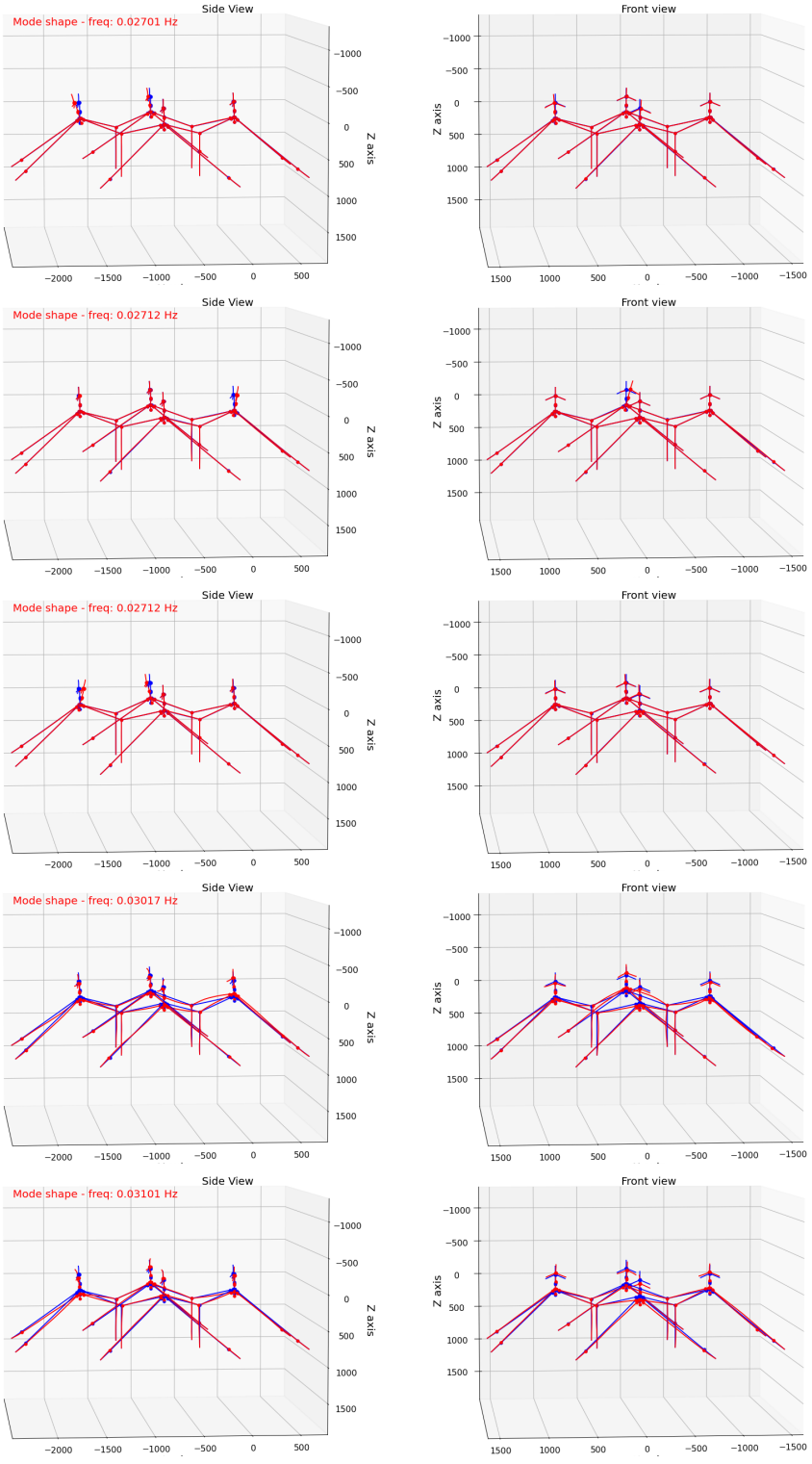
Side View
Mode shape - freq: 0.02701 Hz
Front view
Z axis
Side View
Mode shape - freq: 0.02712 Hz
Front view
Z axis
Side View
Mode shape - freq: 0.02712 Hz
Front view
Z axis
Side View
Mode shape - freq: 0.03017 Hz
Front view
Z axis
Side View
Mode shape - freq: 0.03101 Hz
Front view
Z axis

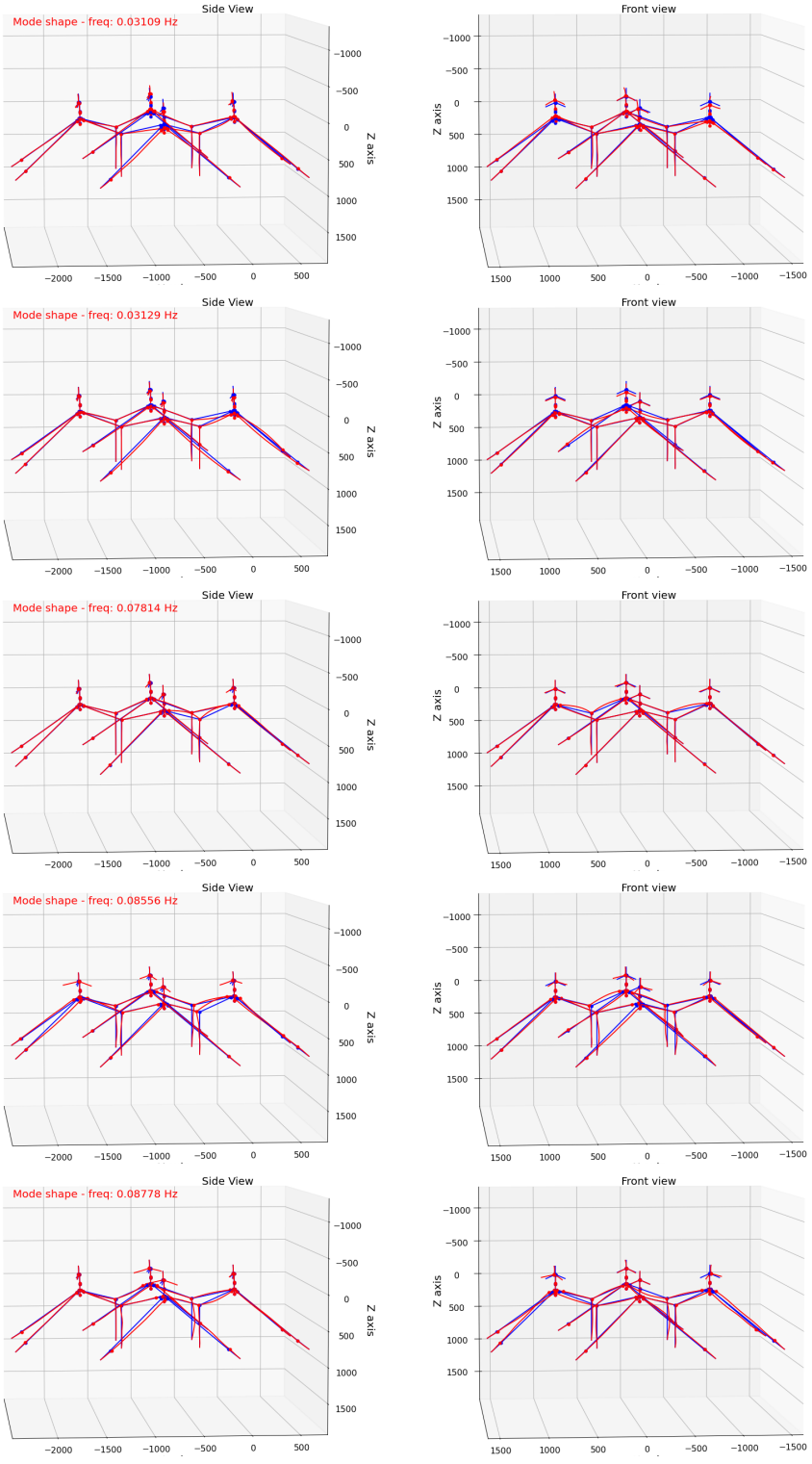
Side View
Mode shape - freq: 0.03109 Hz
Front view
Side View
Mode shape - freq: 0.03129 Hz
Front view
Side View
Mode shape - freq: 0.07814 Hz
Front view
Side View
Mode shape - freq: 0.08556 Hz
Front view
Side View
Mode shape - freq: 0.08778 Hz
Front view
Z axis